Augmented Coronary Vascular Smooth Muscle Response to Endothelin-1 Exacerbates Cardiac Injury Following Pulmonary Exposure to Engineered Nanomaterials

by
Leslie Charles Thompson
December, 3rd 2013
Director of Thesis/Dissertation: Christopher J. Wingard, Ph.D.
Major Department: Physiology

Multi-walled carbon nanotubes (MWCNT) and 60-carbon fullerenes (C60) are important engineered nanoparticles (ENP) used across industry. Exposure to ENP potentially promotes cardiovascular detriments. The hypotheses that exposure to either MWCNT or C60 would exacerbate cardiac ischemia/reperfusion (I/R) injury and promote enhanced coronary artery contraction in response to endothelin-1 (ET-1) by a cyclooxygenase-mediated mechanism were tested. One day following intratracheal instillation of vehicle, 1, 10 or 100 μg MWCNT in male Sprague-Dawley rats, hearts were isolated and mounted on a Langendorff perfusion apparatus. Hearts from animals exposed to 100 μg MWCNT exhibited 3x more premature ventricular contractions during perfusion at baseline. Cardiac perfusion was stopped to induce ischemia for 20 minutes and then restarted to study injuries induced by I/R. Post-reperfusion myocardial infarction expanded 18% in the 100 μg MWCNT group compared to the vehicle group. We also noted that post-ischemia cardiac release of ET-1 was increased 4-fold and coronary reperfusion flow was reduced 30% in the 100 μg MWCNT group compared to the vehicle group. We next evaluated isolated coronary artery ET-1-mediated stress (mN/mm^2) generation by wire myography, 24 hours after intratracheal instillation of 100 μg MWCNT or vehicle. Coronary artery stress generation in response to ET-1 was increased 35% in the MWCNT group compared to the vehicle group and was dependent on cyclooxygenase/thromboxane signaling. Similar endpoints were examined following C60 exposure. We measured myocardial infarction

following I/R*in situ* and coronary artery ET-1-mediated stress responses by wire myography, 24 hours after intratracheal or intravenous administration of vehicle or 28 µg C60. Myocardial infarction expanded between 70% and 110% across all C60 groups. Coronary artery stress generation in response to ET-1 was elevated by 56% in the male intratracheal C60 group compared to the vehicle group and was dependent on cyclooxygenase signaling. ET-1 responses in all other C60 groups were not different than vehicle. These results support the potential for pulmonary exposure to carbon-based ENP to exacerbate cardiac I/R injury and promote dysfunction in coronary arteries associated with ET-1/cyclooxygenase axis. Our results indicate that therapeutic targeting of ET-1 or cyclooxygenase signaling might prevent cardiovascular detriments associated with ENP exposure.

Augmented Coronary Vascular Smooth Muscle Response to Endothelin-1 Exacerbates Cardiac Injury Following Pulmonary Exposure to Engineered Nanomaterials

A Dissertation

Presented to the Faculty of the Department of Physiology

East Carolina University

In Partial Fulfillment of the Requirements for the Degree

Doctor of Philosophy

by

Leslie Charles Thompson

December, 2013

Augmented Coronary Vascular Smooth Muscle Response to Endothelin-1 Exacerbates Cardiac Injury Following Pulmonary Exposure to Engineered Nanomaterials

by

Leslie Charles Thompson

APPROVED BY:

DIRECTOR OF
DISSERTATION/THESIS: _____
Christopher J. Wingard, Ph.D.

COMMITTEE MEMBER: _____
Jared M. Brown, Ph.D.

COMMITTEE MEMBER: _____
Robert M. Lust, Ph.D.

COMMITTEE MEMBER: _____
Michael R. Van Scott, Ph.D.

COMMITTEE MEMBER: _____
Timothy R. Nurkiewicz, Ph.D.

CHAIR OF THE DEPARTMENT
OF PHYSIOLOGY: _____
Robert M. Lust, Ph.D.

DEAN OF THE
GRADUATE SCHOOL: _____
Paul J. Gemperline, Ph.D.

Dedication

I dedicate this dissertation to all of my loving family. They have each contributed to my intellectual growth, my desire to challenge myself, and my will to persevere. When failure seemed close, many people doubted me. Instead, my family gathered around me, loved me, supported me, lifted me up and believed that I would succeed.

ACKNOWLEDGEMENTS

I cannot triumph without challenge, and I was certainly challenged by this dissertation project. I owe many people thanks and gratitude, only a few of which will be listed here.

I would like to thank my mentor, Dr. Chris Wingard, for recruiting me and giving me an opportunity to try my hand at research. He provided an exceptional environment in which I was able to grow and develop as a researcher in physiological sciences. I admire his inquisitive nature, his ability to synthesize new ideas, and his approaches to the problems at hand. He is resourceful, sharp, and truly one of a kind. If he has taught me one thing, it would be to find the right tool for the job and remember where I put it last. I must especially acknowledge his/our funding sources, which include both National Institute of Environmental Health Sciences grants U19 ES019525 and R01 ES016246.

I must provide a special thanks to Dr. Jared Brown for sitting on my dissertation committee. Due to his proximity to my work throughout my first 4 years at ECU, I could not help but be impressed with his success and diligence. Dr. Michael Van Scott was another committee member to whom I am grateful. Despite his busy schedule, he never hesitated to stop and listen when I had a problem, and his responses were always direct, meaningful, and exactly what I needed to hear. Similar thanks go to Dr. Robert Lust for being a wonderful source of guidance, not only as a member of my dissertation committee, but as the Chair of the Department of Physiology. I would also like to humbly thank Dr. Timothy Nurkiewicz for agreeing to sit on my committee, as an external member all the way from West Virginia University. He provided support, important criticism, and a graceful touch of humor during every encounter we shared.

Aside from my committee members, I really must thank Dr. David Tulis, Dr. David Brown, and Dr. Stefan Clemens for their very meaningful input and effort into my growth as a researcher. Dr. Richard Ray, Dr. Robert Carroll, Dr. Jamie Dewitt, Dr. Abdel Abdel-Rahman, Dr. David Taylor, Dr. P. Darrell Neufer, Dr. Brian Shewchuk, Dr. Joseph Chalovich, and Dr. Phillip Pekala all provided excellence in teaching, which inspired me much more than they may be aware of. I would also like to thank Dr. Katwa, Dr. Murashov, Dr. Walters, Dr. Wardle, Dr. Virag and Dr. Ding for their meaningful lectures, conversations, and discussions through my years at ECU.

I would like to thank my classmates Fatiha Moukdar, Joshua Stone, and Tracy Johnson for starting this incredible journey with me. All the other graduate students in the Department of Physiology deserve a really big thanks, especially Drew Holt for all the times I wondered into his workspace and interrupted him to ask if I could borrow something. I would also like to thank previous graduate students who have finished and moved on before me, but whom greatly contributed to my experiences as a graduate student. These include Dr. Achini Vidanapathirana, Dr. Pranita Katwa, Dr. Justin LaFavor, Dr. Chad Frasier, and Dr. Trey Sloan.

Last, but certainly not least, I acknowledge my devoted lab partners. These definitely include Jillian Odom, Nathan Holland, and Daniel Becak. I am not sure how I could have finished all I needed to finish without these three pitching in and helping out. I would like to thank Dr. Jonathan Shannahan, Nicole Sheehan, Alvin Tsang, Erin Mann, and Rakhee Urankar for contributing to my projects over the years. I would also like to thank Brook Cathey and Cathy Stang for helping me get acclimated to Dr. Wingard's laboratory when I was starting at ECU.

TABLE OF CONTENTS

LIST OF TABLES xvi

LIST OF FIGURES xvii

LIST OF SYMBOLS AND ABBREVIATIONS xix

CHAPTER 1: PREAMBLE AND SPECIFIC AIMS 1

1.1. Preamble 1

1.2. Hypotheses 3

1.3. Specific aims 3

1.4. Significance 5

CHAPTER 2: LITERATURE REVIEW 7

2.1. Cardiovascular disease and the contribution of particulate exposure 7

2.2. Mechanisms of cardiovascular toxicity in response to nanoparticles 9

2.3. The era of engineered nanoparticles: tools to study the cardiovascular system? 13

2.4. Engineered nanoparticle examined 15

2.4.1. Multi-walled carbon nanotubes 16

2.4.2. 60-carbon fullerenes 18

2.5. Pulmonary exposure models: intratracheal instillation vs. inhalation 20

2.6. Cardiac endpoints following nanoparticle exposure 20

2.6.1. Cardiac ischemia/reperfusion injury 20

2.6.2. Cardiac ischemia/reperfusion – the *in situ* model 23

2.6.3. Cardiac ischemia/reperfusion – the isolated Langendorff heart model 23

2.6.4. Nanoparticle exposure and the heart 23

2.7. Arterial endpoints following nanoparticle exposure 26

2.7.1. The vascular system 26
2.7.2. Physiological parameters regulated by arteries 28
2.7.3. Isolated artery techniques 29
2.7.4. Nanoparticle exposure and arteries 35
2.8. Key pathways and cardiac/vascular ligands examined 37
2.8.1. Endothelin-1 37
2.8.2. Thromboxane 37
2.9. Conclusion of literature review 39
CHAPTER 3: INTRATRACHEAL INSTILLATION OF MULTI-WALLED CARBON NANOTUBES EXACERBATES CARDIAC ISCHEMIA/REPERFUSION INJURY AND DEPRESSES CORONARY REPERFUSION FLOW 40
3.1. Introduction 40
3.2. Materials and Methods 43
3.2.1. Multi-walled carbon nanotubes and vehicle 43
3.2.2. Hydrodynamic size and zeta potential 43
3.2.3. Particle number assessment 44
3.2.4. Animals 44
3.2.5. Instillations 45
3.2.6. Cardiac ischemia/reperfusion protocol 45
3.2.7. Endothelin-1 and thromboxane in the coronary effluent 46
3.2.8. Statistics 47
3.3. Results 48
3.3.1. Multi-walled carbon nanotube physical characteristics 48

3.3.2. Baseline readings from isolated hearts 49

3.3.3. Coronary reperfusion flow and concentration of endothelin-1 and thromboxane B_2 in effluent 51

3.3.4. Left ventricular pressures 53

3.3.5. Cardiac ischemia/reperfusion injury 54

3.4. Discussion 56

3.5. Chapter 3 Conclusion 62

CHAPTER 4: INCREASED ISOMETRIC STRESS IN RESPONSE TO ENDOTHELIN-1 IN ISOLATED CORONARY ARTERIES 24 HOURS AFTER INTRATRACHEAL INSTILLATION OF MULTI-WALLED CARBON NANOTUBES 63

4.1. Introduction 63

4.2. Materials and Methods 66

4.2.1. Multi-walled carbon nanotubes and vehicle 66

4.2.2. Animals 66

4.2.3. Instillations 67

4.2.4. Bronchoalveolar lavage 67

4.2.5. Differential cell counts 67

4.2.6. Protein quantification 68

4.2.7. Isolated wire myography 68

4.2.8. Pharmacological agents for vascular studies 69

4.2.9. Coronary artery assessments of endothelin-1 responses 69

4.2.10. Coronary artery assessments of thromboxane mimetic U46619..... 70

4.2.11. Statistics 70

4.3. Results 71
4.3.1. Pulmonary responses to instillation 71
4.3.2. Intact coronary artery responses to endothelin-1 and thromboxane mimetic 72
4.3.3. Denuded coronary artery responses to endothelin-1 74
4.3.4. Endothelin receptor antagonist-sensitive responses in intact coronary arteries 76
4.3.5. Coronary artery endothelin-1 responses and cyclooxygenase 78
4.3.6. Coronary artery endothelin-1 responses and the thromboxane axis ... 80
4.4. Discussion 83
4.5. Chapter 4 Conclusion 86
CHAPTER 5: PULMONARY EXPOSURE TO C60 PROMOTES EXPANSION OF CARDIAC I/R INJURY AND ENHANCES ET-1/COX MEDITATED STRESS PRODUCTION IN ISOLATED CORONARY ARTERY CONTRACTION 87
5.1. Introduction 87
5.2. Materials and Methods 90
5.2.1. 60-carbon fullerenes 90
5.2.2. Particle number assessment 91
5.2.3. Animals 91
5.2.4. Instillations 92
5.2.5. Bronchoalveolar lavage 92
5.2.6. Differential cell counts 92
5.2.7. Protein quantification 93

5.2.8. Cardiac ischemia/reperfusion injury *in situ* 93
5.2.9. Determination of post-I/R infarct size 94
5.2.10. Post-ischemia/reperfusion cytokines 94
5.2.11. Coronary artery isolation and vessel viability assessment 95
5.2.12. Pharmacology of the isolated coronary artery 96
5.2.13. Isolated coronary artery endothelin-1 responses 97
5.2.14. Statistics 97
5.3. Results 99
5.3.1. 60-carbon fullerene characterization 99
5.3.2. Bronchoalveolar lavage fluid analysis 100
5.3.3. Cardiac ischemia/reperfusion injury 101
5.3.4. Post-I/R serum cytokines 103
5.3.5. Male rat coronary artery pharmacology 106
5.3.6. Female rat coronary artery pharmacology 109
5.3.7. Male and female rat coronary responses to endothelin-1 112
5.3.8. Indomethacin-sensitive coronary artery responses to endothelin-1 115
5.4. Discussion 118
5.5. Chapter 5 Conclusion 124
CHAPTER 6: INTEGRATED DISCUSSION AND CONCLUSION 125
6.1. Integrated discussion 125
6.1.1. Summary of findings 125
6.1.2. Considerations 127
6.1.2.1. Particle characteristics 127

6.1.2.2. Particle dosimetry 129

6.1.3. Interpretation of results 134

6.2. Dissertation conclusion 142

REFERENCES 143

APPENDIX A: IACUC APPROVAL LETTERS FOR ANIMAL USE PROTOCOLS 159

LIST OF TABLES

Table 3.1 Multi-walled carbon nanotube particle characterization..... 48

Table 4.1 Bronchoalveolar lavage from multi-walled carbon nanotube studies 71

Table 4.2 Coronary artery EC_{50}s from multi-walled carbon nanotube studies..... 82

Table 4.3 Coronary artery Hillslopes from multi-walled carbon nanotube studies 82

Table 5.1 60-carbon fullerene particle characterization 99

Table 5.2 Bronchoalveolar lavage from 60-carbon fullerene studies in male rats 100

Table 5.3 Bronchoalveolar lavage from 60-carbon fullerene studies in female rats 100

Table 5.4 Male rat coronary artery EC_{50}s from 60-carbon fullerene studies..... 109

Table 5.5 Male rat coronary artery Hillslopes from 60-carbon fullerene studies..... 109

Table 5.6 Female rat coronary artery EC_{50}s from 60-carbon fullerene studies 112

Table 5.7 Female rat coronary artery Hillslopes from 60-carbon fullerene studies 112

Table 6.1 Particle suspension comparisons 129

LIST OF FIGURES

Figure 1.1 Visual representation of how the aims of this dissertation are related 6

Figure 2.1 Potentialmechanisms of nanoparticle-induced cardiovascular toxicity..... 11

Figure 2.2 Research on carbon nanotubes and fullerenes has increased 14

Figure 2.3 Structure of multi-walled carbon nanotube..... 18

Figure 2.4 Carbon organization of 60-carbon fullerene 19

Figure 2.5 Ischemic injury compared to reperfusion injury in the heart 22

Figure 2.6 Arterial active length-tension shape depends on technique 33

Figure 3.1 Increased premature ventricular contractions at baseline in isolated hearts. 59-50

Figure 3.2 Coronary reperfusion flow and effluent endothelin-1 and thromboxane B_2. 52

Figure 3.3 Left ventricular pressures..... 53

Figure 3.4 Cardiac ischemia/reperfusion injury..... 54-55

Figure 4.1 Intact coronary artery response to endothelin-1 and thromboxane mimetic. 73

Figure 4.2 Denuded coronary artery responses to endothelin-1 75

Figure 4.3 Endothelin receptor antagonist-sensitive responses in intact coronary arteries 77

Figure 4.4 Cyclooxygenase inhibition in intact coronary arteries 79

Figure 4.5 Thromboxane axis blockade in intact coronary arteries 81

Figure 5.1 Cardiac ischemia/reperfusion injury with 60-carbon fullerene exposure..... 102

Figure 5.2 Post-ischemia/reperfusion serum cytokine concentrations..... 104-105

Figure 5.3 Coronary artery pharmacology in male rats..... 107-108

Figure 5.4 Coronary artery pharmacology in female rats..... 110-111

Figure 5.5 Male and female coronary artery responses to endothelin-1 113-114

Figure 5.6 Indomethacin-sensitive coronary artery responses to endothelin-1 116-117

Figure 6.1 Coronary artery endothelin-1 stress responses as a function of dosimetry... 133

Figure 6.2 In Chapter 3 premature ventricular contractions from baseline correlated withmyocardial infarct size following cardiac ischemia/reperfusion 136

Figure 6.3 Proposed mechanism of increased coronary artery stress in response to Endothelin-1 following pulmonary exposure to multi-walled carbon nanotubes 138

Figure 6.4 Potential cardiovascular consequences of dysregulated endothelin-1 signaling..... 141

LIST OF SYMBOLS AND ABBREVIATIONS

Symbols and equations:

ΔD – change in diameter

ΔF – Change in force

$\Delta F/mm$ – Change in tension

$\Delta F_{total} = \Delta F_{passive} + \Delta F_{active}$ – Change in total force is the sum of passive and active force

ΔR – Change in resistance

$\Delta R = P/\Delta Q$ – Equation to derive change in resistance from change in flow (constant pressure)

$\Delta R = Q \bullet \Delta P$ – Equation to derive change in resistance from change in pressure (constant flow)

$2r$ – Diameter

P_i – Internal pressure

$P\ (\Delta P)$ – Pressure (change in pressure)

$Q\ (\Delta Q)$ – Flow (change in flow)

r – Radius

T_A – Active tension

$T_A = T_T - T_P$ – Equation to derive active tension from total and passive tensions

T_P – Passive tension

T_T – Total tension

$Wall\ tension = P_i \bullet r$ – Law of Laplace

Abbreviations:

5-HT – Serotonin

AA2414 – Thromboxane receptor antagonist

ACh – Acetylcholine

BAL – Bronchoalveolar lavage

C60 – 60-carbon fullerenes

COX – Cyclooxygenase

COX-2 – Cyclooxygenase-2

DUP-697 – Cyclooxygenase-2 selective inhibitor

EC – Vascular endothelial cells

ECG – Electrocardiogram

ENP – Engineered nanoparticles

ET-1 – Endothelin-1

ETAR – Endothelin $_{A}$ receptor

ETBR – Endothelin $_{B}$ receptor

FR139317 – selective endothelin $_{A}$ receptor antagonist

IL-6 – Interleukin-6

Indomethacin – General cyclooxygenase inhibitor

I/R – Ischemia/reperfusion

IT – Intratracheal

IV – Intravenous

LAD – Left anterior descending coronary artery

LVDP – Left ventricular developed pressure

Max. LV – Maximum left ventricular (pressure)

MCP-1 – Monocyte chemotactic protein-1

Min. LV – Minimum left ventricular (pressure)

MOPS – 3-[N-morpholino]-propane sulfonic acid

MWCNT – Multi-walled carbon nanotubes

NP – Nanoparticles

Ozagrel HCl – Thromboxane synthetase inhibitor

PSS – Physiological saline solution

PVC – Premature ventricular contractions

PVP – Polyvinylpyrrolidone

SNP – Sodium nitroprusside

Stress – Measure of force per square area of tissue (mN/mm^2)

SWCNT – Single-walled carbon nanotubes

TP – Thromboxane receptor

TXA2 – Thromboxane

TXB2 – Thromboxane B2, derivative of thromboxane A2

TXS – Thromboxane synthetase

U46619 – Thromboxane mimetic

UFP – Ultrafine particles

VEGF – Vascular endothelial growth factor

VSMC – Vascular smooth muscle cells

VT/VF – Ventricular tachycardia or ventricular fibrillation

ZAR – Zone at risk, an area of cardiac tissue at risk for infarction

CHAPTER 1

PREAMBLE AND SPECIFIC AIMS

1.1. Preamble

Inhalation of ultrafine/nanoparticles (NP) associated with air pollution may increase cardiac mortality and underlie cardiovascular disease prevalence in the United States (39). Modern technology has increased the use of engineered NP (ENP) in modern goods and likewise human occupational exposure to ENP has increased (74). Pulmonary instillation of ambient ultrafine particles (UFP) collected from the lower atmosphere and ENP have both been shown to exacerbate cardiac ischemia/reperfusion (I/R) injury (36; 165), but the mechanisms by which the injuries increaseare unknown. Endothelin-1 (ET-1) is important in cardiovascular physiology (161), andderangements in ET-1 signaling could contribute to exacerbation of cardiovascular injury following NP exposure. Cyclooxygenases (COX) can also contribute to the regulation of vascular tone via the release of prostaglandin derivatives like thromboxane (TXA2) (52), especially in cases of inflammation-induced cyclooxygenase-2 (COX-2) expression (138). Pulmonary inflammation induced by exposure to NP could activate COX-2, thereby disrupting coronary arterial tone and exacerbating cardiac injury.

Multi-walled carbon nanotubes (MWNCT) and 60-carbon fullerenes (C60) are ENP found in a growing number of consumer goods (90; 112). MWCNT and C60 are also gaining promise in medical applications as drug delivery devices and contrast imaging agents (133). The hydrophobic core of fullerene molecules, like MWCNT and C60, make the ideal carriers for hydrophobic pharmacological agents, while functionalization of the normally hydrophobic

fullerene surface with hydrophilic moieties can enhance their solubility in physiological systems (7). Manipulation of MWCNT composites and raw C60 during manufacturing processes can generate airborne particulate that could potentially be inhaled by workers in the immediate environment. Physiological responses to MWCNT, C60 and other ENP are not well understood and should be examined to assess the potential for adverse endpoints.

It is also important to note that both epidemiological and basic science studies indicategender disparities to particulate matter exposures with premenopausal females beingmore resistant than males to the cardiovascular detriments associated with air pollution constituents (71; 134) and less prone to cardiac I/R injury in general (172). The same gender protection against cardiovascular responses to ENP may hold true, but evidence supporting or refuting this claim is absent in scientific literature.

Our laboratory has previously reported an exposure mass-dependent expansion of cardiac I/R injury, 24 hours following pulmonary instillation of MWCNT in mice (165). A similar extent of I/R myocardial infarct expansion was found in mice following instillation of ultrafine particular matter (36). The purpose of this dissertation project was to explore and identify factors intrinsic to the heart that could potentially increase myocardial vulnerability to I/R injury following pulmonary exposure to engineered NP.Once identified, these factors could be utilized to assess and classify cardiotoxicity of other ENP. Basal intrinsic heart rhythm, coronary perfusion, release of cardiac-active and vascular-active autocrine/paracrine agents, and pharmacological stress production generated by isolated coronary artery preparationswere examined following pulmonary instillation of MWCNT. Stress generated by isolated coronary arteries in response to

pharmacological agents following exposure to C60 was examined to explore a unified mechanism associated with cardiotoxicity resulting from exposure to different types of ENP. We further determined if theresponses were unique to NP exposure at the pulmonary interface and whether they were gender-dependent.

1.2. Hypotheses

We hypothesized that pulmonary instillation of ENP would exacerbate cardiac I/R injury by (i) increasing intrinsic cardiac arrhythmia, (ii) increasing the release of ET-1 and thromboxane from the heart during cardiac I/R, and (iii) enhancing coronary vascular resistance via ET-1/thromboxane mediated coronary vasoconstriction. We further hypothesized that exacerbated cardiac I/R injury and enhanced coronary artery stress responses following ENP exposure would be exacerbated in males.

1.3 Specific Aims

The primary aim of this dissertation was to investigate the effects of an acute exposure to ENP on subsequent cardiac I/R injury (see Figure 1.1). The following Specific Aims were developed to test the primary and secondary hypotheses.

Specific Aim 1: Determine if pulmonary exposure to MWCNT*in vivo* leads to altered cardiac functionbefore and after I/R *ex vivo.*

Aim 1.1. - Assess baseline coronary flow, heart rhythm, ET-1 release, and thromboxane release in isolated hearts 24 hours following pulmonary instillation of MWCNT or vehicle.

Aim 1.2. - Determine if the onset of I/R alters coronary flow, heart rhythm, and ET-1 and thromboxane release during myocardial reperfusion between the MWCNT and vehicle groups.

Specific Aim 2: Determine if isolated coronary artery contraction is augmented following pulmonary exposure to MWCNT or vehicle.

Aim 2.1 - Assess coronary artery stress generation in response to ET-1 and TXA2 stimulation.

Aim 2.2 - Determine the role of COX-1 or COX-2 in influencing the stress generation in isolated coronary artery preparation.

Aim 2.3 - Determine if augmented coronary stress generation is endothelial-dependent and/or sensitive to receptor antagonism of ET-1 and TXA2 signaling cascades.

Specific Aim 3: Using an alternative ENP, C60, identify common underlying mechanisms to ENP cardiotoxicity.

Aim 3.1 - Determine effects of pulmonary and intravenous exposure to C60 on cardiac I/R injury.

Aim 3.2 - Determine effects ofpulmonary andintravenous exposure to C60 on coronary artery smooth muscle stress generation in response to ET-1.

Aim 3.3 - Determine if COX signaling contributes to coronary artery augmented contraction following C60 exposure.

Aim 3.4 - Determine if gender is a discriminator for the extent of NP exposure-mediated cardiac I/R injury and/or coronary artery contraction.

1.4. Significance

Inhalation of NP can injure the cardiovascular system in general. Epidemiological data suggests that short-term exposure (days) to ambient air pollution, including ultrafine particulate, increases cardiovascular mortality, cardiovascular hospitalizations, and vascular/endothelial cell

dysfunction (16). Premenopausal females are generally protected against cardiovascular dysfunction associated with pulmonary exposure to airborne particulate (71) and diesel components (134). Development of ENP is rapidly advancing in commercial, military, and medical industries and as a consequence the potential for human exposures are increasing (133). While mechanisms underlying the cardiovascular toxicity of NP inhalation have been proposed (39; 144), few mechanisms have been defined. Given that the number of ENP reaching the industrial and medical settings is increasing rapidly, being able to rapidly classify which types of ENP are cardiotoxic across genders may be very beneficial. Therefore, the contents of this dissertation should advance the scientific understanding of the physiological mechanisms by which negative cardiovascular endpoints result from pulmonary exposure to NP and further establish experimental cardiovascular endpoints based on those mechanisms that can be used to test the cardiotoxicity of ENP.

Figure 1.1 Visual representation of how the aims of this dissertation are related

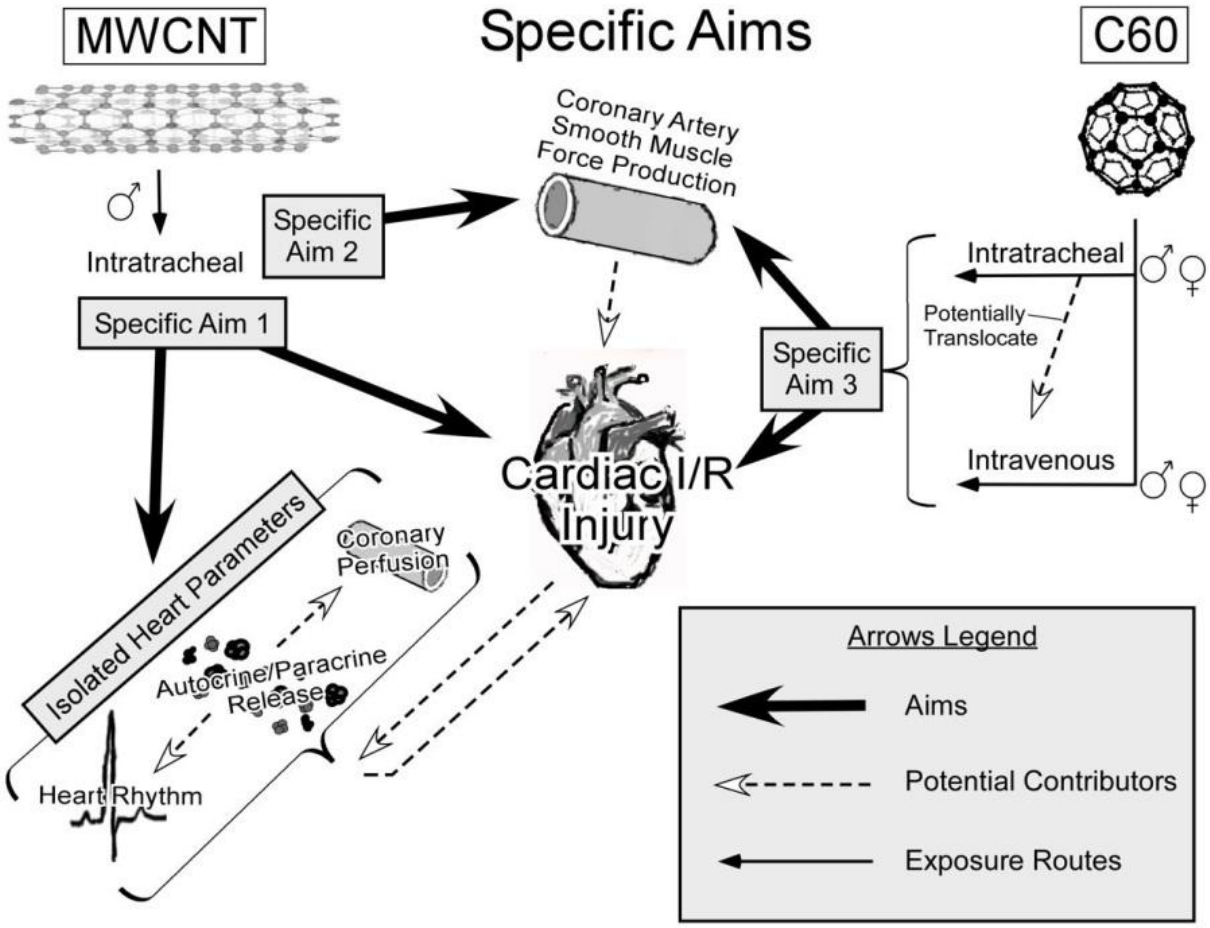

CHAPTER 2

LITERATURE REVIEW

Acknowledgement

Small portions of this chapter have been reproduced in part from the following citation:

Mann EE, Thompson LC, Shannahan JH and Wingard CJ. Changes in cardiopulmonary function induced by nanoparticles. *Wiley Interdiscip Rev Nanomed Nanobiotechnol* 4: 691-702, 2012.

2.1. Cardiovascular disease and the contribution of particulate exposure

Despite advances in the modern age of medicine and the current volume of knowledge about life-style and cardiovascular health, heart disease still accounts for 1 in 3 deaths in the United States every year, totaling approximately 788,000 lives lost (62). Of all heart diseases, coronary heart disease is the most common and costs the United States $108.9 billion annually for health care services, medications and lost productivity (www.cdc.gov/heartdisease). 635,000 Americans have their first heart attack every year and an additional 280,000 have a second or subsequent heart attack (62).

Genetics and sedentary lifestyle are key contributing risk factors for heart disease and cardiovascular emergencies, but air pollution and aerosolized particulate matter exposures are also key risk factors that are relatively under-recognized (167). According to the American Lung Association's State of Air Report in 2011, 20% of people in the United States (61 Million

Americans) live in areas where spikes in particulate air pollution occur at rates and concentrations capable of increasing the probability of heart attack, stroke and cardiovascular-related premature death. Several time-course-dependent cardiovascular endpoints have been identified from epidemiological, panel and controlled exposure studies. These include increased probability of enhanced arterial vasoconstriction/arterial tone, cardiac arrhythmia, thrombus formation and myocardial ischemia, all documented within 24 hours of exposure to air pollution (94). Many of the cardiovascular consequences of air pollution have been linked to the fine particulate fraction possessing aerodynamic diameters <2.5 μm, but the contributions of the ultrafine particulate fraction, those with aerodynamic diameters <0.1 μm, have been hard to distinguish from gaseous/vapor phase compounds in air pollution mixtures because of variation in their relative concentrations and chemical make-up (16; 64). Gender itself may also have an important role in the cardiovascular consequences of air pollution exposure. Specifically, premenopausal females have been shown to be more resistant than males to the cardiovascular detriments associated with air pollution constituents (71; 134) and less prone to cardiac I/R injury when compared to age-matched males (118; 172).

In general, toxicity to particulate has been expected to increase as particle size decreases on an equal mass basis. This assumption is based on the physical principle that smaller sized particles have increased particle numbers and surface areas per mass than larger sized particles of similar composition. The smaller size/mass particles should also have an increased probability of deep lung penetration, barrier permeability and interaction with subcellular components within physiological systems (74). Since particle size is expected to dictate lung penetration, a consideration of particle aspect ratio is also important because aspect ratio can impact the

aerodynamic properties of a particle apart from only the particle's mass. For example, a carbon nanotube is considered "nano" because of its nanoscale diameter but the micron scale length of a carbon nanotube may have an impact on its aerodynamic properties. In any case, if these expectations and assumptions about size/mass-related particle toxicity are true, then it is critical to better understand the role that ENP can have in cardiovascular toxicity.

2.2. Mechanisms of cardiovascular toxicity in response to nanoparticles

Mechanisms of cardiovascular toxicity resulting from inhalation of ambient particulates have been proposed (15; 166) and the mechanisms of extrapulmonary toxicity from NP inhalation have recently been reviewed (144). These proposed mechanisms of NP-induced cardiovascular toxicity include: (i) direct NP interaction with cells of the cardiovascular system after NP translocate from the lung; (ii) pulmonary tissue injury that generates an inflammatory/oxidative response that propagates throughout the systemic circulation, and (iii) interaction of NP with sensory nerve endings in the lung and subsequent dysregulation of autonomic cardiovascular reflexes (see Figure 2.1).

Various inhalation, instillation, and aspiration models of NP exposure in rodents have been shown to cause pulmonary inflammation, apoptosis, oxidative stress, fibrosis, damage to the pulmonary epithelial barrier, and eventually reductions in lung function (10; 32; 72; 100; 104; 171; 173; 174; 179). Following pulmonary exposure to NP, a fraction has been documented to translocate systemically (125; 157). After inhalation CeO_2 has been found in the testis, liver, spleen, kidney, brain, and epididymis as early as 6 hrs after a single exposure in rats (60). Intravenously administered iron oxide NP have been found within hepatic endothelial cells and Kupffer cells, but perhaps more importantly withincells within the renal proximal tubule (76).

This is important because even if NP thatreach the systemic circulation are filtered through the glomerulus, they may be reabsorbed in the renal proximal tubule rather than being cleared by the kidney. Extrapulmonary translocation has been shown to be related to NP size, charge, and surface modifications (61; 143) and could occur as a result of increases in pulmonary epithelial permeability, allowing NP to pass directly into alveolar capillaries or the lymphatic system (33). There has been a large concern for how NP surface chemistry can impact cellular interaction, but upon reaching a biological environment soluble proteins (or other biomolecules) may form a fluxing molecular corona around NP, ultimately altering biological/NP interactions (51). The flux of biomolecules that comprise the NP corona can be driven by electrochemical interactions, like van der Waals and electrostatic charges, causing evolution of the corona constituents as the NP moves through the circulation or different cellular environments (113). The translocation of NP may allow for direct interactions with circulating platelets, vascular endothelial cells, vascular smooth muscle cells and/or cardiac myocytes. These interactions may possibly initiate cardiovascular oxidative stress, inflammation, fibrosis, and prothrombosis, ultimately impairing cardiovascular function.

Figure 2.1 Potential mechanisms of nanoparticle-induced cardiovascular toxicity (105)

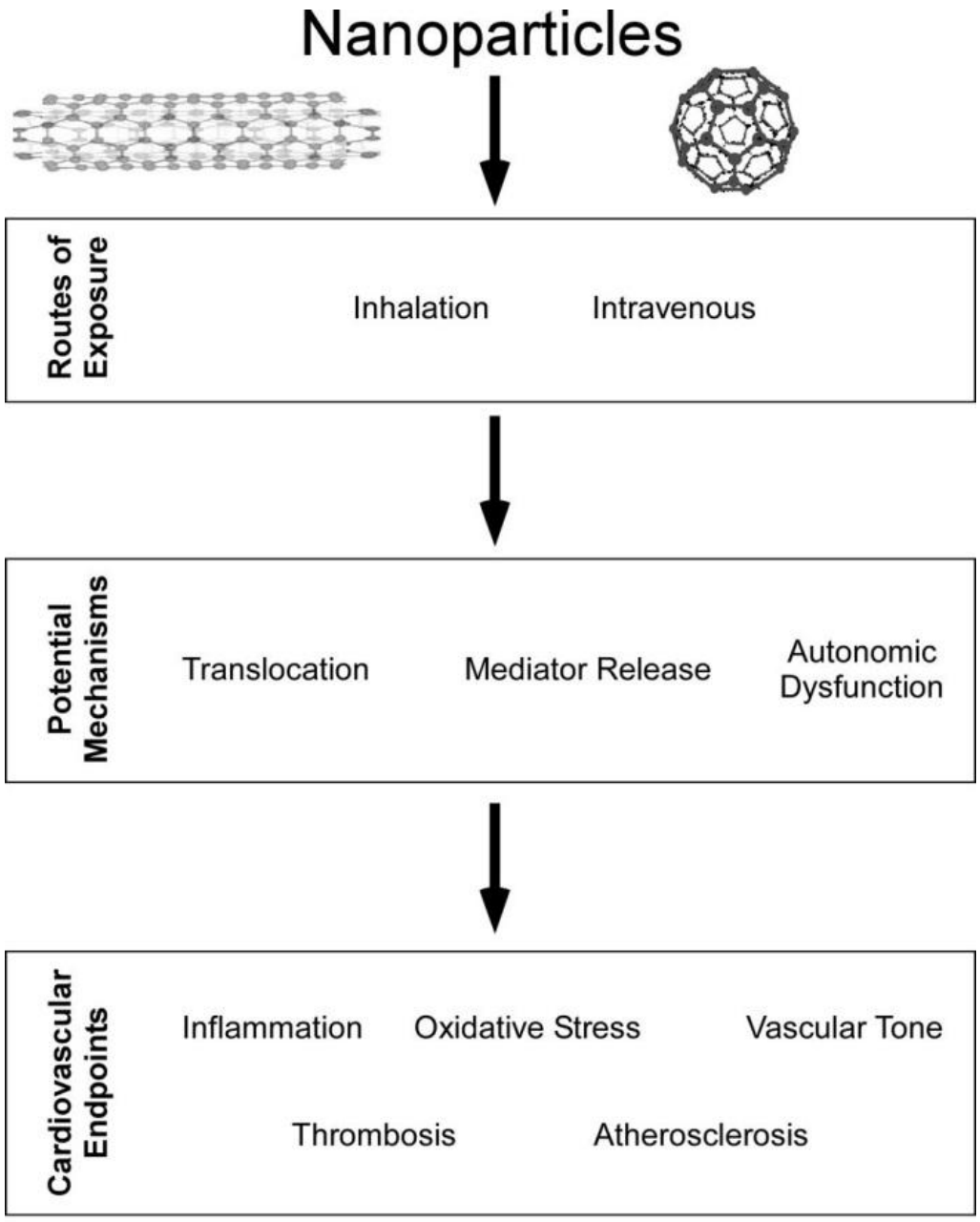

Modified from:
Mann EE, Thompson LC, Shannahan JH and Wingard CJ. Changes in cardiopulmonary function induced by nanoparticles. *Wiley Interdiscip Rev Nanomed Nanobiotechnol* 4: 691-702, 2012.

The release of various soluble factors into the circulation after NP exposure may also mediate cardiovascular toxicity. Intratracheal instillation of carbon black NP demonstrated increases in pulmonary and hepatic transcription of genes related to inflammation and acute phase response (13). After 4 weeks of carbon black NP inhalation, Sprague-Dawley rats were found to express increased pulmonary mRNA for the inflammatory cytokines interleukin-6 (IL-6) and monocyte chemotactic protein-1 (MCP-1), with elevated systolic blood pressure and circulating levels of the pro-inflammatory markers IL-6, MCP-1, and C-reactive protein (122). These inflammatory cytokines have been linked to cardiovascular disease processes and may increase both cardiac and vascular inflammation(14; 56; 181). Pulmonary exposure to NP could also result in autonomic dysregulation, which can also influence cardiovascular health effects. NP could modulate autonomic regulation through the stimulation of vagal sensory nerves within the lung via direct interactions with NP or via inducible pulmonary inflammation similar to other forms of inhaled particulate matter (63; 98; 119). This nerve stimulation could be exacerbated by NP compared to larger inhalable particles due to their potential to evade clearance mechanisms and possibly result in sustained level of pulmonary inflammation (42; 100). These findings support the possible link between pulmonary NP exposure and subsequent and detrimental cardiovascular endpoints.

2.3. The era of engineered nanoparticles: tools to study the cardiovascular system

Since their development, ENPuse in consumer goods, structural engineering components and electrothermal conductors has increased dramatically. Research in ENP has also increased dramatically over the last two decades, as indicated by the number of publications on the carbon-based NP, MWCNT and C60, in scientific journals (Figure 2.2). ENP have been proposed for use in biomedical applications as antimicrobials, antivirals, drug delivery devices and contrast imaging agents. While the unique physicochemical properties of ENP increase their applicability, they also raise concerns for potential adverse human exposure outcomes. Despite apprehensions, the broad application of ENP has increased human exposures in occupational settings (74). While dermal, oral/gastrointestinal, and inhalation exposures to NP are all relevant to the occupational setting, pulmonary exposures have been the principle route of NP administration in toxicological studies (124). These investigations have shown that despite minimal pulmonary outcomes, in many cases, the cardiovascular system may be a key site of NP-induced toxicity (29; 95).

Figure 2.2 Research on carbon nanotubes and fullerenes has increased

As the use of engineered nanoparticles expands across industry and medicine, research on these materials does as well. (A) PubMed search results show that research has increased steadily over the last decade, but research on multi-walled carbon nanotubes (MWCNT) and associated toxicity make up a much smaller fraction of the search results. (B) PubMed search results for fullerene shows a similar pattern but with 60-carbon fullerenes (C60) and associated toxicity make up a small fraction of the search results.

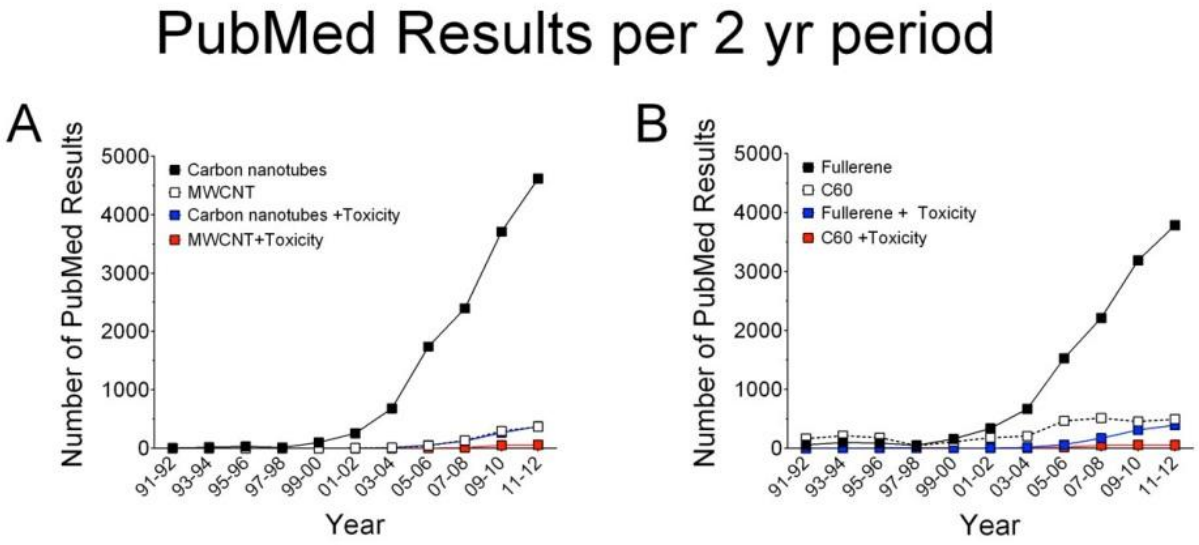

Elucidation of the cardiovascular derangements associated with pulmonary exposure to ENP has two potentially important benefits. First, mechanisms of toxicity based on physicochemical characteristics of ENP couldsupport development of new or modified ENP with reduced cardiovascular-related toxicity. Second, we may uncover mechanisms of cardiovascular toxicity in response to ENP that also underlie the elements of cardiovascular disease brought about by the exposure to NP fractions in air pollution. While the emergence of ENP represents a relatively new paradigm in pulmonary exposure and cardiovascular risks in the occupational setting, pulmonary exposure to naturally occurring NP is not a novel paradigm. Naturally occurring NP are produced in volcanic activity, forest/brush fires, weathering, formation from clay minerals, soil/rock erosion and dessert dust storms (149). Thus, it makes sense that physiological systems have likely evolved mechanisms by which to respond to nano-sized environmental stimuli, *i.e.* NP.

2.4. Engineered nanoparticles examined

Two forms of carbon-based ENP have been selected for study in this dissertation: MWCNT and C60. Both are comprised almost entirely of carbon, but despite having similar chemical make-up, these two ENP have very different aspect ratios, which allow determination of how physical structure may impact the experimental endpoints.

2.4.1. Multi-walled carbon nanotubes

MWCNT consist of multiple layers of graphite sheets rolled into concentrically arranged tubes (See Figure 2.3). They can span microns in length but are only nanometers in diameter. MWCNT have extraordinary physicochemical characteristics that make them promising components in commercial goods (112). Over the last two decades MWCNT have been incorporated into structural, electrical, and thermal engineering applications products. The durability and capacity for electrothermal conduction makes MWCNT attractive for use in compact electronic devices (85; 86; 174). Further, MWCNT are showing promise in many medical applications (133).

As MWCNT use increases there is a greater need to understand thepotential physiological responses or any adverse endpoints following occupational or accidental inhalation (59). For example, asbestos minerals presented many favorable physical properties that made them desirable for widespread use across industry, which was followed by the incorporation of asbestos into thousands of commercial products, and then unfortunately by the asbestos cancer epidemic (91; 92). The same "incorporate before understanding physiological consequences" paradigm was also true for perfluorooctanoic acid, a component of Teflon (155). Given that a complete assessment of biological responses to MWCNT exposure is lacking and the increasing probability of human interaction with MWCNT, there is concern that we may be repeating the "incorporate before understanding physiological consequences" history. Rodent models have shown that pulmonary exposure to MWCNT elicits persistent lung inflammation (133), pulmonary fibrosis (107), and loss of lung function (173). Cardiovascular endpoints following pulmonary exposure to MWCNT have also been investigated in a few cases and were found to

increase microvascular endothelial permeability via oxidative stress (129), diminish endothelial-dependent relaxation in coronary resistance arterioles (153), enhance serum lipid peroxidation (137), diminish serum antioxidant capacity (137), and translocate from the lungs to the heart (153).

Figure 2.3 The structure of a multi-walled carbon nanotube (120)

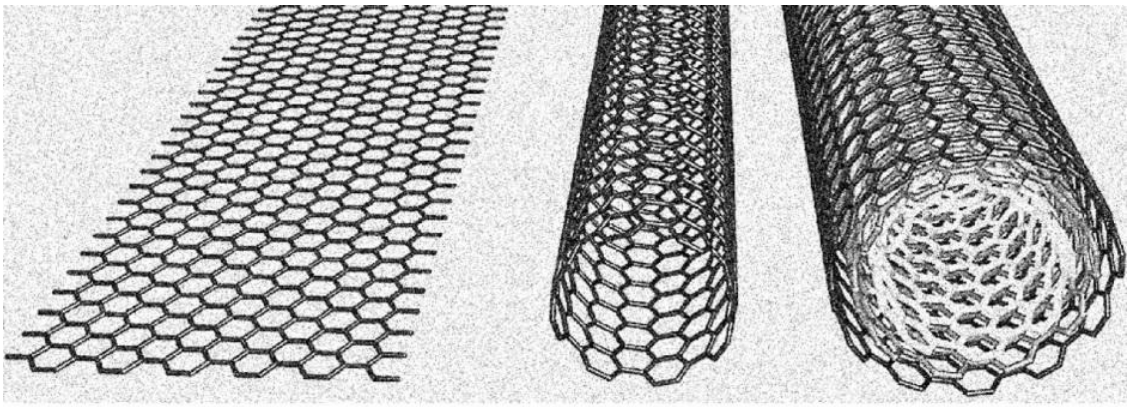

Modified from:
Nessim GD. Properties, synthesis, and growth mechanisms of carbon nanotubes with special focus on thermal chemical vapor deposition. *Nanoscale* 2: 1306-1323, 2010.

2.4.2. 60-carbon fullerene

C60 is a spherical carbon allotrope first generated synthetically in 1985 but has likely been produced naturally in Earth's environment for thousands of years, suggesting that human exposure to C60 is not necessarily a novel (See Figure 2.4) (6). Synthetic production of C60 on a commercial scale has increased the probability of human exposures occupationally and potentially even environmentally (90). The growing number of industrial and medical applications for C60 are not surprising due to its unique physicochemical properties (115). The medicinal uses for C60 spur from its capacity to function as an antiviral, photosensitizer, antioxidant, drug/gene delivery device and contrast agent in diagnostic imaging (7). C60 have been found in occupational environments at concentrations of 23,856 – 53,119 particles/L air (79). Given the potential for humans to encounter C60, assessments of *in vitro* cytotoxicity (22; 78), *in vivo* biodistribution (90; 156), biopersistence (146) and adverse pulmonary responses to C60 have been conducted (6; 114; 126; 145). Despite the effort put into developing a toxicological profile for C_{60}, the potential impacts of C_{60} on the cardiovascular system have rarely been examined.

Figure 2.4 Carbon organization of 60-carbon fullerene (151)

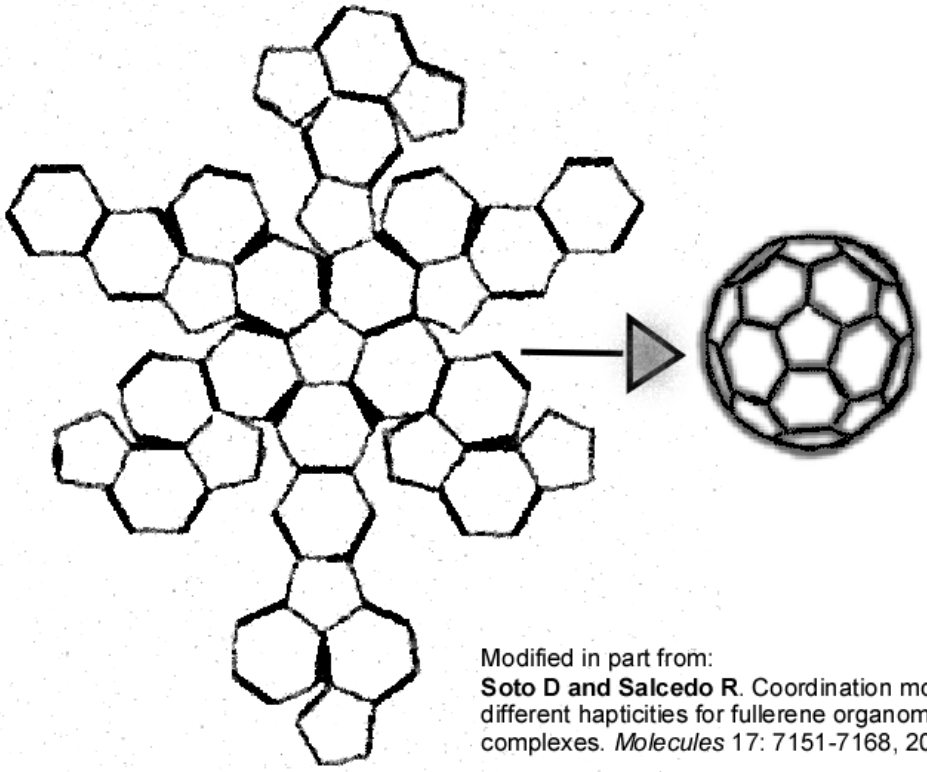

Modified in part from:
Soto D and Salcedo R. Coordination modes and different hapticities for fullerene organometallic complexes. *Molecules* 17: 7151-7168, 2012.

2.5. Pulmonary exposure models: intratracheal instillation vs. inhalation

Two exposure models can be utilized to achieve exposure across the pulmonary interface: (i) intratracheal instillation and (ii) inhalation models. Commentary on these models has been previously provided (154). As it is used in this dissertation project, MWCNT or C60 are dispersed in an aqueous medium and delivered via a bolus droplet into the opening of the trachea of an anesthetized animal. Upon inhalation the droplet is aerosolized and dispersed throughout the lung. Instillation allows for ENP exposure mass to be easily reproduced and delivery of a particle mass into the lungs without ENP deposition in the nasal/upper airways. Alternatively, the inhalation model is achieved by generating and incorporating ENP into an artificial atmosphere, allowing pulmonary deposition of ENP to occur during normal breathing while animals are unrestrained inside a whole body exposure chamber or restrained and exposed by a nose/head only device. The inhalation model is the gold standard for pulmonary exposure models but inhalation facilities are expensive to setup, run, and maintain (43). It is also difficult to determine exactly how much ENP exposure mass will be delivered into the lungs of each animal (177).

2.6. Cardiac endpoints following nanoparticle exposure

2.6.1. Cardiac ischemia and reperfusion injury

In a real world scenario, individuals who experience a coronary artery occlusion (*i.e.* heart attack) will suffer ischemic injury in the zone of the myocardium distal to the occlusion, here after referred to as the zone at risk (ZAR). During ischemia, loss of oxygen delivery to the myocardium stops mitochondrial oxidative phosphorylation in cardiac myocytes and subsequently loss of excitation contraction coupling (21). If the ischemic event is not addressed,

cells within the ZAR are likely to undergo necrosis or apoptosis due to oxygen and nutrient deprivation, resulting in myocardial infarction. In order to spare injury following a myocardial occlusion, catheterization of the occluded artery is performed and the ZAR is reperfused. Dependent upon the timing of intervention, myocardial reperfusion can limit the magnitude of infarction. However, reperfusion generates complex deleterious reactions in the ZAR, which are collectively referred to as reperfusion injury (21; 106). These reactions generated upon reperfusion include free radical production, Ca^{2+} loading and neutrophilia in the ZAR, which promote impaired cardiac function, arrhythmia and accelerated cell death in critically injured myocytes. Both myocardial ischemic injury and reperfusion injury are referred to collectively as cardiac ischemia/reperfusion (I/R) injury (See Figure 2.5).

Figure 2.5 Ischemic injury compared to reperfusion injury in the heart (106)

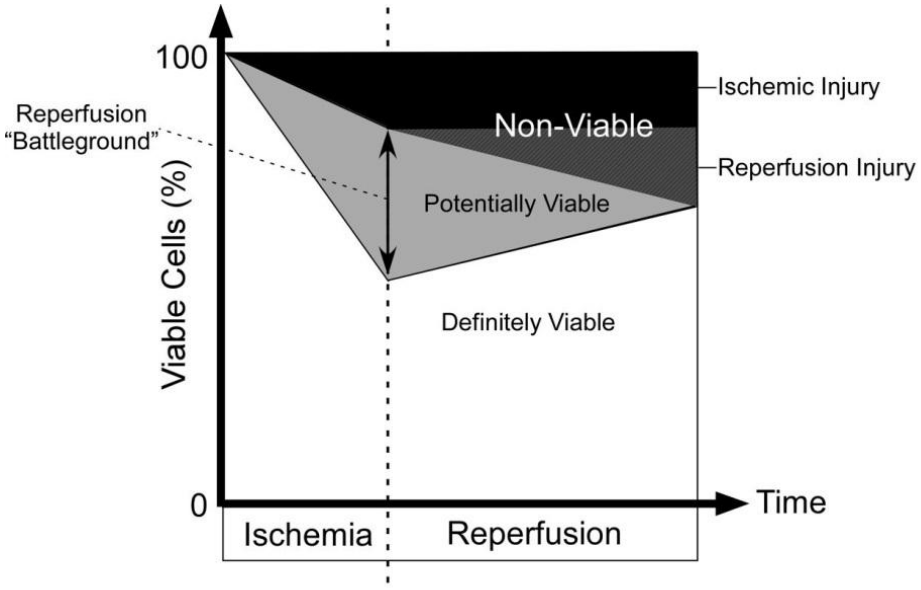

Modified from:
Maxwell SR and Lip GY. Reperfusion injury: a review of the pathophysiology, clinical manifestations and therapeutic options. *Int J Cardiol* 58: 95-117, 1997.

Cardiac I/R injury is complex. The extent of myocardial infarction following I/R can depend upon several properties associated with organ and system levels of physiology. One set of factors that contributes to, or results from, I/R injuryisintrinsic to the heart itself and includes electrical conductive properties of the heart, ventricular function, coronary resistance, and release of soluble factors that can impact heart function and coronary vascular resistance. A second set of factors that can play an important role in cardiac I/R injury response isthe extrinsic factors, or systemic factors originating outside of the heart in the intact animal. These include autonomic innervation/regulation of heart rate and contractility, and circulating endocrine and humoral factors. In this study, two models of cardiac I/R injury were used to delineate between the role of intrinsic and extrinsic factors associated with expansion of I/R injury following NP exposure.

2.6.2. Cardiac ischemia/reperfusion – the *in situ* model

One experimental model of cardiac I/R that accounts for the interplay of organ and system level factors is the *in situ* model. In this model a stably anesthetized animal is intubated, ventilated under positive pressure, and subjected to a thoracotomy. The left anterior descending coronary artery (LAD) is ligated for an ischemic period specified by the investigator and then the ligature is removed and the ZAR is allowed to reperfuse for a period of time (1; 87). Cardiac I/R *in situ* has been described in large mammalian models, like pigs and dogs, and small mammalian models, like rabbits, guinea pigs, rats, and mice (70). Large and small animal models exhibit differences in cardiac vulnerability to arrhythmia, especially lethal arrhythmia, with the incidence of I/R-induced arrhythmia being lower in hearts with smaller physical dimensions. This makes the rodent model of cardiac I/R an attractive choice to avoid unwanted animal losses that result from lethal arrhythmia when myocardial infarction is the desired endpoint. Our laboratory has established an *in situ* model of cardiac I/R induced infarction in mice as a relevant endpoint in the study of pulmonary exposure to UFP (36), MWCNT (82; 165), and cerium oxide NP (176).

2.6.3. Cardiac ischemia/reperfusion – the isolated Langendorff heart model

The isolated Langendorff heart model provides a method of testing I/R injury unique from the *in situ* model. In this model, the heart is isolated from the systemic vasculature, pulmonary system, and neurohumoral influences, allowing autoregulatory functions to be studied. The heart is quickly removed from the animal and the aorta is cannulated for retrograde perfusion (1). By delivering a heated and oxygenated physiological buffer in a retrograde fashion, the aortic valve is maintained in the closed position and the coronary ostia are perfused in a manner that can

sufficiently maintain the heart. The isolated heart model was first established using frog hearts in 1866 by Elias Cyon, which was later modified for the isolated perfused mammalian heart by Oscar Langendorff in 1895 (183). The perfusate in a Langendorff model can be delivered under constant flow with a peristaltic pump or under constant (hydrostatic) pressure using an elevated perfusate reservoir (147). Changes in vascular resistance (ΔR) can be indirectly measured in a Langendorff model by (i) measuring changes in perfusion pressure (ΔP) in the constant flow (Q) model and (ii) by changes in perfusion flow (ΔQ) in the constant pressure (P) model using the following equation:

$$\text{Constant Flow Model: } \Delta R = Q \bullet \Delta P$$

$$\text{Constant Pressure Model: } \Delta R = P/\Delta Q$$

The Langendorff apparatus can also be outfitted to measure volume conducted electrocardiogram (ECG) and left ventricular developed pressure (LVDP) by placing a pressurized balloon inside the left ventricle (1; 180). The ischemic episode can be conducted regionally by ligature of the LAD or globally by shutting off total perfusion to the isolated heart. Reperfusion is then allowed, either by removal of the ligature or continuation of global perfusion (1).

The isolated heart technique eliminates systemic factors during cardiac I/R, but it is important to identify the practical purposes, benefits, and limitations of using a simplified approach, so as not to over interpret the results. For example, myocardial infarction in response to *in situ* cardiac I/R may be exacerbated 24 hours following an acute pulmonary exposure to ENP. It is possible that during the 24 hour period following the pulmonary exposure prior to I/R, changes could have occurred in coronary arteries that promote impaired reperfusion. This parameter cannot be monitored easily in the *in situ* model of I/R. However, by using an isolated heart model, aberrant

reperfusion flow can be described and thus lead to more well informed hypotheses of cardiac I/R injury mechanisms.

2.6.4. Engineered nanoparticle exposure and the heart

Despite the absolute vitality of the heart in the cardiovascular system and the overwhelming prevalence of heart disease, only a few studies have examined changes in heart function or alterations in cardiac injury in response to I/R induced by ENP. One experiment showed that direct delivery of TiO_2, SiO_2, or Printex90 NP in the perfusate of an isolated Langendorff guinea pig heart model, the NP induced tachycardia, compensatory coronary flow, arrhythmia, ST elevation, and atrioventricular block (152). Pulmonary exposure to ENP can also alter I/R injury in a Langendorff heart model. Specifically, acid functionalized single-walled carbon nanotubes (SWCNT) were intratracheally instilled 24 hours prior to heart isolation and I/R (162). They conducted 20/120 minutes of I/R, respectively, and found decreased LVDP during reperfusion and expansion of post-I/R myocardial infarction. Work from our own group has demonstrated 20/120 minutes of cardiac I/R *in situ* expands myocardial infarction in mice 24 hours after intratracheal instillation of CeO_2 (176) or MWCNT (165).

One study examined the ability of ENP exposure to influence autonomic regulation of the heart and found that multiple intratracheal instillations of SWCNT in rats decreased heart rate and increased in baroreflex sequences (98). These findings suggested that baroreflex function might have been impaired due to a loss of arterial pressure sensitivity. Such derangements are prognostic for cardiac mortality, perhaps to a greater extent in individuals with ischemic cardiomyopathy and myocardial infarction (93).

2.7. Arterial endpoints following nanoparticle exposure

2.7.1 The vascular system

The vascular system is generally known for oxygen/nutrient delivery and waste removal from tissue. It also plays an important role in the homeostasis of mean arterial pressure, hemostasis, blood coagulation, immunity, inflammation, humoral propagation, fluid/ion balance, angiogenesis, and thermoregulation. The vascular system is arranged into conduit arteries, resistance arteries, arterioles, capillaries, venules and veins. In terms of cellular components, the vascular system is comprised of vascular endothelial cells, vascular smooth muscle cells, autonomic nerve endings, resident mast cells, macrophages, circulating neutrophils, monocytes, perivascular fat, connective tissues, and extracellular matrices. These components assert the complex mechanisms regulating physiological vascular function and can potentially be influenced by NP exposure through direct NP-cell interactions, autonomic dysfunction, and the release of paracrine and autocrinemediators.

Vascular endothelial cells (EC) make up the thin cellular monolayer that lines the entire vasculature. The human vasculature contains approximately 60 trillion EC, which execute many physiological functions that include influences on vascular reactivity, recruitment and adherence of leukocytes, innate and adaptive immune function, and modulation of vascular permeability (2). EC can influence vascular reactivity by first detecting local or systemic signals and then releasing endothelial derived relaxing or contracting factors that act in a paracrine fashion to elicit vascular smooth muscle-mediated changes in arterial diameter. Endothelial function is

often tested by evaluating acetylcholine (ACh)-mediated vasorelaxation, in contrast to a vasorelaxation response stimulated by a NO donor like sodium nitroprusside (SNP).

Nonstriated vascular smooth muscle cells (VSMC) make up the medial wall of arteries and arterioles. They contain the primary machinery by which arteries and arterioles modulate changes in vessel diameter. Under resting conditions the state of VSMC contraction is referred to vascular tone. Tonic contraction of VSMC maintains vessel shape and allows vessels to withstand blood pressure. Vascular tone can be contrasted with the term vascular reactivity, which describes the ability of a blood vessel to sense physical or chemical stimuli, and respond by dilating or constricting appropriately. This is necessary to maintain tissue homeostasis despite changes in the physiological environment. VSMC can sense chemical ligands released locally by autocrine/paracrine mechanisms or systemically by the endocrine and/or autonomic nervous system. VSMC can also develop myogenic responses to changes in transmural pressure (stretch) and changes in wall tension. VSMC contraction or relaxation is primarily driven by changes in intracellular Ca^{2+} concentration, but can also be regulated by changing the Ca^{2+} sensitivity of the VSMC contractile apparatus (73; 150). In contrast to skeletal muscle, VSMC contraction is a response of Ca^{2+} on myosin rather than a response of Ca^{2+} on actin (175). Similar to skeletal muscle a VSMC can undergo concentric and isometric contractions. However, unlike skeletal muscle, VSMC do not undergo eccentric contractions, but do show a nominal property of length-dependence in their contractile responses.

2.7.2. Physiological parameters regulated by arteries

From a fundamental functional standpoint, arteries, resistance arteries and arterioles are critical to match the supply of blood to the demand for blood in an organ or tissue. Change in metabolic demand within an organ/tissue initiates vasoactive signals to the arterial system and the arterial system itself modulates blood flow to an organ/tissue by changing vascular resistance through the regulation of arterial wall tension. For example during exercise, increased oxygen consumption in skeletal muscle increases global oxygen demand and results in increased heart rate and cardiac output. As heart rate increases, oxygen demand in the heart increases. This is met almost immediately by an increase in coronary blood flow. The increase in coronary blood flow is partly related to an increase in mean arterial pressure (driving force), but is due in large part to a decrease in vascular resistance to flow, i.e. vasodilation (46). Total vascular resistance is the sum of passive and active vascular resistance. Passive vascular resistance is that associated with structural components of an artery and active resistance is that associated with VSMC contraction.

Aside from increased metabolic demand, arteries, resistance arteries, and arterioles can autoregulate the maintenance of constant blood flow to an organ in the face of changing perfusion pressure. As transmural pressure (P_i) increases, arteries distend and then respond by vasoconstricting, decreasing lumen diameter ($2r$) and increasing vascular resistance to flow. The opposite also occurs. As P_i decreases, arteries deflate and respond by vasodilating, increasing lumen diameter and decreasing vascular resistance to flow. The Law of Laplace asserts that these phenomena, termed myogenic responses, act to regulate wall tension:

$$\text{Law of Laplace: } \textit{Wall tension} = P_i \bullet r$$

Schubert and Mulvany have reviewed myogenic responses and provide commentary on several mechanisms that may regulate myogenic responses (141). Schubert described the potential mechanisms that possibly initiate the myogenic response as interplay between VSMC membrane depolarization, increase in intracellular Ca^{2+} concentration, and activation of intracellular second messenger systems.

2.7.3. Isolated artery techniques

This dissertation project utilizes wire myography of LAD segments isolated from rats in order to assess changes in coronary artery VSMC force generating capacity after pulmonary exposures to ENP. Wire myography of arterial segments was first developed and reported in *Nature* in 1976 by Michael Mulvany and William Halpern (117). In this technique, as used in this dissertation, LAD segments 0.5 – 2 mm in length were resected from the surrounding cardiac tissue and two 40 μm diameter stainless steel wires were passed through the lumen. The LAD segments were then mounted into a chamber from a DMT 610M myograph chamber (DMT, Inc., Ann Arbor MI, USA) by attaching one wire to an adjustable micrometer and the second was attached to a force transducer. The technique was developed to assess isometric force development in VSMC at an arterial wall tension and internal circumference selected by the investigator (117). The experiments conducted by Mulvany and Halpern demonstrated that (i) the VSMC within an arterial preparation were oriented to contract across the diameter of the artery examined, within the vector of the force transducer and (ii) the length of any selected individual VSMC within an arterial preparation always occupied a fixed proportion of the internal circumference of that artery. Mulvany and Halpern interpreted these findings to mean that active force data collected

from arteries on a wire myograph represented the force generating capacities of the individual VSMC *in situ*.

The wire myography technique can be contrasted against another experimental isolated artery technique called pressure myography. Even though pressure myography is not utilized in this dissertation, due to its importance in the study of vascular physiology, a brief review of pressure myography is provided. Isolated perfused and pressurized small arteries (50 - 250 µm in diameter) was, perhaps, first described by Uchida *et al*. and published in *Circulation Research* in 1967 (164). The pressure myography technique for small arteries (5 - 100 µm in diameter), as it is used today, was described by Duling *et al*. and published in *American Journal of Physiology, Heart and Circulatory Physiology* in 1981 (45). In short, small resistance artery segments are resected from the vascular bed of interest and cannulated on both ends so that intramural pressure can be controlled by the investigator, and changes in diameter are monitored microscopically (116). Pressure myography is an important tool in the field of vascular physiology because it allows the artery being examined to regulate arterial wall tension. The primary endpoint for isolated arteries on a pressure myograph is visual assessment of change in diameter.

Aside from the endpoints measured, the physical conditions utilized to functionally assess VSMC are different between wire myography and pressure myography. A wire myograph measures the change in smooth muscle force ($\Delta F_{total} = \Delta F_{passive} + \Delta F_{active}$) under isometric conditions to derive $\Delta F/mm$ (*i.e.* tension). A pressure myograph measures change in distance (ΔD) per constant internal pressure (*i.e.* opposing force) to derive $\Delta D/mmHg$. Alternatively, the

pressure myograph can be used to mimic isometric contractions by increasing the internal pressure during a contraction in order to maintain the initial lumen diameter. Therefore, internal pressure utilized to distend an arterial segment on a pressure myograph can be considered synonymous with the passive force required to passively stretch an arterial segment on a wire myograph. That being considered, one key similarity between the two techniques is the relationship between Δinternal pressure and Δpassive internal diameter based on the Law of Laplace (23). In other words the change in passive pressure required to displace passive diameter is similar in both preparations. This highlights an important difference between the wire myograph and the pressure myograph technique. That difference is the difference in the shape and slope of active tension curves generated when length-tension relationships have been established. The active tension curve of an arterial length-tension relationship established by wire myography has a broader base, steeper ascending slope and a broader peak in relation to the optimal arterial diameter (182) than the active tension curve established using a pressure myograph, which has a narrower base, flatter ascending slope and narrower peak (35; 38). Thesedifferences are depicted in Figure 2.6, though it should be noted that the data presented are derived from two different vascular beds, from two different species, and were primarily of two different diameters (38; 182). The differences in species, vascular bed and artery diameter are likely of minimal concern since Davis reported that active tension curves were similar in shape across 4 different orders of arterial branches from hamster cheek pouch arteries using pressure myography (38) and Cox has reported the same shape of active tension curves from 3 different canine hind limb arterial beds, of 3 different sizes (35).

Given that active tension (T_A) curves are derived by subtracting passive tension (T_P) from total tension (T_T) it may seem logical to assume that the passive tension curve may be responsible for the difference in derived active tension.

$$T_A = T_T - T_P$$

It is important to note that because the relative thickness of the medial wall increases as artery size decreases, the relative amount of connective tissue in an artery is proportional to the relative wall thickness of the artery (12). This is important because the connective tissue is responsible for passive element of VSMC length-tension curves (175). However, as stated previously, passive tension curves have been reported to be nearly identical between arteries assessed via wire myography and arteries assessed via pressure myography (23). Thus, the difference in the active properties of VSMC can be impacted by the *in vitro* conditions used to assess their mechanical function. In that regard, caution should be used when interpreting data derived from active stress generation in arterial preparations via wire myography.

Figure 2.6 Arterial active length-tension shape depends on technique(38; 182)

Length tension-relationship in small arteries can be assessed via (A) wire myography and (B) pressure myography. The closed squares indicate total/activated response and open squares indicate the passive/inactivated response. The dashed line indicates the active tension response derived by subtracting passive/inactivated response from the total/activated response, which reveals a fundamental difference in the shape and slope to the active tension curve between the two techniques.

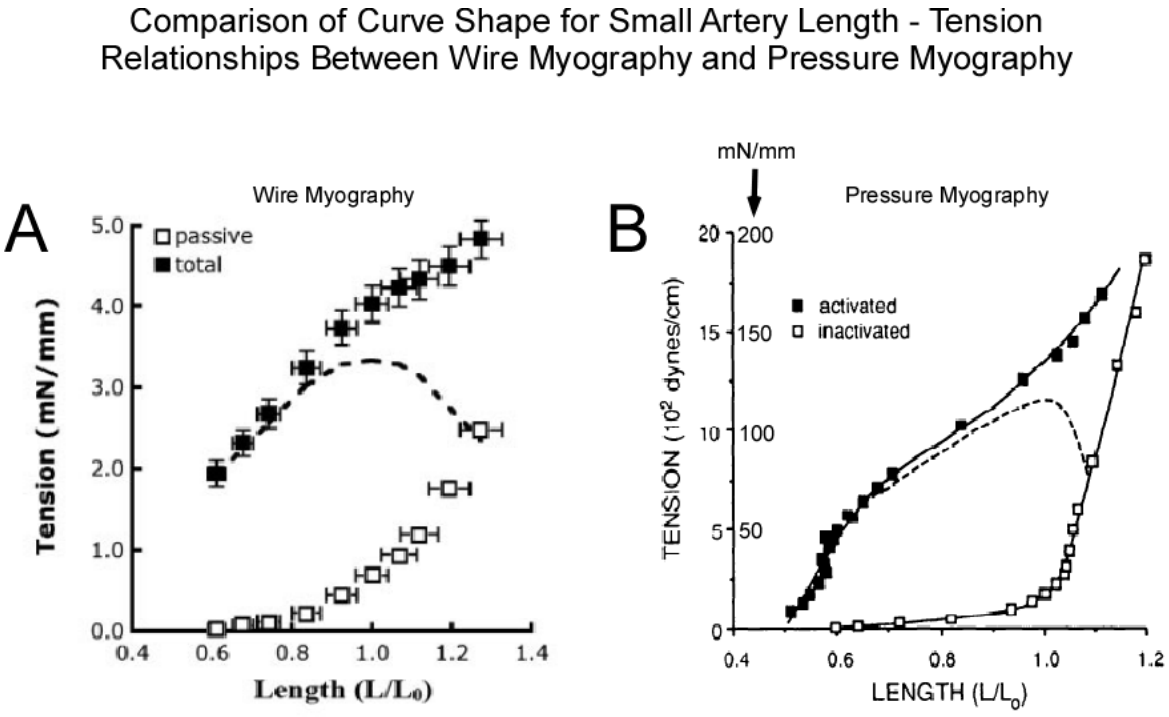

(A) From:
Zhang RZ, Gashev AA, Zawieja DC and Davis MJ. Length-tension relationships of small arteries, veins, and lymphatics from the rat mesenteric microcirculation. *Am J Physiol Heart Circ Physiol* 292: H1943-H1952, 2007.

(B) Modified from:
Davis MJ and Gore RW. Length-tension relationship of vascular smooth muscle in single arterioles. *Am J Physiol* 256: H630-H640, 1989.

Another difference between the techniques is that pharmacological assessment of arteries on a pressure myograph yield lower threshold values and EC_{50} values than pharmacological assessment of arteries on a wire myograph. Arteries pharmacologically assessed on a wire myograph have steeper Hillslope values than arteries pharmacologically assessed on a pressure myograph (23). This highlights another area in which care should be used in the interpretation of pharmacological data generated from arterial preparations on a wire myograph.

Despite the apparent strengths of the pressure myograph approach in vascular physiology, including the use of much more physiologically relevant conditions, it does have a few limitations for examination of VSMC force generating capacity. Maximal VSMC activation can be problematic due to complete closure of the arterial lumen which is difficult to reverse (38; 182). Also, due to VSMC shortening, deactivation of the contractile apparatus can occur and cause underestimation of maximal stress generating capacity (38; 182). Therefore, wire myography is an ideal technique for mechanical arterial studies assessing VSMC stress generating capacity under isometric conditions. However, VSMC contraction/relaxation response profiles obtained under isometric conditions could be due to mechanisms that have less important roles *in vivo*, and careful interpretation of data generated via wire myography is critical (23).

2.7.4. Nanoparticle exposure and arteries

Reviews on mechanisms of NP-induced toxicities have described the ability of NP to induce inflammation which can disrupt vascular function (74; 144). Given that the walls of conduit arteries contain microvessel networks that can intensely regulate vascular inflammation (135), assessment of conduit artery function may be important following NP exposure. We have reported that aortic vascular smooth muscle contraction in response to adenosine was altered 24 hrs following pulmonary instillation of 10 µg and 30 µg of CeO_2 in mice (176). Diminished endothelial-dependent smooth muscle relaxation responses to ACh in isolated aortic segments has also been documented after carbon black NP instillation in mice, in the absence of altered SNP responsiveness (168). Pulmonary exposure to NP may also disrupt smaller conduit artery function. Wire myography analysis of carotid artery segments isolated from mice previously exposed to varying concentrations of $Ni(OH)_2$ nanoparticles (NH-NP) via whole body inhalation chambers for 1, 3, or 5 days (5 hrs/day) showed impaired PE and ACh vasomotor responses in both a NP dose- and time-dependent fashion (37).

Arterioles provide the largest resistance to blood flow in the vasculature and regulate tissue specific flow, thus the response of arterioles to NP exposure is an important area of research. Inhalation-mediated lung deposition of 10 µg of TiO_2 in rats was found to be capable of generating endothelial dysfunction in subepicardial arterioles and increasing heart weight potentially through increased vascular permeability (95). They also suggest inhalation of TiO_2 disrupted microvascular NO bioavailability, and increased oxidative and nitrosative stress in arteriolar walls of the systemic vasculature (123). In other reported studies, endothelium-dependent dilation responses to ACh and the Ca^{2+} ionophore A23187 were both found to be

impaired via pressure myography of coronary and mesenteric arterioles isolated from rats previously exposed to inhalation of MWCNT (153) or intratracheal instillation CeO_2 (111).

While many effects of NP exposure have been associated with endothelium-dependent mechanisms, arteriolar function may also be disrupted following NP exposure via endothelium-independent mechanisms. In one case arterioles of the spinotrapezious muscle were examined by intravital microscopy following TiO_2 NP inhalation in rats (88). In this study arterioles demonstrated heightened sensitivity to α-adrenergic blockade during perivascular nerve stimulation and blunted arteriolar dilation in response to active hyperemia. The dampened active hyperemia-mediated dilation was not exacerbated by the use of a NO synthase inhibitor, suggesting a loss of NO bioavailability. However, COX inhibition did further impair active hyperemia-induced vasodilation, suggesting that arterioles from the TiO_2 exposed animals had compensated for the reduced NO bioavailability by a COX-mediated mechanism. In a different study that examined CeO_2 instillation, endothelium-independent vasodilation responses to SNP and spermine NONOate were also found to be impaired in coronary arterioles on a pressure myograph (111).

2.8. Key pathways and cardiac/vascular ligands examined

2.8.1. Endothelin-1

ET-1 is a dynamic autocrine/paracrine signaling agent involved in the maintenance of many physiological functions and is one of the most potent endogenous vasoconstrictor currently identified (121). ET-1 is a 21 amino acid peptide released from many cell types, including EC, VSMC and cardiac myocytes (84). ET-1 interacts with two receptor subtypes, endothelin $_A$ receptors (ETAR) and endothelin $_B$ receptors (ETBR). VSMC express both ETAR and ETBR receptors, which are G protein-coupled receptors coupled to Gαq. Activation of ETAR or ETBR on VSMC triggers the liberation of inositol triphosphate and diacylglycerol from the cell membrane, causing an increase in intracellular Ca^{2+} concentration and subsequent vasoconstriction. Vascular EC express ETBR receptors that promote vasodilation through the release of NO (131). In the coronary circulation low concentrations of ET-1 promote vasodilation and enhanced coronary flow but at higher concentrations ET-1 produces strong vasoconstriction and reduction of coronary flow (121). ET-1 is arrhythmogenic in cardiac tissue (47) and is also released from the isolated hearts during I/R (19). Given that ET-1 mechanisms have been linked to particulate matter exposure and cardiac ischemic injury (80), perhaps ET-1 is an important target following pulmonary exposure to ENP.

2.8.2. Thromboxane and the cyclooxygenase pathway

TXA2 is an eicosanoid produced by the cyclooxygenase (COX) pathway that is involved in vasoconstriction and platelet aggregation (53). In cells, COX converts free arachidonic acid into prostaglandin H2 which is then converted into TXA2 by TXA2 synthetase (TXS)(52). VSMC contraction occurs when TXA2 activates TXA2 receptor (TP), which is a G protein-coupled

receptor that acts through release of inositol triphosphate and diacylglycerol to promote intracellular Ca^{2+} release. Activation of TP on vascular endothelial cells can stimulate a Rho-kinase-dependent depression of NO release (101), which can potentiate vasoconstriction. Such a loss in NO bioavailability may feed-forward to exacerbate TXA2-mediated vasoconstriction by enhancing TXA2 release (52), given that NO-mediated inhibition of TXS has been documented (170). TXA2 is an ideal autocrine/paracrine agent because it has a ~30 second half-life and is rapidly hydrolyzed to the inactive thromboxane B2 (TXB_2) form (97), thus it must act locally. TXA2 is heavily involved in platelet activation, thrombus formation and vasoconstriction and has been identified as an important marker of acute coronary syndromes, like unstable angina and myocardial infarction (54). TXA2 has further been linked to cardiac ischemic injury and arrhythmia (34). Given that MWCNT have been shown to activate platelets via increased TXA2 release (65), perhaps TXA2 may contribute to cardiovascular consequences following ENP exposure in general.

2.9. Conclusion of literature review

The recognition that particulate matter exposure is animportantrisk factor for heart disease has generated concern that occupational exposure to ENP may also have cardiovascular consequences. If the expectation that particle toxicity increases as particle size decreases on an equal mass basis is true, then it is important to improve our understanding of how pulmonary exposure to ENP may contribute to cardiovascular derangements. Since naturally occurring NP have always been present in the environment, mammals have likely evolved physiological mechanisms to respond to such stimuli. This dissertation project proposed to (i) investigate mechanisms responsible for cardiovascular detriments associated with pulmonary exposure to ENP and (ii) identify key cardiovascular endpoints that can potentially be used to screen ENP for cardiotoxic responses in order to protect individuals in the occupational setting. Specifically MWCNT have been shown to increase cardiac I/R injury 24 hours following exposure (165), similar to previous studies of ultrafine particulate matter (36). However, the question remains, how does ENP exposure lead to expansion of myocardial infarction followingI/R? Many investigations have utilized a lungs-forward approach to uncovering the mechanisms of cardiovascular toxicity in response to pulmonary NP exposure. Here we propose to work back from the heart following pulmonary exposure to ENP in order to better understand any derangements inherent to the heart itself, or the coronary vasculature. After doing so we believe we can more clearly hypothesize the mechanisms that caused the derangements. Of the many proposed mechanisms potentially responsible for cardiovascular derangements following pulmonary exposure to NP, ET-1 and TXA2 could contribute to cardiac arrhythmia and enhanced coronary artery contraction, ultimately exacerbating cardiac I/R injury.

CHAPTER 3

INTRATRACHEAL INSTILLATION OF MULTI-WALLED CARBON NANOTUBES EXACERBATES CARDIAC ISCHEMIA/REPERFUSION INJURY AND DEPRESSES CORONARY REPERFUSION FLOW

Acknowledgement

Elements of this chapter have been adapted from the following citation (159):

Thompson LC, Frasier CR, Sloan RC, Mann EE, Harrison BS, Brown JM, Brown DA and Wingard CJ. Pulmonary instillation of multi-walled carbon nanotubes promotes coronary vasoconstriction and exacerbates injury in isolated hearts. *Nanotoxicology*(November 23, 2012); doi:10.3109/17435390.2012.744858.

3.1. Introduction

Over the last two decades, structural, electrical, and thermal engineering has been enhanced with the development of MWCNT. These materials are layers of graphite sheets rolled into concentrically arranged tubes that span microns in length but only nanometers in diameter (128). MWCNT have extraordinary physicochemical properties and versatility that have made them promising materials to improve many modern goods (112). Their durability and capacity for electrothermal conduction makes them attractive for use in compact electronic devices (85; 86; 174), and MWCNT are showing promise in many medical applications (133). With the increasing use of MWCNT comes a greater need to understand the potential consequences of occupational inhalation and the resulting physiological responses (59). In rodent models,

pulmonary responses to MWCNT include persistent lung inflammation (133), pulmonary fibrosis (107), and loss of lung function (173). Cardiovascular endpoints are far less studied following pulmonary exposure to MWCNT, but a few studies have demonstrated that MWCNT exposure canresult in translocation from the lung to the heart (153), increase microvascular endothelial permeability via oxidative stress (129), enhance serum lipid peroxidation (137), and diminish serum antioxidant capacity (137). It is reasonable to closely examine cardiovascular endpoints following MWCNT exposure because deleterious cardiovascular consequences have been shown to result from pulmonary exposure to other nanomaterials and particulates. Those consequences have been linked to oxidative stress (28; 36; 95), systemic inflammation (176), and/or altered endothelin signaling (30; 31).

The isolated Langendorff heart model has been used to examine cardiovascular endpoints following nanoparticle exposure (152) and has also been used to assess changes in cardiac electrophysiology and ischemia/reperfusion (I/R) injury, in responses to various chemical compounds and pathological conditions (9; 147). ET-1 is a key autocrine/paracrine mediator during myocardial I/R due to its arrhythmogenic properties (47) and its vasoconstrictive effect, which impairs reperfusion flow (131). ET-1 is released during reperfusion in hearts subjected to I/R injury (19) and both endogenous and exogenous ET-1 has been shown to contribute to infarct expansion during cardiac I/R (127). Thromboxane (TXA2) is another autocrine/paracrine agent thathas been linked to cardiac ischemic injury and arrhythmia (34). TXA2 is heavily involved in platelet activation, thrombus formation and vasoconstriction and has been identified as an important marker of acute coronary syndromes, like unstable angina and myocardial infarction (54). MWCNT have also been shown to directly activate platelets via increased TXA2 release

(65). Collectively, perhaps ET-1 and TXA2 are important ligands to study following pulmonary exposure to MWCNT and myocardial infarction.

The impacts of MWCNT exposure *in vivo* on isolated heart function and I/R injury have not been investigated. The purpose of this study was to investigate baseline isolated heart function and cardiac I/R injury 24 hours after pulmonary exposure to MWCNT*in vivo*. Specifically, we tested the hypothesis that intratracheal instillation of MWCNT would enhance the release of ET-1 and TXA2 during reperfusion and impair coronary reperfusion flow and result in the expansion of myocardial infarction following I/R.

3.2. Materials and Methods

3.2.1. Multi-walled carbon nanotubes and vehicle

Vehicle instillate (10% surfactant/saline): Solution by volume is 90% sterile saline (0.9 % NaCl) and 10% pulmonary surfactant (Infasurf™, a gift from ONY, Inc., Amherst, NY). Infasurf™ contains: (per mL of 0.9% NaCl solution) 35 mg total bovine phospholipids, of which 16 mg are disaturated phosphatidylcholine, and 0.7 mg bovine proteins, of which 0.44 mg are hydrophobic surfactant-associated protein C and 0.26 mg are hydrophobic surfactant-associated protein B (http://www.infasurf.com/about-infasurf/#composition).

MWCNT instillate: MWCNT were provided by NanoTechLabs, Inc. (Yadkinville, NC, USA). For 100 µg dosing suspensions, MWCNT were added to the vehicle instillate to a concentration of 0.5 mg/mL. For 10 µg and 1 µg dosing solutions, 1:10 serial dilutions were performed with vehicle instillate. Immediately prior to instillation MWCNT suspensions were sonicated in a cup-horn sonicator (Qsonica, LLC - Newton, CT, USA) for 2 minutes at 65% amplitude to reach and approximate energy output of 10,800 J.

3.2.2. Hydrodynamic size and zeta potential

The MWCNT and suspensions used in this study were characterized previously (173). MWCNT were analyzed in 10%SS suspensions for hydrodynamic size by dynamic light scattering using a Nanosizer S90 (Malvern Instruments, Worcestershire, UK) and zeta potential was determined using a Zeta ZS (Malvern Instruments).

3.2.3. Particle number assessment

MWCNT particle numbers were analyzed in solution by counting events in 10 µl of sample using a BD Accuri C6 flow cytometer (BD, San Jose CA, USA). Briefly samples were prepared as described above. Each sample was run through the flow cytometer to collect a total of 10 µl and analyzed for total events using BD Accuri C6 software with background events subtracted. Samples were analyzed on 3-4 separate runs with a cleaning cycle run between each sample measurement. Each measurement was multiplied by 20 to obtain the particle number delivered to each rat (10 µL x 20 = 200 µL). The mean of the triplicate measurement is reported.

3.2.4. Animals

Male Sprague-Dawley rats were purchased from Charles River (Morrisville, NC, USA). Rats were 10-12 weeks of age at the time of purchase and housed in the Department of Comparative Medicine at East Carolina University. Each rat had access to standard laboratory chow and water *ad libitum* in a temperature regulated facility (23 ± 1°C) under 12:12 hour light-dark cycles. We provided each rat with a minimum of 5 days to acclimate prior to experimental manipulations. All use of rats in this study complied with protocols approved by the East Carolina University Institutional Animal Care and Use Committee.

3.2.5. Instillations

One day prior to sacrifice, rats were anesthetized with Isoflurane. A bolus of 1, 10, or 100 µg of MWCNT suspended in 200 µl of vehicle, or vehicle only (200 µl) was delivered into the opening of the trachea using a micro-pipette. Rats were monitored until normal grooming habits resumed.

3.2.6. Cardiac ischemia/reperfusion protocol

One day following MWCNT or vehicle instillations, rats were anesthetized with an intraperitoneal injection of ketamine/xylazine (85/15 mg/kg, respectively). After reflexes subsided, hearts were excised and mounted onto a modified Langendorff apparatus utilizing aortic retrograde perfusion under constant pressure (75 mmHg), without electrical pacing, as previously described (57). Perfusion buffer contained (mM) 118 NaCl, 24 $NaHCO_3$, 1.2 KH_2PO_4, 4.75 KCl, 1.2 $MgSO_4$, 2.0 $CaCl_2$, and 10 glucose (equilibrated with 95/5 % O_2/CO_2), heated to 37°C, as previously described (17; 57). After 5 minutes of stable parameter recordings established a baseline, hearts were challenged with 20 minutes of global ischemia and then reperfused for 120 minutes. Reported data for ECG, left ventricular developed pressure (LVDP) and coronary flow rate were recorded throughout the each experiment using a PowerLab interface (ADInstruments, Inc., Colorado Springs, CO) and LabChart software (ADInstruments, Inc.). Premature ventricular contractions (PVC) were counted during the stable baseline period.Cardiac arrhythmia was scored during the 2 hour reperfusion period as previously described (57). Coronary flow rate was digitally monitored in real time using a flow probe (Transonic Systems, Ithaca, NY) connected in series with the perfusion cannula. Raw flow rates were normalized to the wet weight of the corresponding heart. The wet weight of each heart was obtained immediately after the end of the perfusion protocol. Though wet:dry weight ratios were

not collected in this study, there is no evidence of marked edema formation in our model, with wet:dry ratios normally ranging between 75-78%. Afterwards hearts were serially sectioned and incubated in a 1% triphenyltetrazolium chloride/0.9% NaCl solution for the determination of infarct size, as described previously (17; 148).

3.2.7. Endothelin-1 and thromboxane in the coronary effluent

During I/R experiments the vena cava were occluded and coronary effluent was collected by cannulating the pulmonary artery. Effluent samples (4-5 mL) were collected from the vehicle and 100 µg MWCNT groups at baseline, at the onset of reperfusion (0 min), at 5 min, and at 10 min into reperfusion (samples collected for approximately 30-50 sec at each time-point). Effluent samples were snap-frozen in liquid nitrogen and stored at -80°C until analysis. An ET-1 enzyme immunoassay plate (ADI-900-020A, Enzo Life Sciences, Farmingdale, NY) was used to determine ET-1 levels in the coronary effluent samples, per the manufacturer's instructions. Optical densities were determined with a plate reader (Synergy HT, BioTek Instruments, Winooski, VT) using Gen5 software. The assay detection limit for conversion to ET-1 concentration occurred at optical densities of 0.098, corresponding to 0.1 pg/ml. Optical densities <0.098 were taken as 0 pg/ml. ET-1 concentrations were then normalized per gram of the corresponding wet heart weight (pg/mL/g of tissue). Since TXA2 is rapidly hydrolyzed to TXB2, a TXB2 ELISA (ADI-900-002, Enzo Life Sciences) was used to quantifyTXA2 release from isolated hearts into the coronary effluents. TXB2 concentrations were normalized per gram of the corresponding wet heart weight (pg/mL/g of tissue).

3.2.8. Statistics

All data are reported as mean ± SEM. Graphpad Prism software (version 5, LaJolla, CA) was used to conduct statistical analyses. A Student's t-test was performed to determine statistical significance against vehicle data for premature ventricular contractions, ending left ventricular pressure, infarct size, coronary flow, and ET-1 concentration in coronary effluent during reperfusion.

3.3. Results

3.3.1. Multi-walled carbon nanotube physical characteristics

The MWCNT suspension characteristics are reported in Table 3.1. Hydrodynamic sizes were found in a bimodal distribution. The major peak occurred at particle sizes of 200 nm and a smaller peak occurred at particle sizes of approximately 1000 nm. The zeta potential of the MWCNT suspension was determined to be -44.6 mV indicating that the MWCNT were stably dispersed in the 10% surfactant/saline. Flowcytometry analysis of10 μL of 0.5 mg/mL MWCNT suspension showed a particle count of 37,147 ± 625 particles. The surface area was approximated to be 655 μm^2 per 10 μL of 0.5 mg/mL MWCNT suspension based on the MWCNT characterization in a previous study (173).

Table 3.1 Multi-walled carbon nanotube particle characterization

Physical characterization of MWCNT suspensions (mean ± SEM)	
Hydrodynamic size, nm	200 ± 50, 1000 ± 150
Zeta potential	-44.6 mV
0.5 mg/mL suspension particle number (per per 10 μL)	37,147 ± 625
Calculated surface area of 0.5 mg/mL suspension (per 10 μL)	23.4 mm^2

3.3.2. Baseline recordings from isolated hearts

Baseline measurements for ECG, PVC, coronary flow, ET-1 concentration, and TXB2 concentration are shown in Figure 3.1. These data indicate that MWCNT exposure increased aberrant ECG tracing as depicted by representative ECG tracings taken from the 5 minute baseline periods (Figure 3.1A). The mean total number of premature ventricular contractions counted during baseline recordings was also elevated significantly in the 10 μg and 100 μg MWCNT groups compared to the vehicle and 1 μg MWCNT groups (Figure 3.1B). The mean minute coronary flow rate (Figure 3.1C) and mean total coronary flow (Figure 3.1D) were not significantly different between groups during baseline recordings. ET-1 concentrations measured in coronary effluents collected at baseline were below detectable limits in the 100 μg and vehicle groups (Figure 3.1E). TXB2 concentrations in coronary effluents collected at baseline were slightly elevated ($P = 0.06$) in the 100 μg MWCNT group compared to the vehicle group (Figure 3.1F).

Figure 3.1 Increased premature ventricular contractions at baseline in isolated hearts

MWCNT exposure increased aberrant ECG and PVC in isolated rat hearts at baseline. (A) Representative ECG tracings taken from baseline. (B) Number of premature ventricular contractions counted during baseline. (C) Minute coronary flow rate for each group during baseline recordings. (D) Total coronary flow during baseline recording. (E) ET-1 concentrations measured in coronary effluents collected at baseline (below detectable limits). (F) TXB2 concentrations measured in coronary effluents collected at baseline. Data are mean ± SEM. *$P < 0.05$.

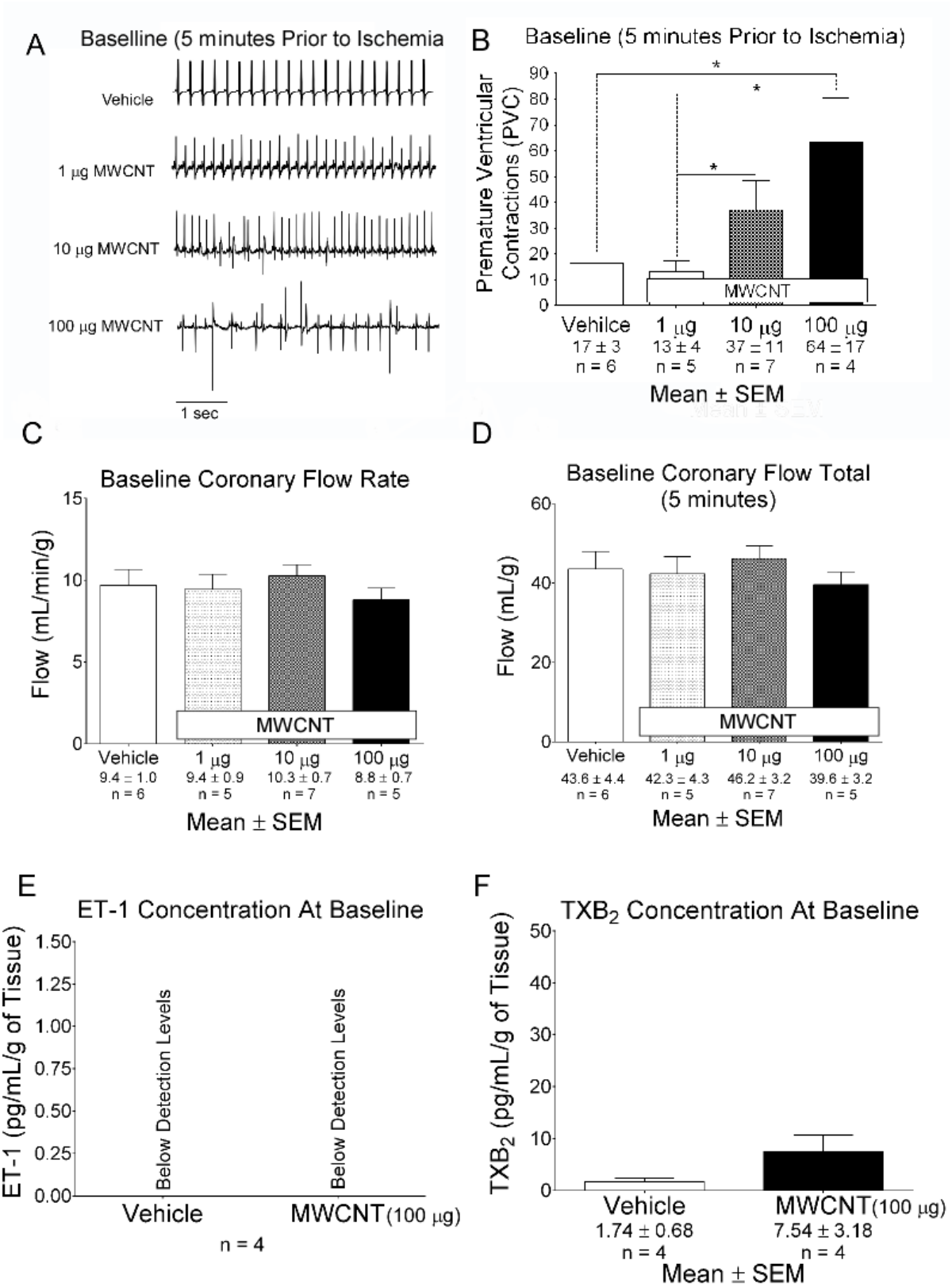
A
Baselline (5 minutes Prior to Ischemia
Vehicle
1 μg MWCNT
10 μg MWCNT
100 μg MWCNT
1 sec
B
Baseline (5 minutes Prior to Ischemia)
Premature Ventricular Contractions (PVC)
MWCNT
Vehilce 17 ± 3 n = 6
1 μg 13 ± 4 n = 5
10 μg 37 ± 11 n = 7
100 μg 64 ± 17 n = 4
Mean ± SEM
C
Baseline Coronary Flow Rate
Flow (mL/min/g)
MWCNT
Vehicle 9.4 ± 1.0 n = 6
1 μg 9.4 ± 0.9 n = 5
10 μg 10.3 ± 0.7 n = 7
100 μg 8.8 ± 0.7 n = 5
Mean ± SEM
D
Baseline Coronary Flow Total (5 minutes)
Flow (mL/g)
MWCNT
Vehicle 43.6 ± 4.4 n = 6
1 μg 42.3 ± 4.3 n = 5
10 μg 46.2 ± 3.2 n = 7
100 μg 39.6 ± 3.2 n = 5
Mean ± SEM
E
ET-1 Concentration At Baseline
ET-1 (pg/mL/g of Tissue)
Below Detection Levels
Below Detection Levels
Vehicle
MWCNT(100 μg)
n = 4
F
TXB2 Concentration At Baseline
TXB2 (pg/mL/g of Tissue)
Vehicle 1.74 ± 0.68 n = 4
MWCNT(100 μg) 7.54 ± 3.18 n = 4
Mean ± SEM

3.3.3. Coronary reperfusion flow and concentrations of endothelin-1 and thromboxane B_2 in effluent

Coronary flow and ET-1/TXB2 data are shown in Figure 3.2. Coronary flow was depressed by ~30% ($P < 0.05$) during the first 30 min of reperfusion in isolated hearts from rats instilled with 100 μg MWCNT compared to those from rats instilled with the vehicle (Figures 3.2A and 3.2B).The mean ET-1 concentrations in coronary effluent during early reperfusion were increased ($P < 0.05$) in the 100 μg MWCNT group compared to the vehicle group (Figure 3.2C). The mean TXB2 concentrations in coronary effluent during early reperfusion were also slightly elevated ($P = 0.06$) in the 100 μg MWCNT group compared to the vehicle group (Figure 3.2D).

Figure 3.2 Coronary reperfusion flow and effluent endothelin-1 and thromboxane B_2

MWCNT exposure promoted early reperfusion depressions in coronary flow and increased ET-1 release. (A) Mean coronary perfusion flow tracing for vehicle and 100 μg MWCNT. (B) Total coronary flow during 30 minute window identified in panel A, flow for 10 μg and 1 μg MWCNT also provided. (C) ET-1 concentration in effluents collected during early reperfusion (first 15 minutes) in the vehicle and 100 μg MWCNT groups. (D) TXB2 concentration in effluents collected during early reperfusion (first 15 minutes) in the vehicle and 100 μg MWCNT groups. Data are mean ± SEM. *P < 0.05.

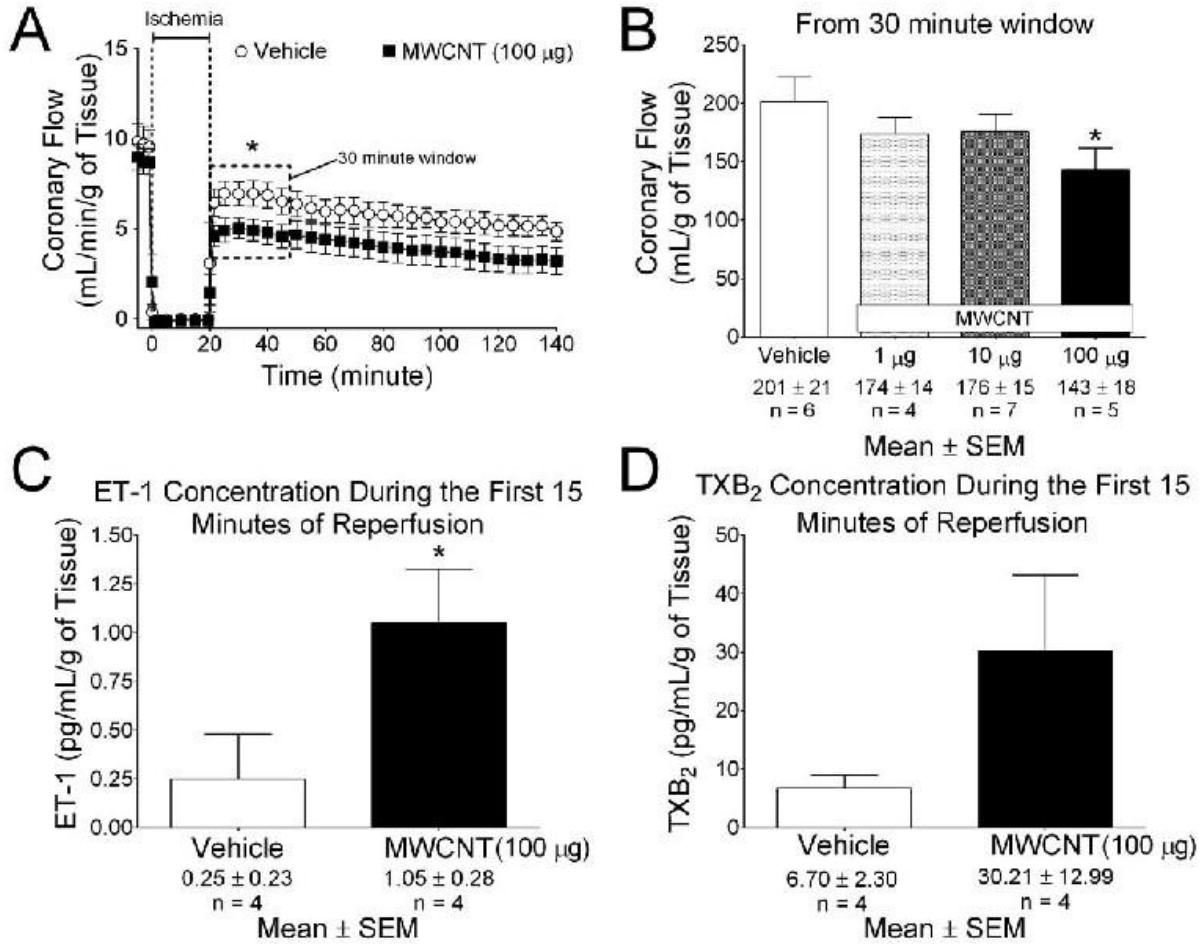

3.3.4. Left Ventricular Pressures

Since left ventricular pressures can impact coronary flow, data on left ventricular pressure is provided for vehicle and 100 µg MWCNT in Figure 3.3. No differences were observed in the maximum left ventricular (Max. LV) pressure in isolated hearts throughout reperfusion from rats instilled with vehicle or 100 µg MWCNT (Figure 3.3A). The minimum LV (Min. LV) pressure was slightly elevated during the first 30 minutes of reperfusion in isolated hearts from the 100 µg MWCNT group compared to the vehicle group (Figure 3.3B).

Figure 3.3 Left ventricular pressures

Depression in coronary flow is not explained by large differences in left ventricular pressures. (A) Tracing of maximum left ventricular (Max. LV) pressure for vehicle and 100 µg MWCNT. (B) Tracing of minimum left ventricular (Min. LV) pressure for vehicle and 100 µg MWCNT. Data are mean ± SEM. *P < 0.05.

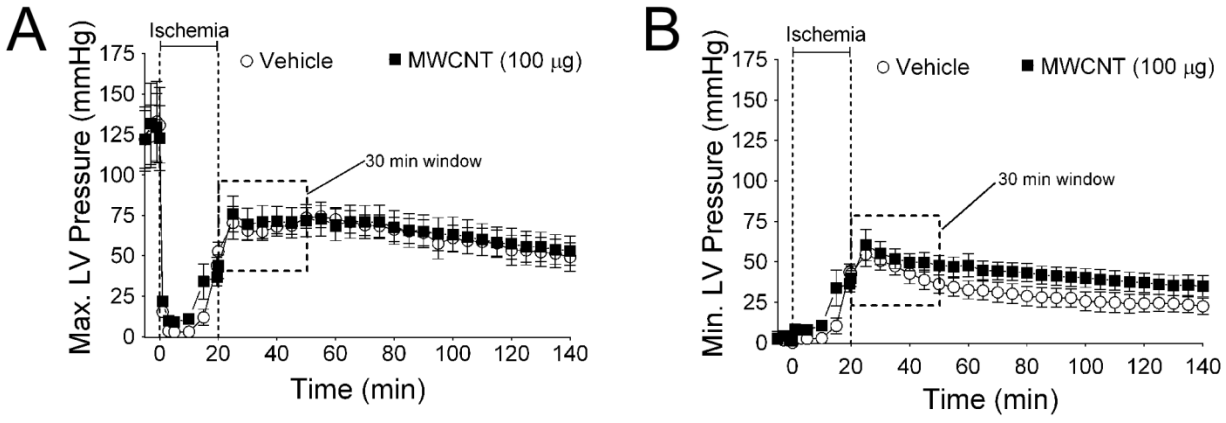

3.3.5. Cardiac ischemia/reperfusion injury

The impacts of MWCNT exposure on *ex vivo* cardiac I/R injury in isolated hearts are presented in Figure 3.4. Following I/R, infarct sizes were larger ($P < 0.05$) in isolated hearts from rats instilled with 100 µg MWCNT compared to hearts isolated from the vehicle group (Figure 3.4A). During reperfusion, the time until the first episode of ventricular tachycardia or fibrillation (VT/VF) was slightly decreased (not statistically different) in isolated hearts from rats instilled with 100 µg MWCNT as compared to vehicle (Figure 3.4B). Additionally, cardiac arrhythmia scores generated for the 2 hr reperfusion period were similar (not shown), ranging from 4.2 ± 0.7 to 4.8 ± 0.4 in hearts isolated from vehicle instilled animals compared to those from the 100 µg MWCNT group, respectively. We derived left ventricular developed pressure (LVDP) by subtracting the Min. LV pressure from the Max. LV pressure. At the end of reperfusion protocols (Time = 140 minutes), ending LVDP was lower ($P < 0.05$) in hearts isolated from rats instilled with either 1 µg or 10 µg MWCNT as compared to hearts from rats instilled with vehicle (Fig. 3.4C). However, the ending LVDP was not significantly lower in isolated hearts from the 100 µg MWCNT group compared to the vehicle group.

Figure 3.4 Cardiac ischemia/reperfusion injury

MWCNT exposure exacerbates cardiac I/R injury. (A) Myocardial infarction following I/R shown as a percent of the zone at risk (ZAR). (B) Time between the onset of reperfusion and the incidence of the first ventricular tachycardia or fibrillation (VT/VF). (C) Mean LVDP values at the end of reperfusion protocols (time =140 minutes). Data are mean ± SEM. *$P < 0.05$.

A

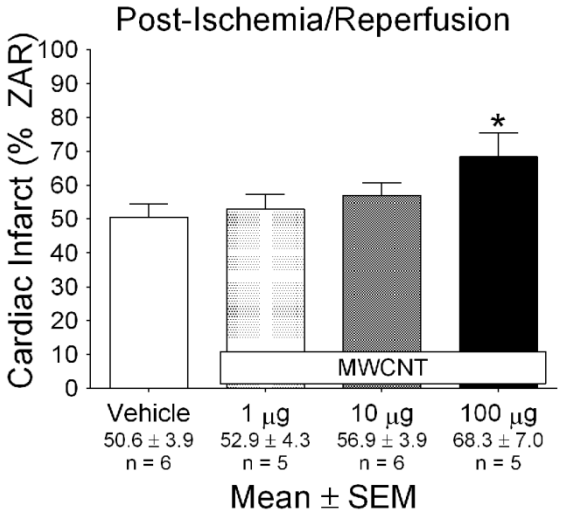
Post-Ischemia/Reperfusion
Cardiac Infarct (% ZAR)
100
90
80
70
60
50
40
30
20
10
0
*
MWCNT
Vehicle
50.6 ± 3.9
n = 6
1 μg
52.9 ± 4.3
n = 5
10 μg
56.9 ± 3.9
n = 6
100 μg
68.3 ± 7.0
n = 5
Mean ± SEM

B

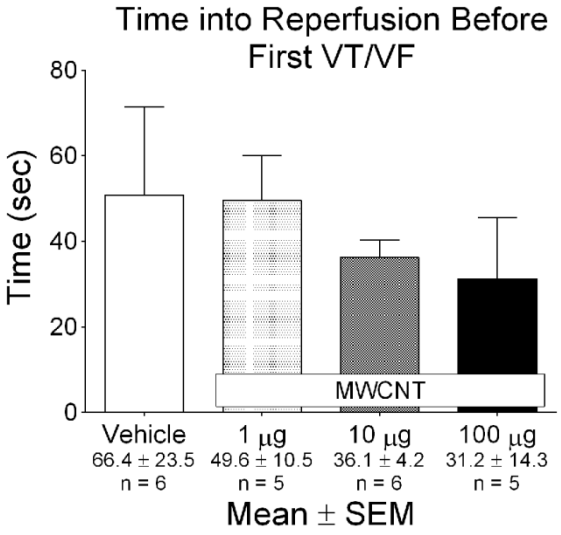
Time into Reperfusion Before First VT/VF
Time (sec)
80
60
40
20
0
MWCNT
Vehicle
66.4 ± 23.5
n = 6
1 μg
49.6 ± 10.5
n = 5
10 μg
36.1 ± 4.2
n = 6
100 μg
31.2 ± 14.3
n = 5
Mean ± SEM

C

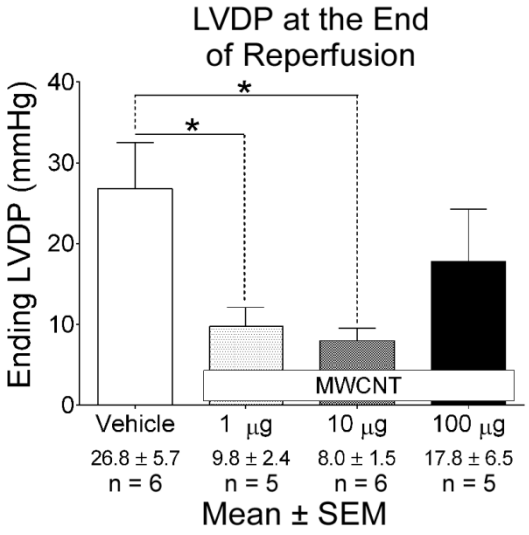
LVDP at the End of Reperfusion
Ending LVDP (mmHg)
40
30
20
10
0
*
*
MWCNT
Vehicle
26.8 ± 5.7
n = 6
1 μg
9.8 ± 2.4
n = 5
10 μg
8.0 ± 1.5
n = 6
100 μg
17.8 ± 6.5
n = 5
Mean ± SEM

3.4. Discussion

This study shows that pulmonary instillation of MWCNT 24 hrs prior to functional assessments in isolated hearts and cardiac I/R resulted in deleterious *ex vivo* cardiovascular endpoints. These included increased myocardial infarction following I/R injury in isolated rat hearts, increased PVC prior to the ischemic bout, and depression of coronary flow during early reperfusion. MWCNT instillation also augmented ET-1 release from isolated hearts during early reperfusion and trends emerged suggesting that TXA2 release from the heart may be augmented prior to I/R and possibly during early reperfusion. These findings are consistent with cardiovascular complications associated with particulate matter and air pollution exposure, which are dependent on decreasing size, increasing number per mass, and increasing surface area per mass of the particulate (16; 75; 98). MWCNT have physicochemical properties similar to particulate matter, which has raised concerns about their ability to initiate cardiovascular complications following pulmonary exposure.However, until now it has not been clear whether pulmonary exposure to MWCNT would generate biological responses capable of altering intrinsic physiological processes of the heart.

The MWCNT utilized in this investigation were physically characterized in a previous study showing that pulmonary exposure generated moderate pulmonary immune cell infiltration, collagen deposition, granuloma formation, and impairment of pulmonary function (173). We used three bolus mass concentrations of MWCNT delivered by intratracheal instillation in rats for the intention of establishing whether MWCNT could exert effects beyond the lung, similar to what is known regarding ambient particular matter. While this approach does not mimic real-world exposure conditions or deposition patterns in the lung that would occur via inhalation, it

provides a model to test whether these MWCNT may influence the cardiovascular system. Future work should focus on similar endpoints following an inhalation exposure, which is more physiologically relevant and would provide critical data needed to develop a risk assessment paradigm.

We used the isolated Langendorff rat heart model of I/R injury to examine cardiac endpoints that were dependent on changes in intrinsic characteristics of the heart and local signaling cascades, rather than MWCNT-induced changes in autonomic outflow and circulating humoral factors at the time of I/R. The isolated heart model has been described elsewhere as an appropriate system for investigating the cardiovascular consequences of direct toxicology (147) or nanoparticle exposure, via delivery of nanoparticles within the isolated heart perfusate (152). Our study demonstrates that the isolated heart model is also useful in assessing cardiovascular endpoints following pulmonary exposure to nanomaterials. The model provided simultaneous measurements of electrical activity/arrhythmogenesis, cardiac function/contractility, and coronary flow throughout the I/R protocol (9). We were able to compare these types of data to subsequent myocardial infarction and loss of LVDP that occurred by the end of I/R.

The first novel finding in this study is that pulmonary exposure to MWCNT resulted in cardiac arrhythmogenic injury. Hearts isolated from animals exposed to 10 or 100 μg of MWCNT had more PVC prior to the ischemic bout than those hearts taken from animals instilled with vehicle or 1 μg MWCNT. These data are consistent with other studies that have noted increased arrhythmogenesis and PVC following pulmonary exposure to particulate matter (69; 80; 83). Contributing factors like MWCNT-dependent effects on autonomic outflow and/or circulating

humeral factors are greatly diminished in the isolated heart model, but neurotransmitter release from the remaining nerve endings in the heart could remain influential (152).

One possible explanation for increased PVC at baseline is a possible increase in circulating oxidants in the hours following MWCNT exposure,which could prime the arrhythmogenic responses seen during the baseline ECG tracings. There is supporting evidence that MWCNT have been shown to increase oxidative burdens in the vascular compartment (137) and increased PVC associated with particulate matter exposure have been linked to oxidative stress (83). Furthermore, it is possible that the basal PVC generation in isolated hearts could be a product of oxidant stress in myocardial tissue following pulmonary exposure to MWCNT. Within the myocardium, oxidative stress is known to increase the propensity for arrhythmia (18), increase spontaneous calcium release from the sarcoplasmic reticulum (8), and introduce heterogeneity into myocardial action potentials (18), all of which are known to increase the proclivity for electrical dysfunction.

Interestingly, during reperfusion, arrhythmia scores were only slightly higher in hearts from MWCNT exposed rats compared to those from the vehicle group, but trends for decreased time until the first VT/VF and increased time spent in VT/VF remained evident. The 20 minute global ischemia challenge and subsequent reperfusion period likely pushed all the hearts in this study into such a highly arrhythmogenic state that MWCNT exposure was unable to worsen arrhythmogenesis during reperfusion. It is also tempting to speculate that the exacerbated size of myocardial infarction in isolated hearts taken from rats instilled with 100 µg MWCNT may have prevented worsening of the arrhythmogenic state of these hearts during reperfusion. It has been

demonstrated that exacerbated myocardial infarction potentially insulatestissue against injury currents, which are abnormal electrical wave front propagations (102), and could also explain the similarity in arrhythmia scores during reperfusion between isolated hearts from rats instilled with vehicle or 100 μg MWCNT. Clearly, further research will be needed in order to substantiate such a claim, but given the complexity and multifaceted aspects of cardiac I/R injury, such research would have multidisciplinary benefits outside of MWCNT-associated cardiotoxicity. In either case, we propose that increased arrhythmogenesis at baseline following pulmonary exposure to MWCNT could possibly serve as an indicator of cardiac vulnerability to I/R, and further investigation of this observation should be warranted.

The second novel finding in this study is the exacerbation of myocardial infarction following I/R in isolated rat hearts. Given that increased levels of endogenous ET-1 has been linked to increasing myocardial infarction following I/R (127), it is possible that the increased ET-1 in the effluents of isolated hearts seen during reperfusion in the 100 μg MWCNT group contributed to the infarct expansion. MWCNT instillation also appeared to have some effect on post-I/R cardiac contractility. In particular, those hearts isolated from rats instilled with lower mass concentration (1 or 10 μg) of MWCNT had lower LVDP by the end of reperfusion than those hearts isolated from the vehicle instilled rats. LVDP is the difference between Min. LV pressure and Max. LV pressure and describes the force generating capacity of the left ventricle, and is thus commonly used as a measure of cardiac function. Such a reduction in LVDP following I/R could result from cardiac stunning, arrhythmia, infarction, or any combination thereof (18; 184). Interestingly, hearts isolated from rats instilled with 100 μg of MWCNT did not demonstrate the same magnitude of LVDP reduction by the end of reperfusion that was seen following 1 μg or 10

μg MWCNT instillations. TXA2 is linked to cardiac I/R and increased arrhythmias (34), and TXA2 has been shown to elevate intracellular Ca^{2+} in cardiac myocytes (41). Considering that our study shows 100 μg MWCNT instillation resulted in slight increases (P = 0.06) in TXB2 concentrations measured in coronary effluents collected at baseline and early reperfusion, perhaps TXA2 briefly localized in high concentrations within zones of the myocardium enhanced myocyte contractility enough to preserve ventricular function in the face of expanding injury.

The third novel finding in this study was that coronary reperfusion flow was depressed in hearts from rats instilled with 100 μg MWCNT when compared to the vehicle group. Adequate coronary reflow is important due to the necessity of oxygen and nutrient delivery to the ischemic region in order to maintain cardiac contractility and myocardial viability, but these benefits are contrasted by increased oxygen free radical production in response to coronary reperfusion (24). Enhanced coronary vasoconstriction, and thus increased vascular resistance, is a central mechanism responsible for decreases in coronary blood flow, ultimately contributing to cardiac arrhythmogenesis and infarction during early post-ischemic reperfusion (99). In this study, the modified Langendorff heart model delivers perfusate under constant pressure. Therefore, the physical relationship of $\Delta R = P/\Delta Q\cdot$ were considered, where ΔR stands for the change in vascular resistance in the face of constant perfusion pressure (P) and an inverse change in the rate of perfusate flow ($\Delta Q\cdot$). The depression in flow during early post-ischemic reperfusion of isolated hearts taken from rats previously instilled with 100 μg MWCNT suggested that vascular resistance was elevated. We documented that Min. LV pressure was slightly increased in early reperfusion, which impart resistance to flow during cardiac diastole.

However, increased vascular resistance is more likely explained by the significant increase in concentration ET-1 that was measured in coronary effluents from the 100 μg MWCNT group,especially considering the possibility of a concomitant elevation in the concentration of the vasoconstrictor TXA2. ET-1 itself is a potent vasoconstrictor (25) and increased ET-1 levels in coronary effluents during reperfusion in hearts from the 100 μg MWCNT group are also consistent with the increased release of endothelins previously documented following particulate matter exposure and myocardial infarction (80). Cardiac responses to arrhythmogenic autocrine/paracrine agents like ET-1 could explain the increases in PVCat baseline (47; 80), though our data shows that ET-1 levels in preischemic coronary effluent samples from both the vehicle and 100 μg MWCNT group were below detectible limits. This brings into question the possibility that MWCNT exposure may perhaps modulate the specific local responses to ET-1 in cardiac myocytes and nodal tissue.

Cardiac infarct size has also been shown to relate to the amount of ET-1 released (127), indicating that elevated ET-1 levels during reperfusion in isolated hearts from rats exposed to 100 μg MWCNT may have also contributed to exacerbated myocardial infarction. The role of ET-1 during myocardial I/R has been extensively reviewed (131), but the impact of MWCNT exposure on cardiac and coronary responses to ET-1 have not been previously identified. Based on this study, a more in-depth assessment of myocardial and coronary artery responses to ET-1 represents a logical focus point for future research following MWCNT exposure.

3.5. Chapter 3 conclusion

Chapter 3 demonstrates that pulmonary exposure to MWCNT can have systemic impacts beyond the lung, and alters intrinsic properties of the heart capable of promoting cardiac I/R injury. One key functional change induced by MWCNT outside of cardiac I/R injury, is baseline non-autonomic cardiac arrhythmogenesis. In terms of changes functional endpoints associated with cardiac I/R, increased release of ET-1, and possibly TXA2, may promote depression of coronary flow during reperfusion. Each of these functional endpoints can provide an explanation for and contribute to post-I/R myocardial infarct expansion. These findings indicate that acute pulmonary exposure to MWCNT, and possibly other ENP, has the potential to promote cardiovascular derangements similar to pulmonary exposure to particulate matter in air pollution.

CHAPTER 4

INCREASED ISOMETRIC STRESS IN RESPONSE TO ENDOTHELIN-1 IN ISOLATED CORONARY ARTERIES 24 HOURS AFTER INTRATRACHEAL INSTILLATION OF MULTI-WALLED CARBON NANOTUBES

Acknowledgement

Elements of this chapter have been reproduced in part from the following citation(159):

Thompson LC, Frasier CR, Sloan RC, Mann EE, Harrison BS, Brown JM, Brown DA and Wingard CJ. Pulmonary instillation of multi-walled carbon nanotubes promotes coronary vasoconstriction and exacerbates injury in isolated hearts. *Nanotoxicology* (November 23, 2012); doi:10.3109/17435390.2012.744858.

4.1 Introduction

The increased use of MWCNT has raised concerns about human exposure. Based on their size, it is possible that pulmonary exposure to MWCNT may generate physiological changes in the cardiovascular system similar to that of NP in air pollution. MWCNT have been shown to translocate from the lung (139; 153). Arterial responsiveness following inhalation of NP have been shown to be augmented COX-dependent mechanisms (88). Pulmonary exposure to NP *in vivo* have been shown to disrupt vascular response profiles in isolate coronary arteries 24 hours after exposure (95; 111), including MWCNT (153). Altered ETBR function has been linked to enhanced ET-1-mediated vasoconstriction following exposure to diesel components (30). The COX pathway has been shown to promote exaggerated vasoconstriction in response to ET-1

during inflammation in other vascular beds, linked to increasing arachidonic acid metabolism through activation of the COX pathway, resulting in release of TXA2, and thus exaggerated vasoconstriction (81; 178). Other evidence suggests that local coronary artery inflammation results in the induction of COX-2 and enhanced coronary vasoconstriction (136). Induction of COX-2 has been linked to MWCNT exposure in macrophages (96), but COX-2 deficiency has been shown to exacerbate airway remodeling disorders in response to MWCNT exposure (140).

In Chapter 3 we found that hearts isolated from rats 24 hours following a pulmonary exposure to100 μg MWCNT demonstrated increased release of ET-1 during post-ischemic reperfusion with concomitant depression in coronary flow suggestive of increased coronary resistance. There were also slight elevations in TXB2 concentrations in isolated heart coronary effluents collected from the MWCNT group at baseline and early reperfusion. Further, enhanced TXA2 production likely reflects a role of COX in the cardiovascular detriments associated with pulmonary exposure to MWCNT. These findings suggest that ET-1, COX and TXA2 may play a role in coronary tone following MWCNT exposure.

Since coronary artery responses to ET-1 and TXA2 have not been studied following pulmonary exposure to MWCNT, it was thus the purpose of this study. Here we used wire myography investigate coronary artery responses to ET-1 and TXA2 and the potential contribution of the COX pathway to enhance coronary artery stress (mN/mm^2) generation following pulmonary exposure to 100 μg MWCNT. Specifically, we tested the hypothesis that intratracheal instillation of 100 μg of MWCNT would enhance coronary smooth muscle stress generating capacity associated with ET-1, ETBR, COX, and TXA2. Since ETBR as associated with the

vascular smooth muscle and endothelial layers of coronary arteries was also tested the endothelial-dependent component of this hypothesis by studying enhanced stress generation in intact and denuded coronary artery segments.

4.2 Materials and Methods

4.2.1. Multi-walled carbon nanotubes and vehicle

Vehicle instillate (10% surfactant/saline): Solution by volume is 90% sterile saline (0.9 % NaCl) and 10% pulmonary surfactant (Infasurf™, a gift from ONY, Inc., Amherst, NY). Infasurf™ contains: (per mL of 0.9% NaCl solution) 35 mg total bovine phospholipids, of which 16 mg are disaturated phosphatidylcholine, and 0.7 mg bovine proteins, of which 0.44 mg are hydrophobic surfactant-associated protein C and 0.26 mg are hydrophobic surfactant-associated protein B (http://www.infasurf.com/about-infasurf/#composition).

MWCNT instillate: MWCNT were provided by NanoTechLabs, Inc. (Yadkinville, NC, USA). For 100 µg dosing suspensions, MWCNT were added to the vehicle instillate to a concentration of 0.5 mg/mL. For 10 µg and 1 µg dosing solutions, 1:10 serial dilutions were performed with vehicle instillate. Immediately prior to instillation MWCNT suspensions were sonicated in a cup-horn sonicator (Qsonica, LLC - Newton, CT, USA) for 2 minutes at 65% amplitude to reach and approximate energy output of 10,800 J.

4.2.2. Animals

Male Sprague-Dawley rats were purchased from Charles River (Morrisville, NC, USA). Rats were 10-12 weeks of age at the time of purchase and housed in the Department of Comparative Medicine at East Carolina University. Each rat had access to standard laboratory chow and water *ad libitum* in a temperature regulated facility (23 ± 1°C) under 12:12 hour light-dark cycles. We provided each rat with a minimum of 5 days to acclimate prior to experimental

manipulations. All use of rats in this study complied with protocols approved by the East Carolina University Institutional Animal Care and Use Committee.

4.2.3. Instillations

MWCNT were administered by intratracheal instillation. Rats were placed under Isoflurane anesthesia and a 200 µL bolus of MWCNT or vehicle was placed at the opening of the trachea until aspirated, 24 hours prior to cardiopulmonary assessments. After instillation, each rat was monitored for until normal grooming habits resumed.

4.2.4. Bronchoalveolar lavage

Rats were anesthetized deeply with Isoflurane and a pneumothorax was induced. The heart was excised for coronary artery dissection and thoracic cage was removed for optimal visualization of the lungs, lower trachea and main bronchi. Connective tissue surrounding the lung was resected and the left main bronchus was ligated. A tracheotomy was performed allowing an 18 gauge angiocatheter to be inserted and secured with 2-0 suture. One bolus of Hanks balanced saline solution (23.1 mL/kg) was lavaged into the right lung three times successively. Recovered bronchoalveolar lavage (BAL) fluid was centrifuged at 1000 x g for 10 minutes at 4°C. The BAL supernatant was used for protein quantification.

4.2.5. Differential cell counts

The cell pellets were resuspended in 1 mL of fresh Hanks balanced saline solution and total cell counts were determined with a Cellometer® Auto X4 (Nexcelom Biosciences, LLC., Lawrence, MA, USA). BAL fluid volumes containing 20,000 cells were centrifuged onto glass slides using

a Cytospin IV (Shandon Scientific Ltd., Cheshire, UK) and stained via a three step hematology stain (Richard Allan Scientific, Kalamazoo, MI, USA). Cell differential counts were determined microscopically based on hematologic stain and cellular morphology. A total of 300 cells per slide were counted to estimate cell percentage.

4.2.6. Protein quantification

BAL fluid protein quantification was performed using a standard Bradford protein assay. In short, BAL fluid proteins were quantified using 5 µL of sample diluted 250 µL of Bradford reagent in duplicate wells of using a 96 well plate. Absorbance values were read at 562 nm using a BIO-TEK® Synergy HT plate reader (Winooski, VT, USA) and data were analyzed with Gen5 software (BIO-TEK®). Absorbance values for each sample were compared to a standard curve generated using 2.0 - 0.0625 mg/mL bovine serum albumin.

4.2.7. Isolated coronary wire myography

After excision hearts were placed in ice cold physiological saline solution (PSS) containing (mM) 140 NaCl, 5.0 KCl, 1.6 $CaCl_2$, 1.2 $MgSO_4$, 1.2 3-[N-morpholino]-propane sulfonic acid (MOPS), 5.6 d-glucose, and 0.02 EDTA with a pH of 7.4 when heated to 37°C. Segments of the LAD were carefully isolated and mounted into the chambers of a multi-channel wire myograph system (DMT 610M, Ann Arbor, MI). Before being mounted into myographs, LAD segments selected for denuding were carefully passed on to a strand of human hair and the LAD lumen was gently rolled and rubbed along the hair to strip away the endothelium. Following a 1 hour equilibration in oxygenated PSS, heated to 37°C with periodic washes, LAD segments were stretched progressively and length-tension relationships were established. The law of Laplace

was used to determine the optimum resting tension for each vessel segment (90% of the internal circumference established at tensions equivalent to 100 mmHg), as described by Halpern and Mulvany (67). After another 30 minute equilibration period, tissue viability was assessed by a 10 minute K^+ depolarization using 109 mM K^+PSS, which is PSS containing equal molar substitution of Na^+ with K^+. After washing out with fresh PSS and return to baseline tension, 1.0 µM serotonin was delivered to precontract the LAD segments, followed by 3.0 µM ACh (5 minutes each) to test for endothelial-dependent relaxation.

4.2.8. Pharmacological agents for vascular studies

Serotonin and ACh(Sigma-Aldrich,St. Louis, MO, USA) used during "wake-up" protocols and were dissolved in PSS.ET-1 (American Peptide Company, Inc., Sunnydale, CA) was dissolved in 0.1% acetic acid. FR139317 (R&D Systems, Inc., Minneapolis, MN) was dissolved in 100 mM DMSO. Indomethacin (Sigma-Aldrich) was dissolved in 100% ethanol. DUP-697 (R&D Systems, Inc.) was dissolved in 100 mM DMSO. Ozagrel HCl (R&D Systems, Inc.) was dissolved in PSS. AA2414 (R&D Systems, Inc.) was dissolved in 100 mM DMSO. U46619 (R&D Systems, Inc.) was dissolved in 100% ethanol. HA-1077 (R&D Systems, Inc.) was dissolved in PSS.

4.2.9. Coronary artery assessment of endothelin-1 responses

After PSS washouts and tension relaxation, LAD segments were subjected to cumulative concentration-responses to ET-1 (0.1 nM - 1.0 µM). Due to the robust nature of ET-1 responses, we conducted pair-wise measurements of ET-1 responses in separate LAD segments from the same heart, with and without pharmacological antagonist and an inhibitor for ET-1 receptors,

COX-1, COX-2, TXSorTP. We used concentrations of the selective ETAR antagonist FR139317 that were selective for ETAR (10 nM) or a higher concentration that would also partially antagonize ETBR (10 μM), based on IC_{50} values reported by the supplier. Indomethacin (10 μM) was used as a general COX inhibitor and 1 μM DUP-697 was used to selectively inhibit COX-2. The TXS inhibitor Ozagrel HCl was used at 10 μM and the TP antagonist AA2414 was used at a 1.0 μM concentration. The concentrations for Indomethacin, DUP-697, and AA2414 were selected just above the IC_{50} values reported by the supplier. The Ozagrel concentration was titrated to response in the MWCNT group and then recapitulated in the vehicle group.

4.2.10. Coronary artery assessments of thromboxane mimetic U46619

Another group of LAD segments was used to develop a concentration-response curve for U46619, a TXA2 mimetic over the concentration range of 1.0 nM - 10 μM.

4.2.11. Statistics

All data are expressed as mean ± SEM and significant P-values (< 0.05) are marked or reported. Graphpad Prism software (version 5, LaJolla, CA, USA) was used to graph and analyze all data. BAL data were analyzed by t-test. Isolated coronary artery vascular response curves were compared using Repeated Measures ANOVA with Bonferroni's post-tests and non-linear regression analysis of the 4 parameter best-fit values (103). Reported EC_{50} and Hillslope values were derived from normalized fits of each individual LAD concentration-response curve (0-100% of response) and were compared by t-test.

4.3 Results

4.3.1 Pulmonary responses to instillation

We conducted BAL studies in order to estimate the extent of lung response following exposure to 100 μg MWCNT, and since Infasurf™ contains non-rat related proteins, we sought to confirm that no adverse pulmonary reactions occurred in response to the exogenous surfactant in vehicle instilled rats. These data are reported in Table 4.1. Total protein concentrations in BAL fluid collected from rats exposed MWCNT were elevated ($P < 0.05$) compared to those from rats instilled with vehicle. While total cell counts, macrophages and neutrophils were slightly in the MWCNT group compared to the vehicle group, the number of eosinophils was significantly elevated.

Table 4.1 Bronchoalveolar lavage from multi-walled carbon nanotube studies

	Total Bronchoalveolar Lavage Fluid (BALF) Protein and Cellularity					
	BAL samples collected 24 hrs following exposure in males, data expressed as mean ± SEM					
	Protein (μg/mL)	**Cell Number (x 10^5)**	**Macrophages (x 10^5)**	**Neutrophils (x 10^3)**	**Eosinophils (x 10^3)**	**Epithelial Cells (x 10^3)**
Vehicle	207 ± 13	3.8 ± 1.2	2.7 ± 0.8	35 ± 12	0.8 ± 0.4	22.7 ± 8.9
MWCNT	272 ± 18*	4.6 ± 1.4	3.4 ± 1.1	42 ± 14	7.6 ± 2.4*	28.2 ± 8.5
n	7-8	7	7	7	7	7

*** P < 0.05 vs. vehicle**

4.3.2. Intact coronary artery responses to endothelin-1 and thromboxane mimetic

Data for coronary artery stress production in response to ET-1 and the TXA2 mimetic U46619 are presented in Figure 4.1 and Tables 4.2 (EC_{50} values) and 4.3 (Hillslope values). Coronary artery stress (mN/mm^2) responses to ET-1 in the MWCNT group yielded significant increases in stress production and altered curve progression compared to isolated LAD responses from the vehicle group (Figure 4.1A). Conversely, smooth muscle stress production in response to U46619 appeared diminished in LAD isolated from MWCNT instilled rats compared to vehicle but the curve progressions were significantly different between the MWCNT and vehicle groups (Figure 4.1B). EC_{50} and Hillslope values for ET-1 and U46619 were all slightly shifted toward a more sensitized state in the MWCNT group compared to the vehicle group.

Figure 4.1 Intact coronary artery response to endothelin-1 and thromboxane mimetic

MWCNT exposure enhances smooth muscle contraction in response to ET-1 in isolated coronary artery segments. (A) Stress response curves for ET-1 in intact coronary artery segments isolated from MWCNT and vehicle instilled rats. (B) Stress response curves for U46619 in intact coronary artery segments isolated from MWCNT and vehicle instilled rats. Data are mean ± SEM. *P < 0.05 vs. Vehicle by Repeated Measures ANOVA. P < 0.05 vs. Vehicle indicated for non-linear regression analysis.

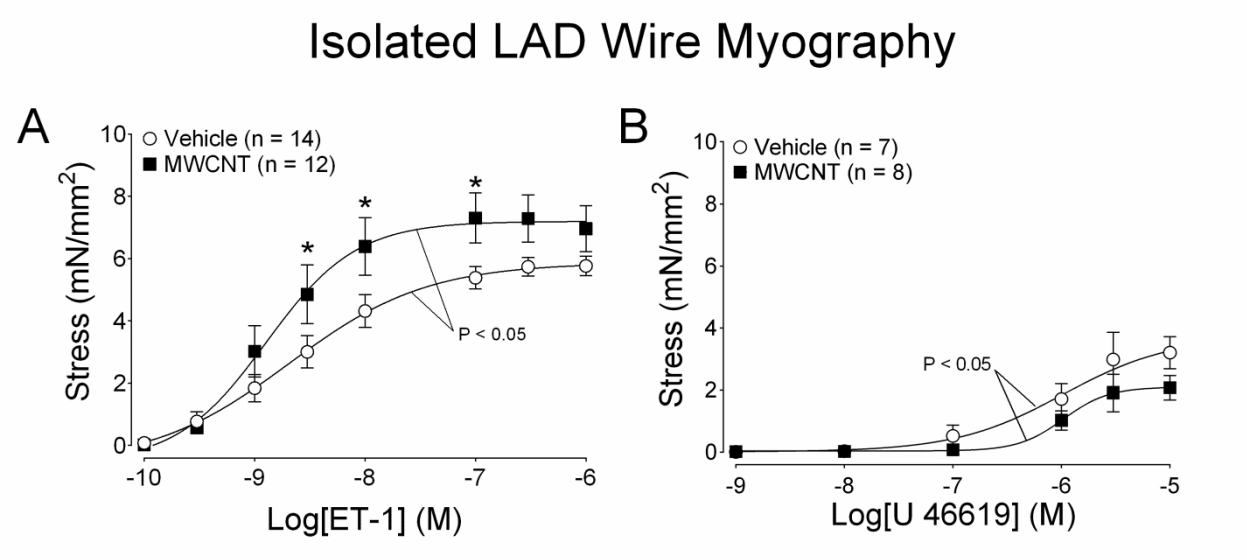

4.3.3. Denuded coronary artery responses to endothelin-1

Data for denuded LAD responses to ET-1 are presented in Figure 4.2, and Tables 4.2 (EC_{50} values) and 4.3 (Hillslope values). Experiments involving denution of coronary arteries had low success rates just above 50% (7/12 survived the denuding process). Intact vessels were only included if the corresponding denuding segment survived. In those segments denuded coronary arteries isolated from rats instilled with MWCNT caused slight reductions in ET-1 stress generation compared to paired intact artery segments, enough so that the denuded MWCNT response curve looked more like the curve from intact LAD isolated from rats instilled with vehicle (Figure 4.2A). However, denuding coronary artery segments also caused a slight diminishment in ET-1 stress response in the vehicle group compared to paired intact vessel segments from the vehicle group (Figure 4.2B).

Figure 4.2 Denuded coronary artery responses to endothelin-1

(A) Stress response curves for ET-1 in denuded coronary artery segments isolated from MWCNT instilled rats. (B) Stress response curves for ET-1 in denuded coronary artery segments isolated from Vehicle instilled rats. Data are mean ± SEM.

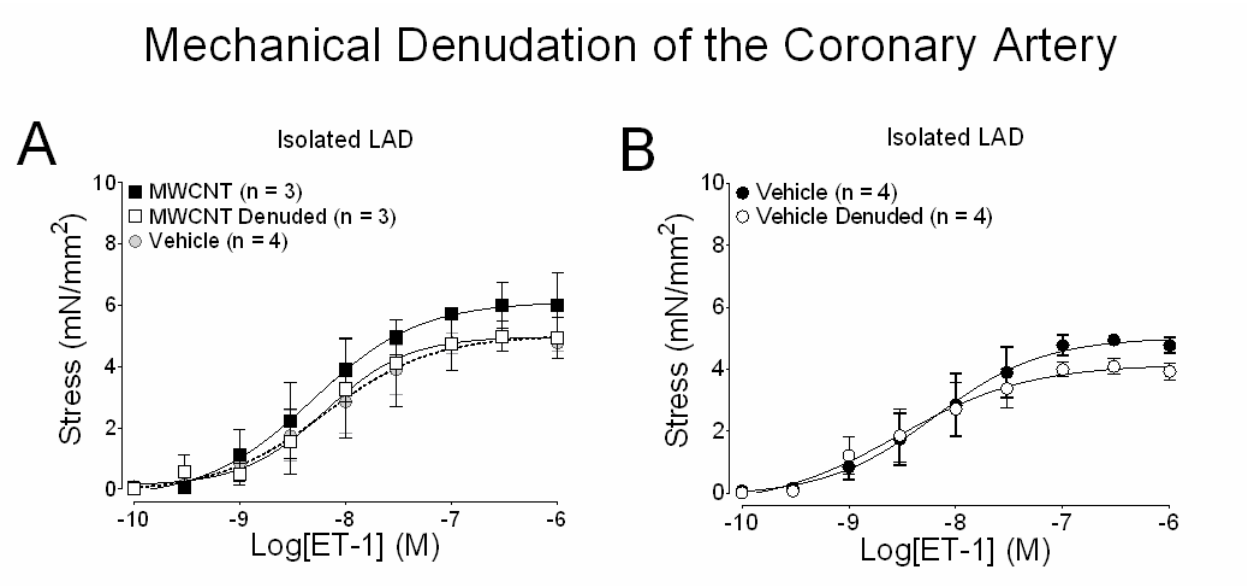

4.3.4. Endothelin receptor antagonist-sensitive responses in intact coronary arteries

The contribution of ETAR in response to ET-1 following MWCNT exposure was tested in Figure 4.3. We incubated intact LAD segments with 10 nM FR139317, an ETAR-selective antagonist. We found that at lower concentrations of ET-1, stress levels were similar between intact LAD isolated from the hearts of MWCNT exposed rats and vehicle exposed rats. However, at higher ET-1 concentrations the stress generated by intact ETAR antagonized LAD from the MWCNT group increased to levels similar to those of intact LAD isolated from the hearts of MWCNT instilled rats not antagonized with FR139317 (Figure 4.3A). We also incubated intact LAD with 10 μM FR139317, which will also partially antagonize ETBR. In these experiments, intact LAD isolated from the hearts of MWCNT instilled rats antagonized with10 μM FR139317 produced stress similar to that seen in intact LAD from the vehicle group at higher ET-1 concentrations (10 nM – 1.0 μM) (Figure 4.3B). EC50 and Hillslope values for ET-1 responses after incubation with 10 nM or 10 μM FR139317 are reported in Tables 4.2 and 4.3 respectively.

Figure 4.3 Endothelin receptor antagonist-sensitive responses in intact coronary arteries

(A) ET-1 stress response curves from isolated LAD incubated with or without 10 nM FR139317, an endothelin A receptor (ETAR)-selective antagonist. (B) ET-1 stress response curves from LAD isolated from rats instilled with 100 μg MWCNT after being incubated with or without 10 μM FR139317, which antagonizes ETAR and partially antagonizes endothelin B receptors (ETBR). Data are mean ± SEM.

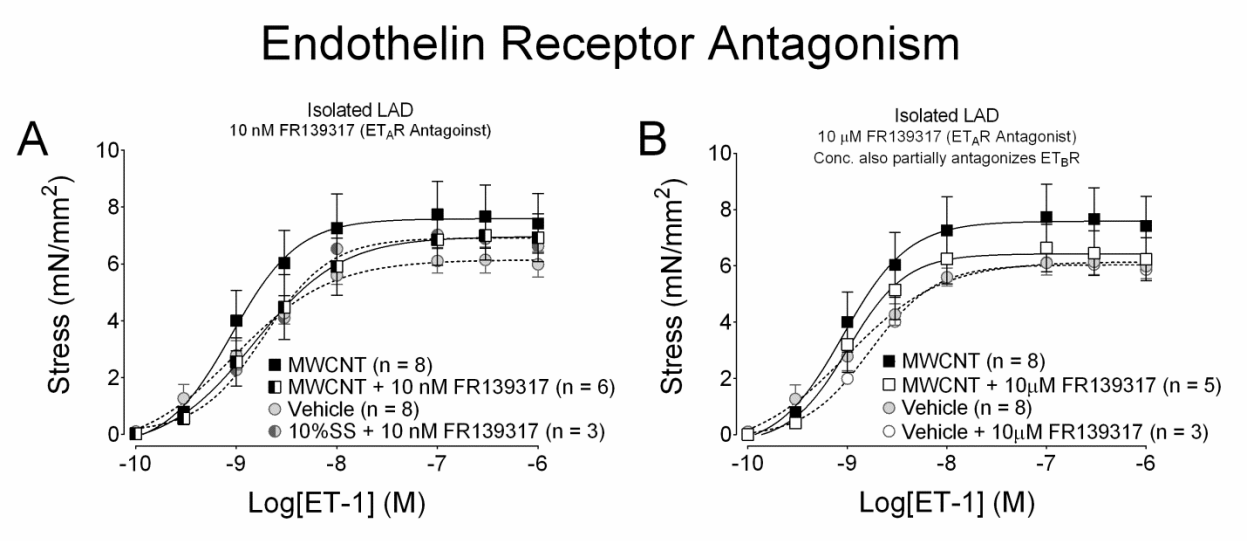

4.3.5. Coronary artery endothelin-1 responses and cyclooxygenase

Data from isolated LAD responses to ET-1 with and without pharmacological manipulation of the COX-1 and COX-2 are shown in Figure 4.4. Inhibition of LAD segments with 10 μM Indomethacin, a general COX inhibitor, produced a 24% reduction in ET-1 stress in the MWCNT group to a level similar to the ET-1 stress responses of uninhibited LAD segments from vehicle instilled rats (Figure 4.4A). The vehicle group showed little differences between ET-1-mediated stress responses in LAD inhibited with Indomethacin and those not inhibited. Inhibition of LAD segments with 1 μM DUP-697, a COX-2 selective inhibitor, produced a 15% reduction in ET-1 stress in segments isolated from rats previously instilled with MWNCT (Figure 4.4B). The vehicle group also showed little differences between ET-1-mediated stress responses in LAD inhibited with DUP-697 and those not inhibited.

Figure 4.4 Cyclooxygenase inhibition in intact coronary arteries

MWCNT exposure induces ET-1 responses in intact coronary arteries that are sensitive to pharmacological manipulation of the cyclooxygenase (COX) pathway. (A) ET-1 stress-response curves from isolated LAD incubated with or without 10 µM Indomethacin, a general COX inhibitor, from rats instilled with 100 µg MWCNT. (B) ET-1 stress-response curves from isolated LAD incubated with or without 1.0 µM DUP-697, a COX-2 selective inhibitor, from rats instilled with 100 µg MWCNT.Data are mean ± SEM. $P < 0.05$ by non-linear regression analysis

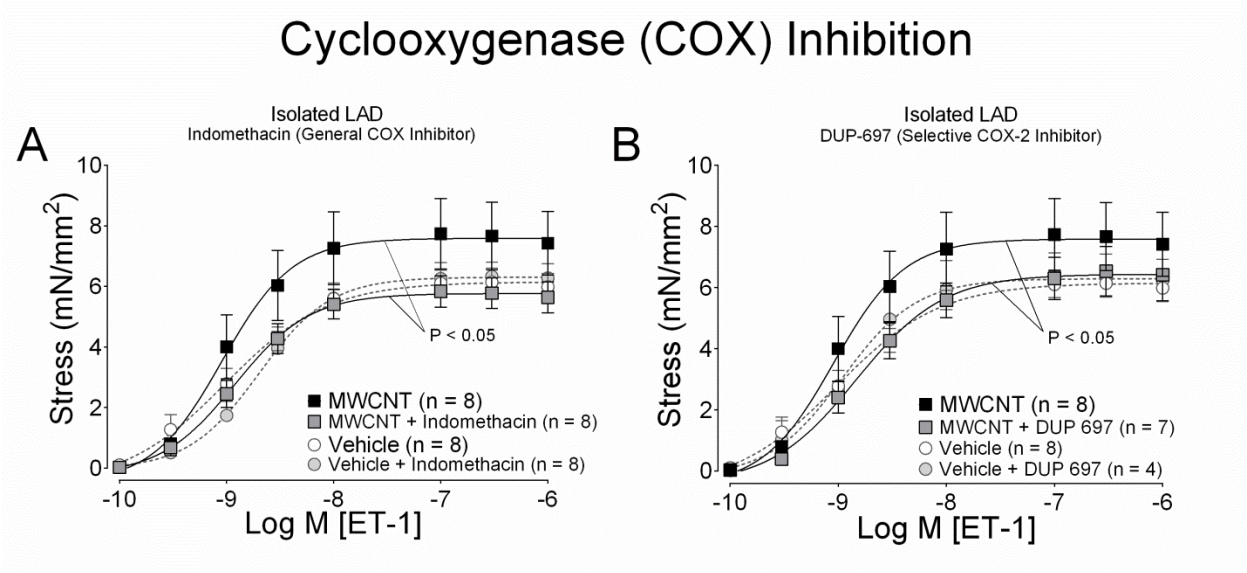

4.3.6. Coronary artery endothelin-1 responses and the thromboxane axis

Data from isolated LAD responses to ET-1 with and without pharmacological manipulation of the TXS and TP are shown in Figure 4.5. Inhibition of LAD segments with 10 μM Ozagrel HCl, a TXS inhibitor, produced a 28% reduction in ET-1 stress in the MWCNT group to a level similar to the ET-1 stress responses of uninhibited LAD segments from vehicle instilled rats (Figure 4.5A). The vehicle group showed little change in LAD stress responses to ET-1 after being inhibited Ozagrel HCl compared to the uninhibited ET-1 stress responses in LAD from the vehicle group. When isolated LAD segments from MWCNT-instilled rats were incubated with 1 μM AA2414 they showed a 27 % reduction in ET-1 stress generation compared to uninhibited LAD from the MWCNT group (Figure 4.5B). LAD from the vehicle group also showed very little change in ET-1-mediated stress responses when inhibited withAA2414 compared to LAD from the vehicle group that were not inhibited.

Figure 4.5 Thromboxane axis blockade in intact coronary arteries

MWCNT exposure induces ET-1 responses in intact coronary arteries that are sensitive to both pharmacological inhibition of TXA2 synthetase and pharmacological antagonism of TXA2 receptor. (A) ET-1 stress-response curves from isolated LAD incubated with or without 10 µM Ozagrel HCl, a TXA2 synthetase inhibitor. (B) ET-1 stress-response curves from LAD incubated with or without 1.0 µM AA2414, a TXA2 receptor antagonist. Data are mean ± SEM. $P < 0.05$ by non-linear regression analysis.

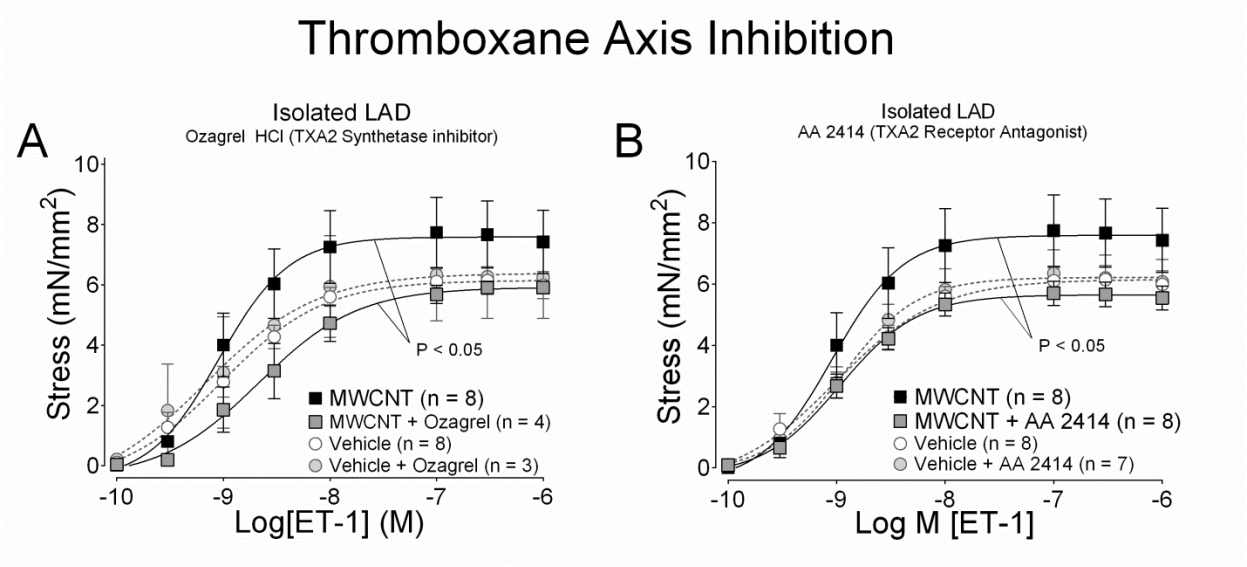

Table 4.2 Coronary arteryEC_{50}s from multi-walled carbon nanotube studies

	EC_{50} Values [nm] (mean ± SEM, n)	
	Vehicle	**MWCNT**
Figure 4.1:ET-1 (total)	14 ± 6.6, 14	4.7 ± 2.6, 12
Figure 4.1:U46619	1930 ± 612, 7	1307 ± 394, 8
Figure 4.2: ET-1 (intact)	16 ± 10, 4	14 ± 10, 3
Figure 4.2: ET-1 (denuded)	12 ± 6.8, 4	17 ± 7.5, 3
Figure 4.3 - 4.5:ET-1	1.7 ± 0.6, 8	1.5 ± 0.3, 8
Figure 4.3:ET-1 + 10 nM FR	1.6 ± 0.9, 3	3.1 ± 1.5, 6
Figure 4.3:ET-1 + 10 µM FR	2.0 ± 0.3, 4	1.6 ± 0.6, 5
Figure 4.4:ET-1 + Indomethacin	2.4 ± 0.5, 8	1.6 ± 0.4, 8
Figure 4.4:ET-1 + DUP697	1.7 ± 0.5, 4	2.5 ± 1.0, 8
Figure 4.5:ET-1 + Ozagrel	1.5 ± 0.5, 3	3.7 ± 1.7, 4
Figure 4.5: ET-1 + AA2414	1.5 ± 0.4, 7	1.4 ± 0.3, 8

Table 4.3 Coronary artery Hillslopes from MWCNT studies

	Hillslope Values (mean ± SEM, n)	
	Vehicle	**MWCNT**
Figure 4.1: ET-1 (total)	1.4 ± 0.1, 14	1.6 ± 0.1, 12
Figure 4.1: U46619	1.3 ± 0.2, 7	1.5 ± 0.2, 8
Figure 4.2: ET-1 (intact)	1.4 ± 0.1, 4	1.4 ± 0.2, 3
Figure 4.2: ET-1 (denuded)	1.5 ± 0.1, 4	1.1 ± 0.1, 3
Figure 4.3 - 4.5: ET-1	1.4 ± 0.1, 8	1.6 ± 0.2, 8
Figure 4.3: ET-1 + 10 nM FR	1.9 ± 0.5, 3	1.3 ± 0.1, 6
Figure 4.3: ET-1 + 10 µM FR	2.1 ± 0.9, 4	1.8 ± 0.1, 5
Figure 4.4: ET-1 + Indomethacin	1.9 ± 0.5, 8	1.6 ± 0.2, 8
Figure 4.4: ET-1 + DUP697	1.7 ± 0.2, 4	1.5 ± 0.2, 8
Figure 4.5: ET-1 + Ozagrel	1.4 ± 0.1, 3	1.4 ± 0.1, 4
Figure 4.5: ET-1 + AA2414	1.7 ± 0.2, 7	1.8 ± 0.3, 8

4.4. Discussion

The major findings from this study are that pulmonary exposure to 100 μg MWCNT resulted in significant enhancement ET-1-mediated stressproduction in coronary arteries isolated from rats 24 hours after exposure. Pharmacological approaches suggested that enhancement of ET-1-mediated stress production is driven in large part by the COX/TXA2 axis. TXS inhibitor Ozagrel and TP antagonist AA2414 both were capable of completely blocking the enhanced ET-1 mediated coronary artery stress in LAD isolated from the rats instilled with 100 μg MWCNT. Examining the differences in the diminishment of ET-1-mediated stress production by the general COX inhibitor Indomethacin and the COX-2 selective inhibitor DUP-697, suggests that COX-2 may be more important in the response than COX-1. These findings are consistent with other research showing that air pollution, particulate matter, and various ENP can yield arterial functional derangements (30; 31; 36; 88; 95; 111; 153; 176). These findings support the concerns that pulmonary exposure to NP could promote cardiovascular derangements by specific physiological mechanisms, and that these physiological mechanisms may have an underlying vascular component.

Since ET-1 has a significant role during cardiac I/R we tested the hypothesis that ET-1 vasoconstriction in isolated LAD segments taken from rats exposed to 100 μg MWCNT would be enhanced in a COX/TXA2-dependent manner. This hypothesis gained substantial support from the findings in Chapter 3 showing that pulmonary exposure to100 μg MWCNT promoted an increase in coronary effluent ET-1 concentrations and depression of coronary flow during early post-ischemic reperfusion.ET-1 is a potent vasoconstrictor released from endothelial cells, though not exclusively, to influence local vascular tone (25). On vascular smooth muscle cells,

ET-1 acts on ETAR or ETBR, which are both coupled to Gq proteins. On vascular endothelial cells, ET-1 can act on ETBR coupled to Gi proteins (40). ETAR activation generally produces strong and prolonged vasoconstriction through Gq activation of phospholipase C, mobilization of inositol triphosphate and diacylglycerol from the lipid bilayer, which in turn activates Ca^{2+} release from the sarcoplasmic reticulum and extracellular Ca^{2+} entry via voltage operated channels, producing vascular smooth muscle contraction (89). ETBR activation on endothelial cells produces vasodilation by stimulating release of NO, which results in vascular smooth muscle relaxation (89).

Research has suggested that tissue insult and inflammation can cause an augmented vasoconstriction in response to ET-1 dependent on ETBR activation (108; 132). In our experiments, pharmacological inhibition of ETAR and partial inhibition of ETBR did not yield strong evidence that ETBR is solely responsible for the increase in ET-1-mediated stress production in coronary arteries following MWCNT exposure, but the claim is still plausible. Similarly, denudation of coronary artery segments did not provide strong support that the enhanced arterial response to ET-1 was entirely dependent upon vascular endothelial cells because denuded arteries from the vehicle group also showed a similar small reduction in stress response to ET-1. These findings suggest that the experiments we preformed could be improved by increasing the N in denuded studies, and in conjunction with endothelium denudation also utilize ETAR and ETBR selective antagonist. Such experiments could provide stronger evidence to support the hypothesis that MWCNT exposure results in endothelial cell/ETBR-dependent enhancement of coronary artery stress production in response to ET-1.

Under inflammatory conditions ET-1 has been linked to increasing arachidonic acid metabolism through activation of the COX pathway, resulting in release of TXA2 and thus exaggerated vasoconstriction (81; 178). Our data suggest that COX and TXA2 play a role in coronary responses to ET-1, 24 hrs following MWCNT exposure. We also showed that LAD stress-responses to U46619, a TXA2 mimetic, generated less stress in the MWCNT group compared to vehicle, possibly indicatingTPdesensitization in LAD isolated from rats exposed to 100 μg MWCNT. Such an agonist-induced desensitization of TP is thought to occur through protein kinase C activation and TP phosphorylation by G-protein receptor kinases (55). Therefore, if COX is basally active following MWCNT exposure, continued TXA2 release could result in coronary artery TP desensitization. In either case, the involvement of the ET-1/COX/TXA2 signaling axis may be a plausible mechanism to explain the depression of coronary flow during early reperfusion seen in the Langendorff isolated heart experiments in, following MWCNT exposure in Chapter 3.

4.5. Chapter 4 conclusion

Chapter 4 demonstrates that pulmonary exposure to MWCNT *in vivo* can promote alterations in coronary artery smooth muscle function capable of enhancing coronary arterial tone. Increased coronary tone, and thus increased coronary resistance, can impair perfusion to the myocardium. The heart is a metabolically active organ and specific adjustments in perfusion are both essentialand dependent upon precise responses of coronary arteries to local autocrine/paracrine agents. If coronary arteries are over-responsive following pulmonary exposure to MWCNT as Chapter 4 suggests, then perfusion supply and demand mismatching could occur in the myocardium and result in cardiac injury.

CHAPTER 5

PULMONARY EXPOSURE TO C60 PROMOTES EXPANSION OF CARDIAC I/R INJURY AND ENHANCES ET-1/COX MEDITATED STRESS PRODUCTION IN ISOLATED CORONARY ARTERY CONTRACTION

Acknowledgement

This chapter has been adapted from (160):

Thompson, L. C., Urankar, R. N., holland, N. A., Vidanapathirana, A. K., Plankenhorn, S., Han, L., Sumner, S. J., Lewin, A. H., Fennell, T. R., Lust, R. M., Brown, J. M., and Wingard, C. J. C60 exposure augments cardiac ischemia/reperfusion injury and coronary tone in Sprague-Dawley rats. Toxicol.Sci. (Resubmitted 11/8/2013)

5.1. Introduction

The heart may be susceptible to infarction in response to I/R injury following pulmonary exposure to multiple types of NP. We have previously reported that post-I/R myocardial infarction worsens in a dose- and time-dependent manner following intratracheal (IT) instillation of MWCNT(165), cerium oxide nanoparticles (176) or ultrafine particulate matter (36). Cardiovascular detriments associated with ultrafine particulate matter may result from pulmonary inflammation, oxidative stress or direct particle effects following translocation (27; 166). Exposure to NP can result in systemic release of IL-6, IL-1β and tumor necrosis factor-α, as well as increased release of ET-1(39; 44; 66; 130). Decreased release of nitric oxide and

hypercoagulability associated with exposure to ENP may contribute to impaired perfusion to zones of the myocardium, potentially increasing propensity for cardiac arrhythmia and myocardial infarction. In Chapters 3, MWCNT were shown to increase PVC in isolated hearts and depress coronary flow during post-ischemic reperfusion, ET-1 release during reperfusion and expansion of post-I/R myocardial infarction (159). Data collected in Chapter 4 data suggested that COX might contribute to enhanced coronary artery stress generation in response to ET-1 in LAD isolated from rats exposed to intratracheal MWCNT. It is not clear whether these cardiovascular endpoints are unique to pulmonary routes of exposure or only occur in response to MWCNT. In this chapter we will examine similar endpoints following exposure to a second carbon NP, C60.

C60 is a spherical carbon allotrope first generated synthetically in 1985 but has likely been produced naturally in Earth's environment for thousands of years, suggesting that human exposure to C60 is not necessarily a novel interaction (6). Synthetic production of C60 on a commercial scale has increased the probability of human exposures occupationally and potentially even environmentally (90). The growing number of industrial and medical applications for C60 are not surprising due to its unique physicochemical properties (115). The medicinal uses for C60 spur from its capacity to function as an antiviral, photosensitizer, antioxidant, drug/gene delivery device and contrast agent in diagnostic imaging (7). C60 have been found in occupational environments at concentrations of 23,856 – 53,119 particles/L air (79). Given this potential for humans to encounter C60, assessments of *in vitro* cytotoxicity (22; 78), *in vivo* biodistribution (90; 156), biopersistence (146) and adverse pulmonary responses to C60 have been conducted (6; 114; 126; 145). Despite the effort put into developing a

toxicological profile for C60, the potential impacts of C60 on the cardiovascular system have rarely been examined.

The purpose of this study was to examine cardiovascular detriments associated with different routes of exposure to C60 and to delineate the responses to C60 exposure in different genders. We examined the highest C60 concentration that we were able to achieve in solution (0.14 μg/μL). Here we delivered 28 μg of C60 total, either by intratracheal or intravenous instillation in rats, a mass smaller than others that have been characterized for C60 exposure in rats (146).

Based upon clinical findings associated with particulate matter exposure and our data with MWCNT, we hypothesized that I/R injury and pharmacological responses in isolated coronary arteries would depend upon the route of exposure and gender in rats instilled with C60.

5.2. Materials and Methods

5.2.1. 60-carbon fullerenes

C60 were formulated, characterized for zeta potential, and hydrodynamic sized by RTI International (Research Triangle Park, NC, USA). Dry C60 was purchased from Sigma-Aldrich (St. Louis, MO, USA; Cat # 379646). Due to its hydrophobicity, C60 was formulated with polyvinylpyrrolidone (PVP), and the dried pellets of C60/PVP were suspended in saline. We dissolved PVP in saline to 1.4% for vehicle samples. For more information about our formulation of C60 see the supplemental materials. PVP coated C60 (C60) and PVP vehicles (vehicle) were analyzed for zeta potential and hydrodynamic diameter using a Malvern Zetasizer NanoZS (Malvern Instruments, Worcestershire, UK) with a 633nm laser source, 173° detection angle, and a clear disposable zeta cell. The following protocol was used to characterize each suspension while at room temperature (25°C) and was designed to mimic the sample preparation for animal exposures. Sterile normal saline (250 μL) was added to the vial containing the C60 or vehicle pellets and the vial was immediately placed in the cup horn sonicator and the sample was sonicated at 50% amplitude to obtain total energy output of 8880 J. This process was repeated for two more vials. The contents of the three vials were combined, vortexed for 10 sec and delivered into the Malvern cell for measurement using a syringe. Size and zeta potential measurements were done using a Malvern disposable capillary cell (Malvern Instruments, #DTS1061C). Measurements were performed in sequence of (i) 1st size determination; (ii) zeta potential measurement; (iii) 2nd size determination to confirm particle size after zeta potential measurement. The sample cell remained undisturbed in the instrument throughout the three measurements, which took approximately 6-8 minutes each. All experiments were performed in triplicate.

5.2.2. Particle number assessment

C60 particle numbers were analyzed in solution by counting events in 10 µl of sample using a BD Accuri C6 flow cytometer (BD, San Jose CA, USA). Briefly samples were prepared as described above. Each sample was run through the flow cytometer to collect a total of 10 µl and analyzed for total events using BD Accuri C6 software with background events subtracted. Samples were analyzed on 3-4 separate runs with a cleaning cycle run between each sample measurement. Each measurement was multiplied by 20 to obtain the particle number delivered to each rat (10 µL x 20 = 200 µL). The mean of the triplicate measurement is reported.

5.2.3. Animals

Male and Female Sprague-Dawley rats were purchased from Charles River (Morrisville, NC, USA). Rats were 10-12 weeks of age at the time of purchase and housed in the Department of Comparative Medicine at East Carolina University. Each rat had access to standard laboratory chow and water *ad libitum* in a temperature regulated facility (23 ± 1°C) under 12:12 hour light-dark cycles. We provided each rat with a minimum of 5 days to acclimate prior to experimental manipulations. All use of rats in this study complied with protocols approved by the East Carolina University Institutional Animal Care and Use Committee.

5.2.4. Instillations

C60 were administered by intratracheal (IT) instillation of intravenous (IV) administration via the lateral tail vein. A 200 µL bolus was delivered to each rat while under Isoflurane anesthesia, 24 hours prior to cardiopulmonary assessments. After instillation, each rat was monitored until normal grooming habits resumed.

5.2.5. Bronchoalveolar lavage

Only animals used for isolated coronary artery wire myography were used for BAL analysis.Rats were anesthetized deeply with Isoflurane and a pneumothorax was induced. The heart was excised for coronary artery dissection and thoracic cage was removed for optimal visualization of the lungs, lower trachea and main bronchi. Connective tissue surrounding the lung was resected and the left main bronchus was ligated. A tracheotomy was performed allowing an 18 gauge angiocatheter to be inserted and secured with 2-0 suture. One bolus of Hanks balanced saline solution (23.1 mL/kg) was lavaged into the right lung three times successively. Recovered BAL fluid was centrifuged at 1000 x g for 10 minutes at 4°C. The BAL supernatant was used for protein quantification.

5.2.6. Differential cell counts

The cell pellets were resuspended in 1 mL of fresh Hanks balanced saline solution and total cell counts were determined with a Cellometer® Auto X4 (Nexcelom Biosciences, LLC., Lawrence, MA, USA). BAL fluid volumes containing 20,000 cells were centrifuged onto glass slides using a Cytospin IV (Shandon Scientific Ltd., Cheshire, UK) and stained via a three step hematology stain (Richard Allan Scientific, Kalamazoo, MI, USA). Cell differential counts were determined

microscopically based on hematologic stain and cellular morphology. A total of 300 cells per slide were counted to estimate cell percentage.

5.2.7. Protein quantification

BAL fluid protein quantification was performed using a standard Bradford protein assay. In short, BAL fluid proteins were quantified using 5 µL of sample diluted 250 µL of Bradford reagent in duplicate wells of using a 96 well plate. Absorbance values were read at 562 nm using a BIO-TEK® Synergy HT plate reader (Winooski, VT, USA) and data were analyzed with Gen5 software (BIO-TEK®). Absorbance values for each sample were compared to a standard curve generated using 2.0 - 0.0625 mg/mL bovine serum albumin.

5.2.8. Cardiac Ischemia/Reperfusion Injury *in situ*

Cardiac I/R and myocardial infarct size analysis were performed by modifying the protocol we have previously reported using mice (165). I/R experiments were conducted in a cohort of rats separate from those used for BAL, histology and coronary vascular studies. Twenty-four hours following exposure to C60 or vehicle, male and female rats were anesthetized by an intraperitoneal injection of ketamine/xylazine (85/15 mg/kg, respectively) and given supplemental injections throughout the procedure to maintain anesthesia. Body temperature was maintained at 37°C with a heating pad and TC-1000 Temperature Controller (CWE, Inc., Ardmore, PA, USA). Rats were intubated via tracheostomy with a 16 gauge angiocatheter and mechanically ventilated at 81 breaths/minute with 100% O_2 using a Harvard Inspira Advanced Safety Ventilator (Holliston, MA, USA). Male rats were ventilated with 3.0 mL tidal volumes and female rats were ventilated with 2.8 mL tidal volumes. A left parasternal thoracotomy was

performed and the pericardium was gently removed. The LAD was identified and ligated ~4 mm distal to its origin between the conus arteriosus and the left atrium with 6-0 prolene suture tied over polyethylene tubing. Effective occlusion of the LAD was confirmed visually by pallor distal to the ligature. After 20 minutes of ischemia the tubing was removed and reperfusion was allowed for 2 hours. One milliliter of blood was drawn from the inferior vena cava at the end of reperfusion for serum analysis.

5.2.9. Determination of post-I/R myocardial infarct size

Myocardial infarct size was determined by replacing the ligature at the original point of occlusion. The aortic arch was cannulated and 1% Evans blue dye was perfused retrograde to delineate the myocardium subjected to I/R from the myocardium perfused throughout the procedure. Hearts were excised and cut serially into 1 mm sections from the point of ligation to the apex. Sections were incubated for 20 minutes in 0.1 - 1.0% triphenyltetrazolium chloride solution to demarcate infarcted from non-infarcted tissue. Triphenyltetrazolium chloride is reduced enzymatically to a brick red color in viable tissue, while infarcted tissue remains pale. Both sides of all heart sections were digitally imaged. Image J software was downloaded from the National Institutes of Health website (http://rsbweb.nih.gov/ij/) and used to determine the size of the left ventricle, zone at risk and the area of infarction.

5.2.10. Post-ischemia/reperfusion cytokines

Post-I/R serum cytokine concentrations were analyzed using serum samples collected 24 hours following exposure to C60 or vehicle. Serum from male and female ratssubjected to I/R (Post-I/R) were tested for concentrations of IL-6, MCP-1 and vascular endothelial growth factor

(VEGF) using a custom Milliplex MAP Cytokine/Chemokine Panel and Immunoassay (EMD Millipore, Billerica, MA, USA). The assays were run according to the manufacturer's instructions. Assays were analyzed using a Luminex 200 (Luminex, Austin, TX, USA) and results reported using Luminex xPONENT® software version 3.1. Any sample concentration that fell below the detection limit of the assay was reported as 0 pg/mL.

5.2.11. Coronary artery isolation and vessel viability assessment

Isolated coronary artery smooth muscle assessments were conducted 24 hours after IT or IV exposure to C60 or vehicle in male and female rats not subjected to I/R. Rats were anesthetized deeply with Isoflurane and a pneumothorax was induced immediately. One milliliter of blood was drawn directly from the right ventricle of the heart for serum analysis and then each animal was exsanguinated by cutting the inferior vena cava. Coronary artery isolation was performed as we have previously described (159). The heart was excised and placed in cold physiological saline solution (PSS); [mM] 140.0 NaCl, 5.0 KCl, 1.6 $CaCl_2$, 1.2 $MgSO_4$, 1.2 MOPS, 5.6 D-glucose, and 0.02 EDTA (pH 7.4 @ 37°C). Paired segments of the LAD, ~1 mm in length, were dissected away from the left ventricle between the circumflex artery and the first major bifurcation of the LAD. Segments were mounted into chambers of a 610M multichannel wire myograph (DMT, Ann Arbor, MI, USA) using 0.04 mm diameter stainless steel wire. After a 45 minute equilibration period, length and lumen diameter were determined using the reticle micrometer of a stereo dissecting scope positioned over the chambers. Resting tension was established by determining diameter-tension relationships and setting each segment to 90% of the lumen circumference achieved at 13.3 kPa (67). An additional 45 minute equilibration period was allowed and then tissue viability was assessed by potassium depolarization for 7

minutes with 109 mM K^+PSS (Equal molar substitution of K^+ for Na^+). LAD segments were relaxed using successive washes with fresh PSS and endothelial integrity was tested by precontracting with 1.0 µM serotonin for 3 minutes followed by addition of 3.0 µM ACh. Each LAD segment was washed with fresh PSS every 10 minutes for 30 minutes before starting experimental pharmacology protocols. Myograph data was recorded in mN and was collected via computer using a PowerLab8/35 data acquisition interface (ADInstruments, Colorado Springs, CO, USA) and LabChart 7 Pro software (ADInstruments). Data from each vessel segment were normalized to the vessel surface area (length x 2 x width) to yield segment stress (mN/mm^2). LAD segments that generated less than 2.0 mN/mm^2 in response to K^+PSS, 1.0 mN/mm^2 in response to 1.0 µM serotonin or relaxed less than 70% of the serotonin precontraction were not considered viable and excluded from further study.

5.2.12. Pharmacology of the isolated coronary artery

LAD were evaluated using cumulative concentration-response protocols designed to test endothelial-dependent vasorelaxation, modified from Tawfik et al. (158). Paired LAD segments isolated from IT or IV exposed male and female rats were subjected to cumulative concentrations of serotonin (10 nM - 3.0 µM, 5-HT) and given 3 minutes to respond at each concentration before proceeding to the next concentration. The coronary artery vascular smooth muscle stress (mN/mm^2) generated in response to 5-HT of paired segments was averaged at each concentration for data reporting. Upon verifying stable tension after addition of the highest concentration of 5-HT, one of the paired segments was subjected to ACh (1.0 nM - 1.0 µM, ACh) to assess endothelial-dependent smooth muscle relaxation and the other segment was subjected to cumulative concentrations of the nitric oxide donor SNP (1.0 nM - 1.0 µM) to assess endothelial-

independent smooth muscle relaxation. Each LAD segment was given 3 minutes to respond at each concentration before proceeding to the next concentration.

5.2.13. Isolated coronary artery endothelin-1 responses

Coronary artery smooth muscle ET-1 responseswere conducted as we reported in Chapter 4. Following ACh and SNP protocols paired LAD segments from each group was subjected to ET-1 concentration-response experiments. These LAD segments were washed with fresh PSS every 10 minutes for a minimum of 30 minutes before starting ET-1 protocols. After confirming that basal resting tension had been reestablished, one of the paired LAD segments was incubated with 10 μM of the non-selective COX inhibitor Indomethacin (Sigma-Aldrich, St. Louis, MO, USA) for 20 minutes. Indomethacin remained in the preparation throughout the remaining protocol. ET-1was added cumulatively to each vessel chamber from 0.1 nM to 1.0 μM and given 7 minutes to respond at each concentration before the next concentration was applied.

5.2.14. Statistics

All data are expressed as mean ± SEM unless otherwise reported with significant P-values (< 0.05) marked. Graphpad Prism software (version 5, LaJolla, CA, USA) was used to graph and analyze all data. Cardiac I/R data were compared by ANOVA with Dunnett's Multiple Comparison post-tests. Isolated coronary artery vascular response curves were compared using Repeated Measures ANOVA with Bonferroni's post-tests and non-linear regression analysis of the 4 parameter best-fit values (103). Reported EC_{50} and Hillslope values were derived from normalized fits of each individual LAD concentration-response curve (0-100% of response) and were compared by t-test across treatment within delivery routes and by ANOVA against matched

treatments across delivery routes and naïve controls. Statistical power and group size were based on power analysis of our cardiac I/R experiments in order to understand variability in physiological mechanisms that may contribute to any myocardial vulnerability to infarction following C60 exposure.

5.3 Results

5.3.1. 60-carbon fullerene characterization

The physical characteristics of both PVP vehicle and C60/PVP suspensions are outlined in Table 5.1. The hydrodynamic size characteristics varied only slightly over a 38 minute testing period despite the fact that a zeta potential in the range of 0-5 mV is indicative of rapid flocculation or coagulation. The flowcytometery data indicated that there were approximately 25,791 ± 1351 particles of C60/10 µL of sample. This means that approximately 515,825 ± 27,014 C60 particles were delivered to each rat in the IT and IV C60 groups. If theC60/PVP particles are spherical, we can estimate that a particle surface area of 23.2 mm^2 was administered to each rat. Based on calculations, the dispersion of the PVP samples should equal 21.6 µg/µL and for C60 samples should equal 21.3 µg/µL.

Table 5.1 60-carbon fullerene particle characterization

Physical characterization ofC60 suspensions (mean ± SEM)	
Hydrodynamic size, nm	371 ± 0.6
Zeta potential	1.6 mV
Particle number (per per 10 µL)	25,791 ± 1351
Calculated surface area (per 10 µL)	11.15 mm^2

5.3.2. Bronchoalveolar lavage fluid analysis

BAL protein and differential cell counts for male rats are reported in Table 5.2. BAL protein and differential cell counts for female rats are reported in Table 5.2. Only two important differences were identified, including increased total protein concentrations ($P < 0.05$) in BAL fluid collected from male rats exposed to IV C60 compared to IT C60 exposed males, and increased number of eosinophils in BAL fluid collected from IT C60 females compared to IT vehicle females.

Table 5.2 Bronchoalveolar lavage from 60-carbon fullerene studies male rats

	Total Bronchoalveolar Lavage Fluid (BALF) Protein and Cellularity											
	BAL samples collected 24 hrs following exposure in males, data expressed as mean ± SEM											
	Protein (µg/mL)		Cell Number (x 10^5)		Macrophages (x 10^5)		Neutrophils (x 10^3)		Eosinophils (x 10^3)		Epithelial Cells (x 10^3)	
	IT	IV	IT	IV	IT	IV	IT	IV	IT	IV	IT	IV
Vehicle	560 ± 149	638 ± 100	5.7 ± 1.4	3.5 ± 0.9	5.3 ± 1.3	5.7 ± 0.7	14.2 ± 10	2.1 ± 0.3	1.9 ± 1.1	2.4 ± 2.4	6.6 ± 2.4	1.7 ± 1.7
C60	316 ± 55	750 ± 138*	3.9 ± 0.8	6.9 ± 1.7	4.0 ± 0.7	2.5 ± 1.2	13.3 ± 12	1.7 ± 1.4	0.5 ± 0.5	<1	2.8 ± 0.3	8.2 ± 2.6
n	4-5		4-6		3-5		3-5		3-5		3-5	

*** P < 0.05 vs. IT C60**

Table 5.3 Bronchoalveolar lavage from 60-carbon fullerene studies female rats

	Total Bronchoalveolar Lavage Fluid (BALF) Protein and Cellularity											
	BAL samples collected 24 hrs following exposure in females, data expressed as mean ± SEM											
	Protein (µg/mL)		Cell Number (x 10^5)		Macrophages (x 10^5)		Neutrophils (x 10^3)		Eosinophils (x 10^3)		Epithelial Cells (x 10^3)	
	IT	IV	IT	IV	IT	IV	IT	IV	IT	IV	IT	IV
Vehicle	252 ± 28	195 ± 8.2	7.8 ± 1.9	4.1 ± 0.6†	1.6 ± 0.9	3.3 ± 0.4	35.0 ± 25.3	<1	0.25 ± 0.25*	1.7 ± 1.7	132 ± 90	346 ± 132
C60	206 ± 24	226 ± 41	7.1 ± 1.2	3.5 ± 0.5*	0.9 ± 0.3	3.1 ± 1.1	27.5 ± 11.1	<1	12.5 ± 7.5	3.6 ± 0.6	75.0 ± 32.8	362 ± 59*
n	5-6		4-6		4-6		4-6		4-6		4-6	

*** P < 0.05 vs. IT C60, †P < 0.05 vs. IT vehicle**

5.3.3. Cardiac ischemia/reperfusion injury

The impact of IT or IV exposure to C60 on cardiac I/R injury in male and female rats is represented in Figure 5.1. Following I/R we found expansion of myocardial infarction in male rats exposed to C60 suspensions when compared to the infarct size measured in the vehicle groups. Male rats demonstrated no significant differences between the extent of I/R injury across IT or IV exposure routes. Female rats also suffered myocardial infarct expansions following I/R in both C60 exposed groups compared to infarct sizes in hearts from vehicle groups. Female rats did show significantly larger myocardial infarctions following IT exposure to C60 as compared to IV exposure to C60.

Figure 5.1 Cardiac ischemia/reperfusion injury with 60-carbon fullerene exposure

Male and Female rats were subjected to regional cardiac I/R (20/120 minute) injury *in situ,* 24 hrs following intratracheal (IT) or intravenous (IV) delivery of C60 or vehicle. In either case C60 exposure exacerbated myocardial infarction. Within each delivery route, infarct sizes in the male groups were larger than those in females. Between delivery routes, the females had larger infarctions in response to IT C60 exposure compared to IV exposure. *P < 0.05 by two-way ANOVA, N = 4-5

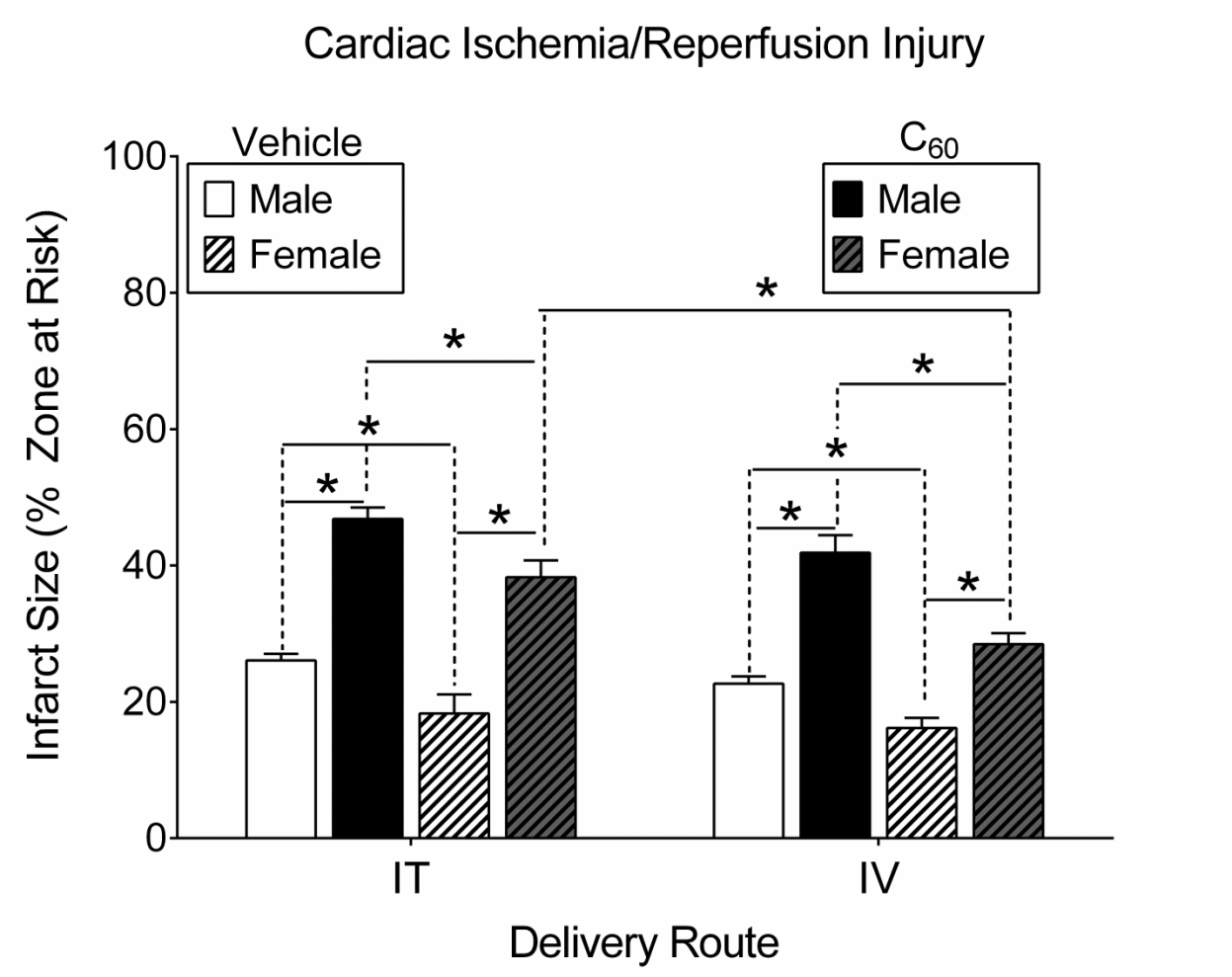

5.3.4. Post-I/R serum cytokines

The influence of IT or IV exposure to C60 on post-I/R concentrations of serum IL-6, MCP-1 and VEGF from male and female rats is presented in Figure 5.2. IL-6 concentrations were greater in serum collected post-I/R from male rats exposed to IV C60 when compared to serum collected from male rats exposed to IV vehicle and male rats exposed to IT C60 (Figure 5.2A). Female rats exposed to IV C60 had significantly lower serum IL-6 concentrations than IV C60 exposed males. Serum IL-6 concentrations were unaltered between all IT groups and IV exposed females. MCP-1 showed a similar profile to IL-6. MCP-1 concentrations were greater in serum collected post-I/R from male rats exposed to C60 IV when compared to serum collected from male rats exposed to IV vehicle, male rats exposed to IT C60 and female rats exposed to C60 IV (Figure 5.2B). Female rats exposed to IV C60 had significantly lower serum MCP-1 concentrations than IV C60 exposed males. Serum MCP-1 concentrations were unaltered between all IT groups and IV exposed females. VEGF was variable and slightly elevated in females exposed to IT and IV C60, though not significantly different than any other group (Figure 5.2C).

Figure 5.2 Post-ischemia/reperfusion serum cytokine concentrations

Serum samples were collected from male or female rats subjected to cardiac I/R injury, 24 hrs following intratracheal (IT) or intravenous (IV) delivery of C60 or vehicle. (A) Interleukin-6 (IL-6) concentrations were significantly higher in serum collected from male rats exposed to IV C60 compared to male IV vehicle, male IT C60, and female IV C60. (B) Monocyte chemotactic protein-1 (MCP-1) concentrations were also increased in serum collected from male rats exposed to IV C60 compared to male IV vehicle, male IT C60, and female IV C60. (C) Vascular endothelial growth factor (VEGF) concentrations were similar in serum collected from all groups. *P <0.05 by two-way ANOVA, N = 3-4.

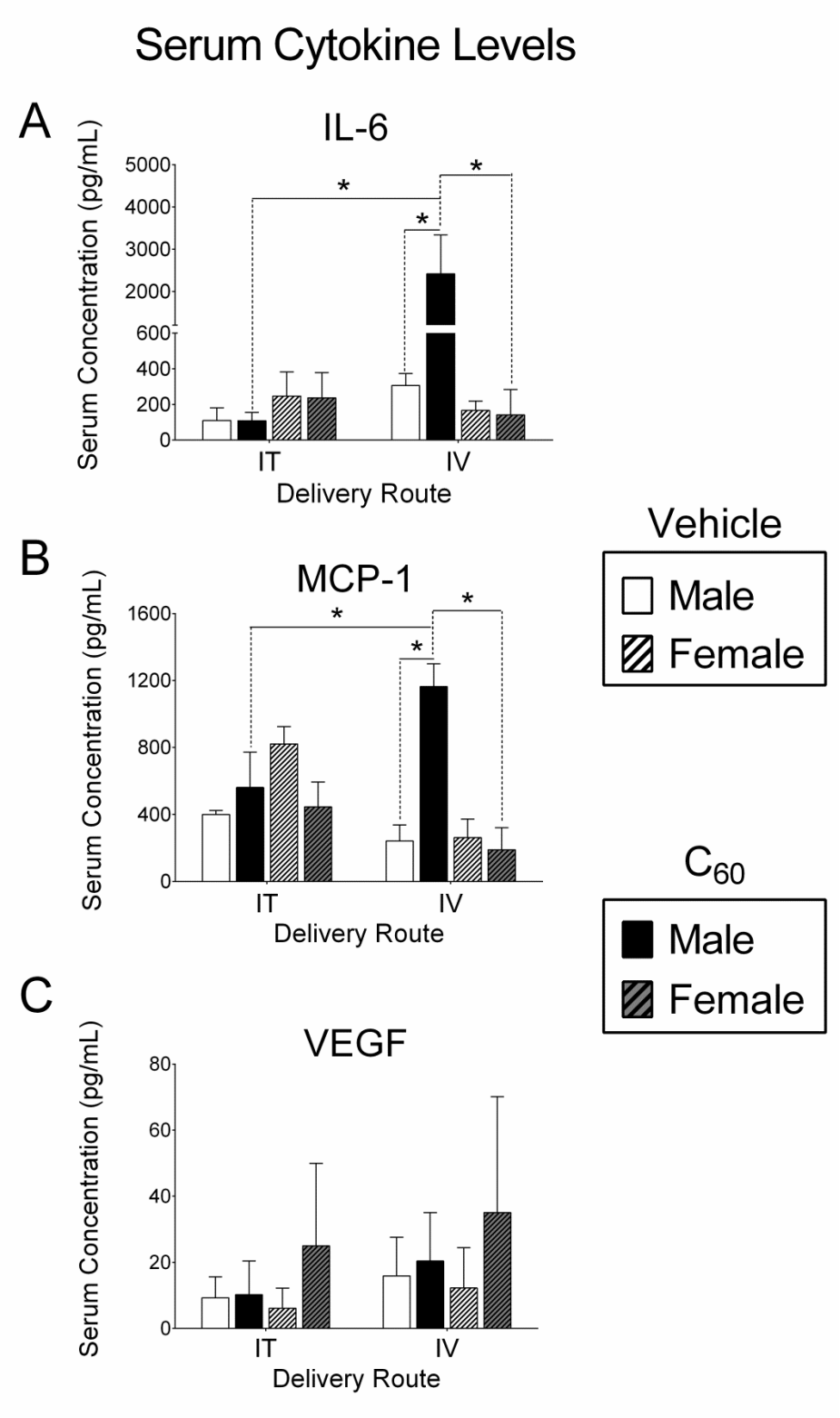
Serum Cytokine Levels
A
IL-6
Serum Concentration (pg/mL)
5000
4000
3000
2000
600
400
200
0
*
*
*
IT
IV
Delivery Route
B
MCP-1
Serum Concentration (pg/mL)
1600
1200
800
400
0
*
*
*
IT
IV
Delivery Route
C
VEGF
Serum Concentration (pg/mL)
80
60
40
20
0
IT
IV
Delivery Route
Vehicle
Male
Female
C60
Male
Female

5.3.5. Male rat coronary artery pharmacology

Pharmacological response curves generated in coronary artery (LAD) segments isolated from male rats 24 hrs after exposure to IT and IV administration of C60 or vehicle suspensions are shown in Figure 5.3. The associated EC_{50}values are reported in Table 5.4 and associated Hillslope values are reported in Table 5.5. LAD isolated from male rats exposed to IT C60 showed vascular smooth muscle stress (mN/mm^2) generation curves for 5-HT trending toward ($P = 0.06$) a leftward shift (*i.e.* sensitization) compared to the vehicle group (Figure 5.3A). Stress response curves for 5-HT were not altered in LAD isolated from male rats treated with IV C60 or vehicle (Figure 5.3B). ACh vascular smooth muscle relaxation responses were not different between LAD isolated from male rats exposed to IT C60 and vehicle (Figure 5.3C). The LAD from IV C60 exposed males yielded an ACh vascular smooth muscle relaxation response curve with significantly different best-fit values than the curve generated by LAD isolated from vehicle exposed males, despite the overall variability ACh sensitivity (Figure 5.3D). As indicated in Table 3, IT vehicle and IT C60 ACh EC_{50}s from male rats were significantly higher than those from naïve males. The ACh response curve produced by LAD from IV vehicle exposed males was not different from ACh responses in LAD isolated from naïve controls (curves not shown). Vascular smooth muscle relaxation curves generated by LAD in response to SNP were not different between IT exposed males (Figure 5.3E) or IV exposed males (Figure 5.3F).

Figure 5.3 Coronary artery pharmacology in male rats

Segments of the coronary artery (LAD) were isolated from male rats 24 hrs following intratracheal (IT) or intravenous (IV) delivery of C60 or vehicle. (A) Cumulative concentration-response curves for serotonin (5-HT) revealed a trend for sensitized vascular smooth muscle contraction in coronary arteries from IT C60 exposed rats, which were not seen following IV delivery of C60. (B) Cumulative concentration-response curves for 5-HT in coronary artery smooth muscle of LAD segments isolated from IV exposed rats. (C) Cumulative concentration-response curves for acetylcholine (ACh) showed no changes following IT exposure. (D) The IV C60 ACh curve was rightward shifted compared to the vehicle curve. (E) Cumulative concentration-response curves for sodium nitroprusside (SNP) were similar between vehicle and C60 groups following IT exposure and IV exposure. (F) Cumulative SNP concentration-response curves from LAD isolated from IV exposed rats. †for $P < 0.05$ by regression analysis of best-fit curve values. Reported P-values for ΔEC_{50} were determined by t-test, N = 4-5.

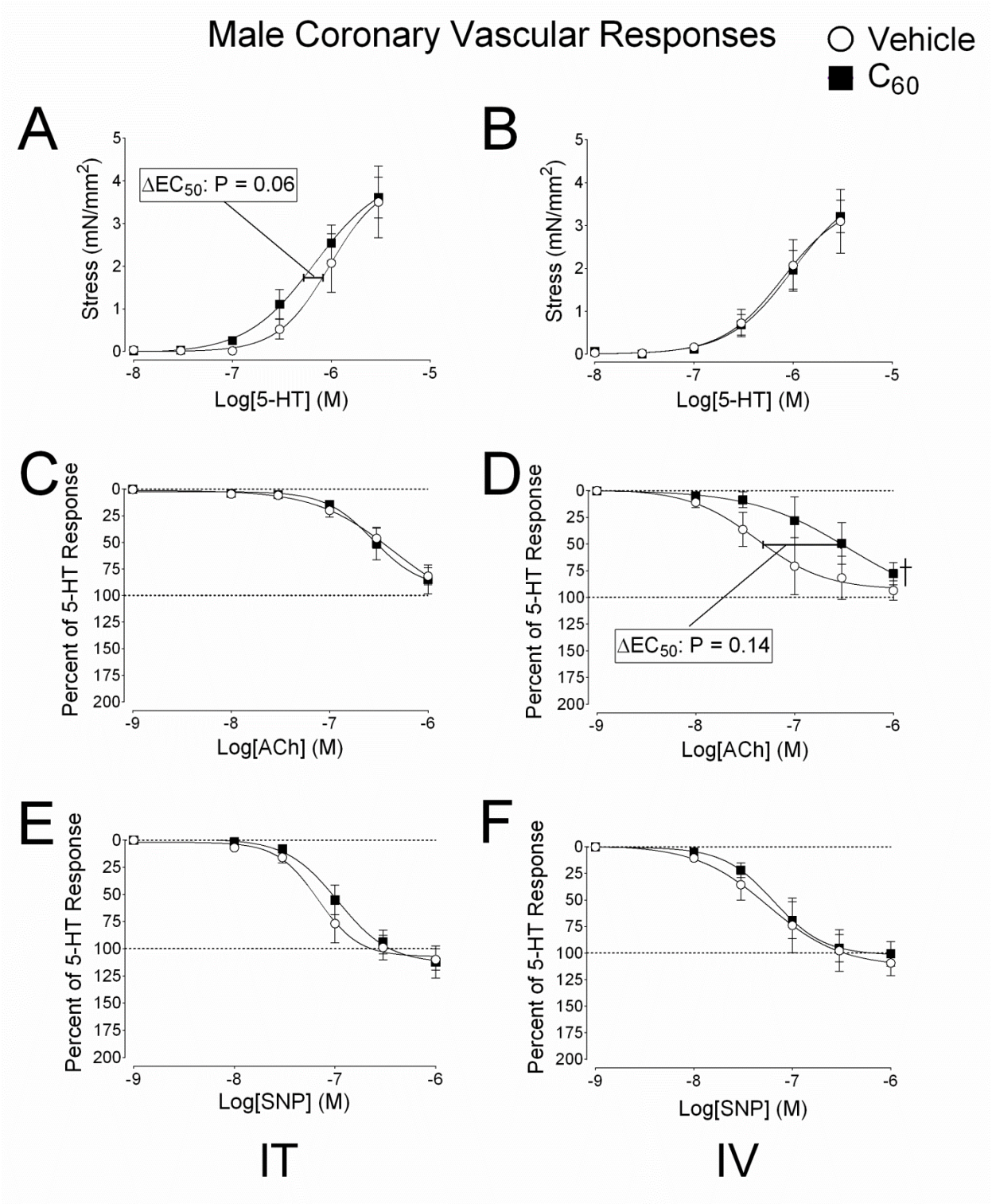
Male Coronary Vascular Responses
Vehicle
C60
A
Stress (mN/mm2)
ΔEC50: P = 0.06
Log[5-HT] (M)
B
Stress (mN/mm2)
Log[5-HT] (M)
C
Percent of 5-HT Response
Log[ACh] (M)
D
Percent of 5-HT Response
ΔEC50: P = 0.14
Log[ACh] (M)
E
Percent of 5-HT Response
Log[SNP] (M)
IT
F
Percent of 5-HT Response
Log[SNP] (M)
IV

Table 5.4 Male rat coronary artery EC_{50}s from 60-carbon fullerene studies

	Male Rat EC_{50}s [nM] (mean ± SEM)					
	Intratracheal (IT) Delivery			Intravenous (IV) Delivery		
	C60	Vehicle	P-Value, n	C60	Vehicle	P-Value, n
5-HT	559 ± 104	871 ± 130	0.06, 4	766 ± 113	675 ± 59	0.25, 4
ACh	265 ± 45	239 ± 34	0.33, 4	231 ± 80	97 ± 69	0.14, 4
SNP	116 ± 24	76 ± 18	0.13, 4	76 ± 21	104 ± 53	0.32, 4
ET-1	38 ± 20	48 ± 15	0.49, 6	26 ± 18	113 ± 86	0.35, 5

Table 5.5 Male rat coronary artery Hillslopes from 60-carbon fullerene studies

	Male Rat Hillslope Values (mean ± SEM)					
	Intratracheal (IT) Delivery			Intravenous (IV) Delivery		
	C60	Vehicle	P-Value, n	C60	Vehicle	P-Value, n
5-HT	1.7 ± 0.1	3.2 ± 0.7	0.10, 4	2.0 ± 0.2	1.9 ± 0.1	0.57, 4
ACh	2.6 ± 0.4	1.7 ± 0.1	0.10, 4	3.8 ± 0.8	1.8 ± 0.1	0.09, 3-4
SNP	2.4 ± 0.6	2.2 ± 0.3	0.77, 4	2.1 ± 0.3	1.9 ± 0.1	0.50, 4
ET-1	1.3 ± 0.2	1.0 ± 0.05	0.09, 6	1.1 ± 0.1	1.0 ± 0.2	0.67, 5

5.3.6. Female rat coronary artery pharmacology

Pharmacological response curves generated in coronary artery (LAD) segments isolated from female rats 24 hrs after exposure to IT and IV administration of C60 or vehicle suspensions are shown in Figure 5.4. The associated EC_{50} are reported in Table 5.6 and Hillslope values are reported in Table 5.7. Stress generation curves for 5-HT were not significantly different between LAD isolated from female rats exposed to IT C60or vehicle (Figure 5.4A). LAD vascular smooth muscle stress generationin response to 5-HT wasnot different between LAD from the female IV C60 or IV vehicle groups (Figure 5.4B). Vascular smooth muscle relaxation in response to ACh was not different between LAD isolated from female rats exposed to IT C60 orIT vehicle (Figure 5.4C). The vascular smooth muscle relaxation response curves for ACh appeared to show a desensitization in the LAD from IV C60 exposed femalesbut the responses were not statistically different from females exposed to IV vehicle (Figure 5.4D). The best-fit values for the vascular smooth muscle relaxation curve for SNP in IT C60 exposed females were

significantly differentthan those from coronary arteries isolated from IT vehicle exposed females (Figure 5.4E). SNP smooth muscle relaxation responses in isolated coronary artery segments isolated from IV C60 exposed females were only slightly leftward shifted compared to coronary artery segments from IV vehicle exposed females (Figure 5.4F).

Figure 5.4 Coronary artery pharmacology in female rats

Segments of the coronary artery (LAD) were isolated from female rats 24 hrs following intratracheal (IT) or intravenous (IV) delivery of C60 or vehicle. (A) Cumulative concentration-response curves for serotonin (5-HT) mediated vascular smooth muscle contraction in LAD from IT C60 exposed rats. (B) Cumulative concentration-response curves for 5-HT in coronary artery smooth muscle of LAD segments isolated from IV exposed rats. (C) Cumulative concentration-response curves for acetylcholine (ACh) showed no changes following IT exposure. (D) The IV C60 ACh curve a slight rightward shifted compared to the vehicle curve. (E) Cumulative concentration-response curves for sodium nitroprusside (SNP) showed less smooth muscle relaxation in LAD isolated fromIT C60 compared to IT vehicle groups. (F) Cumulative SNP concentration-response curves from LAD isolated from IV exposed rats showed slight leftward shifts in EC_{50} from LAD coronary artery smooth muscle relaxation responses from C60 exposed females compared to the IV vehicle curves. †for $P < 0.05$ by regression analysis of best-fit curve values. Reported P-values for ΔEC_{50} were determined by t-test, N = 4-5.

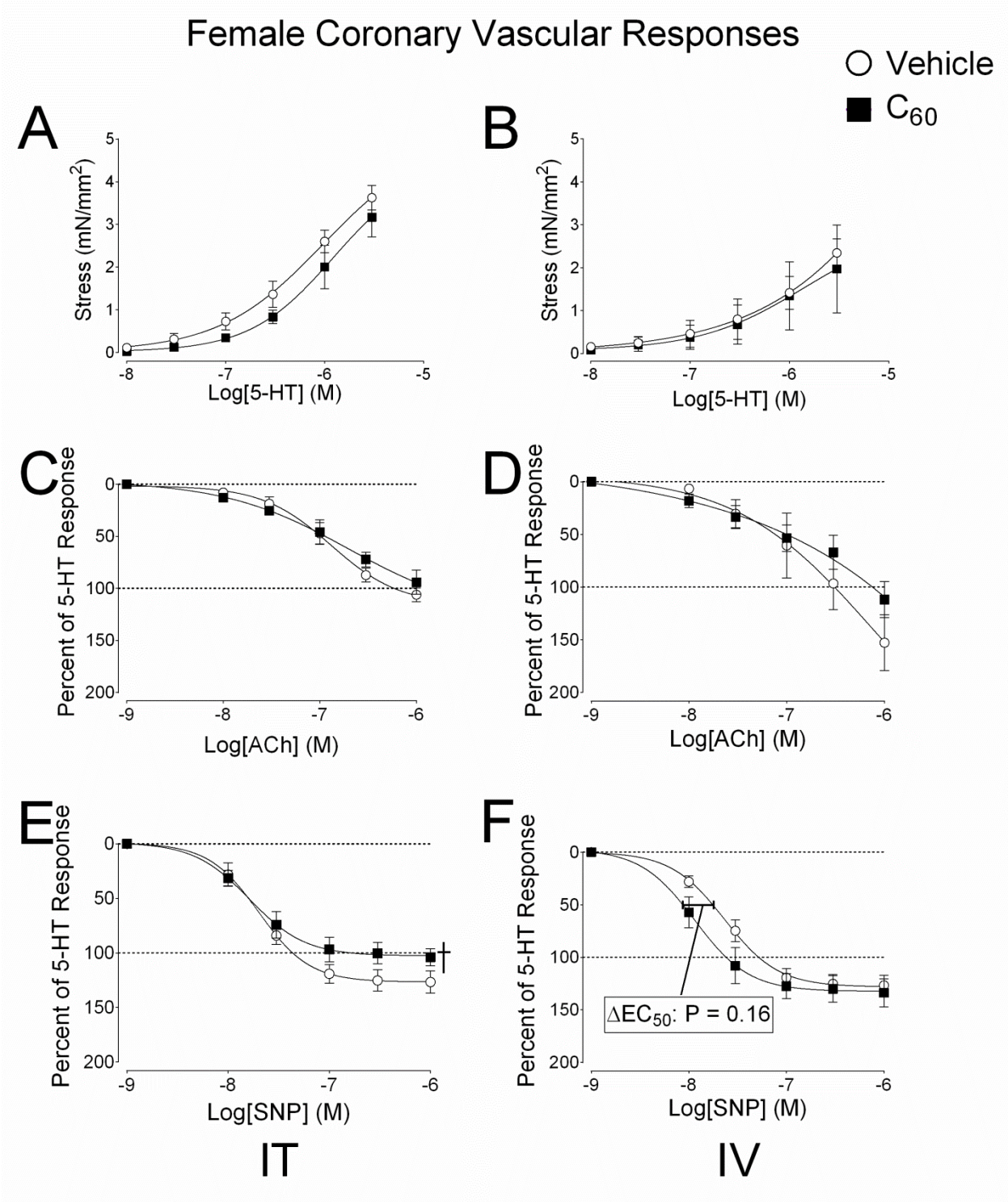
Female Coronary Vascular Responses
Vehicle
C60
A
Stress (mN/mm2)
Log[5-HT] (M)
B
Stress (mN/mm2)
Log[5-HT] (M)
C
Percent of 5-HT Response
Log[ACh] (M)
D
Percent of 5-HT Response
Log[ACh] (M)
E
Percent of 5-HT Response
Log[SNP] (M)
IT
F
Percent of 5-HT Response
ΔEC50: P = 0.16
Log[SNP] (M)
IV

Table 5.6 Female rat coronary artery EC_{50}s from 60-carbon fullerene studies

	Female Rat EC_{50}s [nM] (mean ± SEM)					
	Intratracheal (IT) Delivery			Intravenous (IV) Delivery		
	C60	Vehicle	P-Value, n	C60	Vehicle	P-Value, n
5-HT	813 ± 128	1268 ± 497	0.40, 5	932 ± 156	990 ± 275	0.86, 5
ACh	1419 ± 843	139 ± 28	0.16, 5	619 ± 233	1085 ± 558	0.46, 5
SNP	19 ± 3	21 ± 4	0.64, 5	14 ± 4	24.1 ± 4.1	0.16, 5
ET-1	29 ± 20	6.5 ± 2.4	0.31, 5	13 ± 7	23 ± 16	0.56, 5

Table 5.7 Female rat coronary artery Hillslopes from 60-carbon fullerene studies

	Female Rat Hillslope Values (mean ± SEM)					
	Intratracheal (IT) Delivery			Intravenous (IV) Delivery		
	C60	Vehicle	P-Value, n	C60	Vehicle	P-Value, n
5-HT	1.4 ± 0.4	1.0 ± 0.2	0.39, 5	1.3 ± 0.4	1.3 ± 0.2	0.95, 5
ACh	1.0 ± 0.4	1.6 ± 0.3	0.29, 5	1.0 ± 0.2	1.7 ± 0.5	0.19, 5
SNP	1.6 ± 0.3	2.1 ± 0.4	0.35, 4	2.0 ± 0.3	1.9 ± 0.3	0.79, 5
ET-1	1.4 ± 0.3	1.1 ± 0.3	0.41, 5	1.1 ± 0.2	1.0 ± 0.2	0.67, 5

5.3.7. Male and female coronary artery responses to endothelin-1

Vascular smooth muscle contraction responses to ET-1 are shown in Figure 5.5 for LAD segments isolated from male and female rats exposed to IT or IV C60 and vehicle. EC_{50} and Hillslope values for ET-1 concentration-response curves are also provided in Tables 5.4 and 5.5 for LAD collected from male rats and Tables 5.6 and 5.7 for LAD collected from female rats. Male rats instilled with C60 IT demonstrated enhanced stress in response to ET-1 compared to vehicle (Figure 5.5A). This response was not seen in male rats following IV C60 exposure (Figure 5.5B) or female rats instilled with C60 IT (Figure 5.5C) or C60 IV (Figure 5.5D).

Figure 5.5 Male and female coronary artery responses to endothelin-1

Segments of the coronary artery were isolated from male and female rats 24 hrs following ITor IV delivery of C60 or vehicle. (A) Cumulative concentration-response curves for ET-1 showed enhanced stress generation during isometric vascular smooth muscle contraction in LAD from IT C60 instilled male rats compared to vehicle. (B) Cumulative concentration-response curves for ET-1 stress generation during isometric vascular smooth muscle contraction in LAD from IV C60 or vehicle instilled male rats. (C) Cumulative concentration-response curves for ET-1 stress generation during isometric vascular smooth muscle contraction in LAD from IT C60 instilled female rats. (D) Cumulative concentration-response curves for ET-1 stress generation during isometric vascular smooth muscle contraction in LAD from IV C60 instilled female rats. †for $P < 0.05$ by regression analysis of best-fit curve values. N = 5-6.

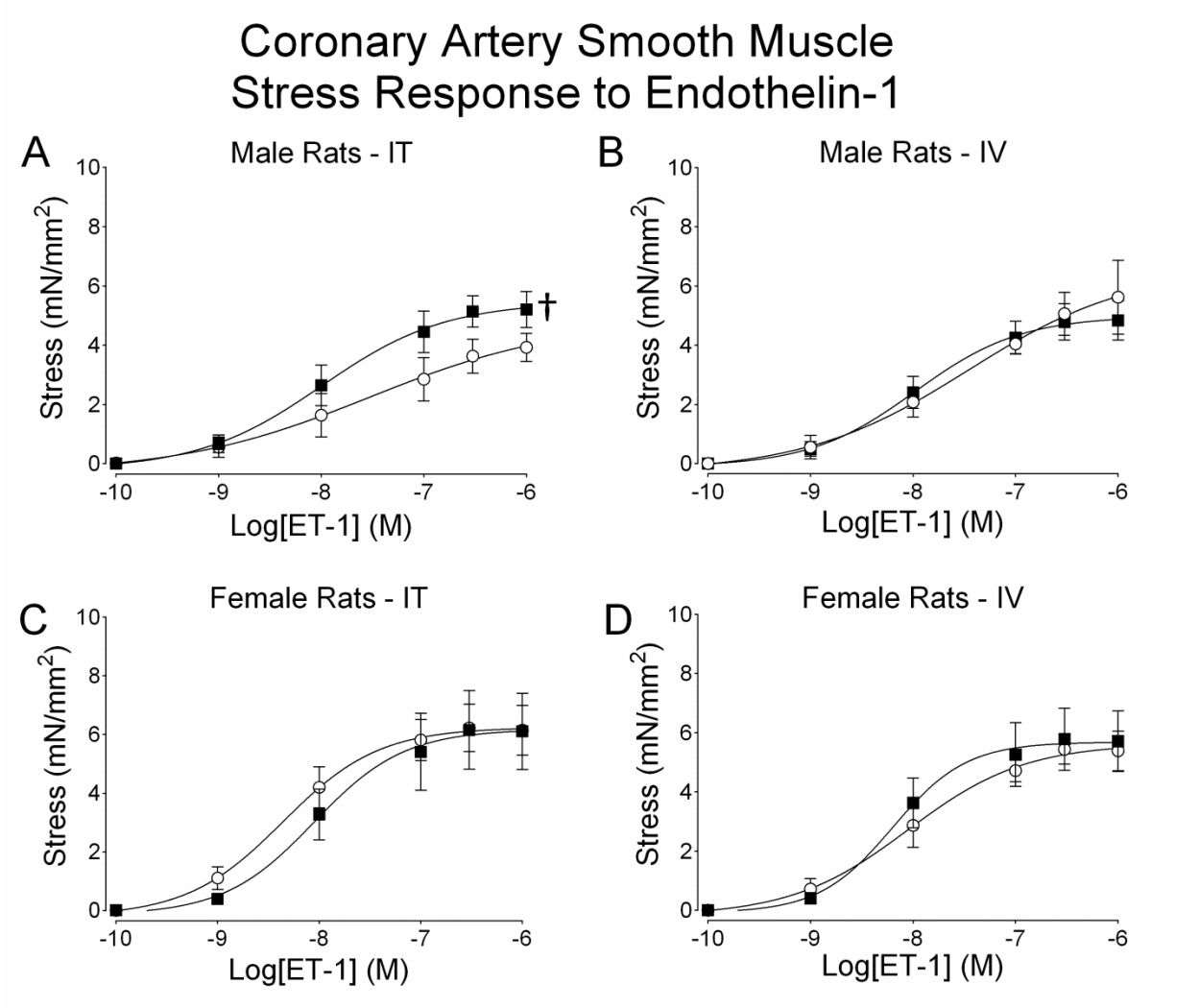
Coronary Artery Smooth Muscle
Stress Response to Endothelin-1
A
Male Rats - IT
B
Male Rats - IV
C
Female Rats - IT
D
Female Rats - IV
Stress (mN/mm2)
Log[ET-1] (M)
†

5.3.8. Indomethacin-sensitive coronary artery responses to endothelin-1. The ability of Indomethacin, a general COX inhibitor, to influence ET-1 mediated isometric stress (mN/mm^2) generation in LAD isolated from male rats exposed to IT C60is depicted in Figure 5.6. LAD segments isolated from rats exposed to C60 generated more stress in response to ET-1 than LAD collected from vehicle exposed rats (Figure 5.6A). Enhanced stress was lower in paired LAD isolated from C60 exposed rats that were incubated with 10 μM Indomethacin, a general COX inhibitor, for 20 minutes immediately prior to ET-1 protocols (Figure 5.6B). LAD collected from vehicle instilled rats did not show sensitivity to Indomethacin inhibition of COX during ET-1 mediated vascular smooth muscle contractionbut Indomethacin inhibition was able to restore the C60 stress generation response to ET-1 to the level of the vehicle group (Figure 5.6C).

Figure 5.6 Indomethacin-sensitive coronary artery responses to endothelin-1

Segments of the coronary artery were isolated from male rats 24 hrs following IT delivery of C60 or vehicle. Paired LAD segments isolated from each of the IT exposed male rats were also treated with 10 μM Indomethacin, a general COX inhibitor, 20 minutes prior to ET-1 administration. (A) Cumulative concentration-response curvesdeveloped in response to ET-1 revealed enhanced isometric stress generation in coronary arteries from C60 exposed rats when compared to vehicle. (B) Coronary segments isolated from C60 exposed rats showed sensitivity to Indomethacin during cumulative concentration-responses to ET-1 when compared to vehicle. (C) Data combined from vehicle and C60 groups during ET-1/Indomethacin experiments showed that LAD isolated from vehicle instilled rats were not sensitive to Indomethacin during cumulative concentration-responses to ET-1 and that Indomethacin restored LAD smooth muscle contractile response from IT C60 exposed rats to the level of those from the vehicle group. †for $P < 0.05$ by regression analysis of best-fit curve values, * for $P < 0.05$ by Repeated Measures ANOVA on matching concentration data points, $N = 6$.

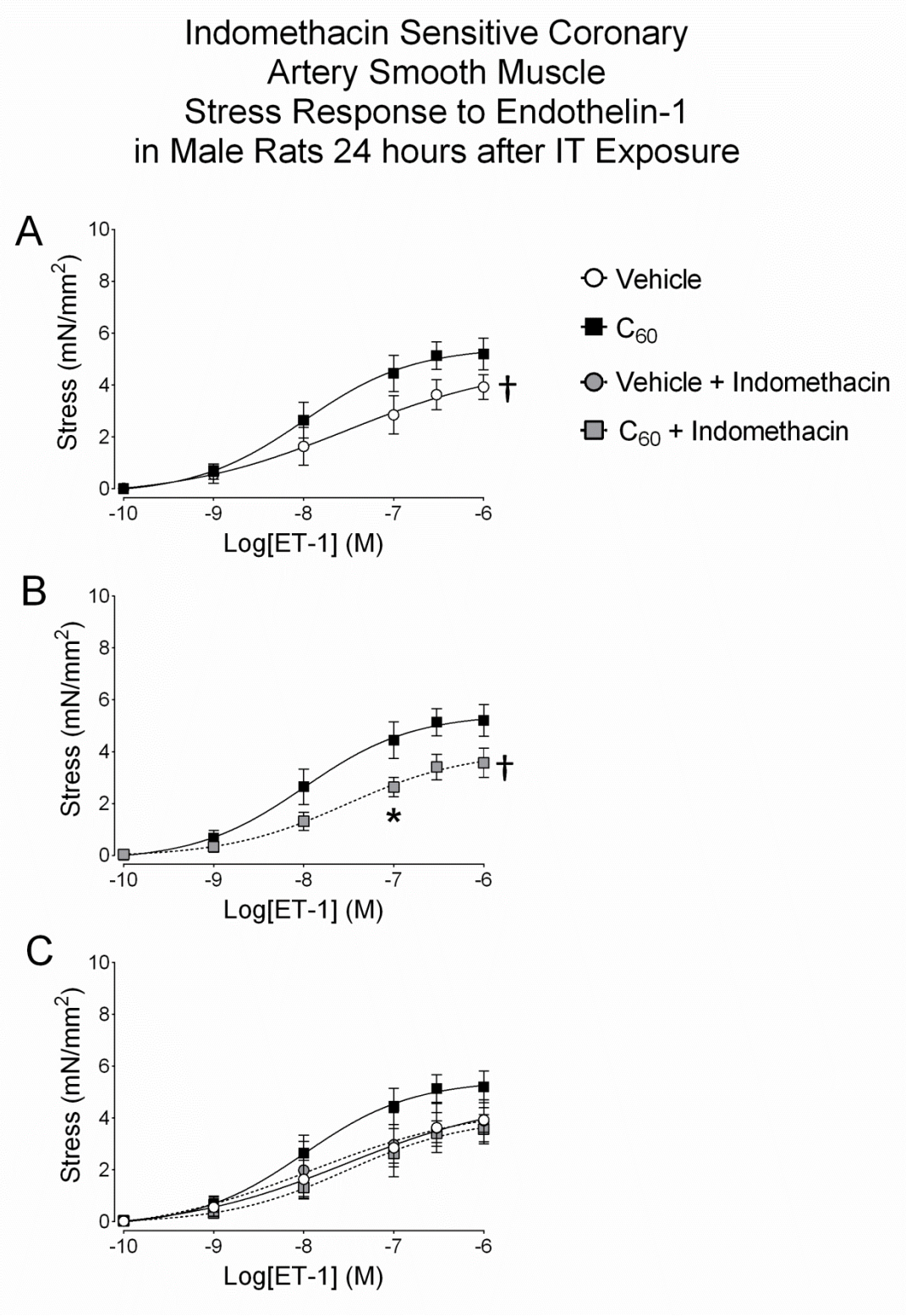
Indomethacin Sensitive Coronary
Artery Smooth Muscle
Stress Response to Endothelin-1
in Male Rats 24 hours after IT Exposure
A
B
C
Stress (mN/mm2)
Log[ET-1] (M)
Vehicle
C60
Vehicle + Indomethacin
C60 + Indomethacin
†
*

5.4. Discussion

This study demonstrated that IT C60 exposure of Sprague-Dawley rats resulted in deleterious cardiovascular consequences. This included C60 induced expansion of myocardial infarction following cardiac I/R and enhancement of ET-1 mediated stress generation of isolated segments of the LAD, potentially indicative of increased coronary vascular resistance. These results align with the paradigm that pulmonary exposure to nanosized particles has the potential to generate cardiovascular impairments (16; 105; 109; 144) and supports our previous report that enhanced coronary artery tone following IT exposure to engineered carbon nanomaterials may exacerbate cardiac I/R injury (159). The present study goes further to demonstrate that IT exposure to C60 may generate cardiovascular detriments via mechanisms unique from those produced by IV exposure to C60. While expansion of post-I/R myocardial infarction resulted from both IT and IV exposure to C60, our study uncovered impairment of ACh mediated coronary artery relaxation, increased serum IL-6 and serum MCP-1 associated with IV C60 exposure and not IT C60 exposure in male rats. This study also offers other evidence of potential importance in that female rats were more susceptible to I/R injury following IT C60 exposure than they were following IV C60 exposure, a trend that did not emerge in male rats. Female rats also showed C60 exposure route sensitivity in coronary artery relaxation responses for SNP. The diminished SNP response in the female IT C60 group was not seen in the female IV C60 group. The female IT C60 group also had significant eosinophilia when compared to the IT vehicle female group. These findings provide a possible explanation for why infarct sizes were larger in the female IT C60 group than infarcts in the female IV C60 group. These types of gender sensitivities to nanomaterials are not well understood and may be an important area for future research.

C60 fullerene is emerging as an advantageous engineered nanoparticle due to its highly modifiable structure, potentially providing it with countless applications in material science (110), optics, cosmetics (163), electronics, green energy (115) and medicine (50). With C60 use increasing, the toxicological and regulatory communities have been investigating the potential adverse impacts associated with C60 exposure, bringing into question potential routes of exposure and use of comparable doses. Pulmonary exposure is expected to occur in occupations requiring direct work with raw C60. In occupational settings C60 have been detected at concentrations ranging from 23,856 - 53,119 particles/L air (79). Considering that humans breathe between 360 - 600 L of air an hour, even a brief 1 hour occupational inhalation exposure could deposit 8,500,000 - 31,500,00 C60 particles into the lungs. We delivered 515,825 ± 27,014 C60 particles to each rat in the C60 groups from our study. Given the size difference between rats and humans, the 28 μg C60 burden we administered to each rat was relatively large, but comparable to potential human doses.

Studies have shown that IT instillation of 100 μg C60 in rats resulted in a pulmonary burden half-life of about 15 days (146) and minimal pulmonary inflammation 3 days after exposure (126). The medical applications of C60 suggest that IV exposure in humans is likely. In a study where C60 was administered IV to male rats once per day for four days (approximately 929 μg C60 total), C60 accumulation in the lungs was prominent from 1 day post-exposure out to 28 days post-exposure (90). Another IV study on the biodistribution of radiolabeled C60 in pregnant and lactating rats showed moderate accumulation of C60 in the lungs (156). We delivered 28 μg of C60 per rat in this study (93.33 μg/kg based on a 300 g rat). This exposure mass is comparable and often times lower than the doses of other C60 studies cited. Though we

found an increase in eosinophils in the female IT C60 group compared to the female IT vehicle group, our study falls in line in line with many of those studies supporting the possibility that C60 delivered IT or IV may produce minimal pulmonary inflammation, if any.

Despite the various investigations into pulmonary and *in vitro* responses to C60, examinations of cardiovascular impacts are scarce. The model of *in situ* cardiac I/R injury used in this study has been well established in our laboratory as a toxicological endpoint following pulmonary exposure to various types of ultrafine and nanosized particles (36; 82; 165). Here we tested the hypothesis that pulmonary exposure to C60 would result in expansion of myocardial infarction in rats subjected to cardiac I/R injury 24 hours post-exposure. Our results maintain that IT exposure to nanoparticles exacerbates myocardial infarction in a male rat model. We further tested the possibility that route of exposure may uniquely alter the I/R injury between IT and IV exposure to C60. This did not appear to be the case in male rats as shown in Figure 7. However the extent of post-I/R myocardial infarction in female rats was significantly larger in the IT C60 exposed female group compared to the IV C60-exposed female group, suggesting that gender may influence the biological response to C60 exposure.

Though post-I/R myocardial infarct sizes were not greatly different between IT and IV C60 exposed males, serum IL-6 and MCP-1 concentrations were significantly elevated post-I/R in the IV C60 group compared to the IT C60 group. It is unclear if these elevated serum components found after cardiac I/R contributed to the infarct expansion or were merely a reflection of the infarct size. Further, it is unclear as to why male rats produced an IL-6/MCP-1 response following I/R in the IV C60 group but the female group did not. We can speculate that perhaps a

link between cardioprotection and estrogen may also contribute to reduced IL-6 and MCP-1 release in response to cardiac I/R. In any case, IL-6 and MCP-1 have each been linked to impaired fibrinolysis/hemostasis following exposure to particulate matter (20; 48), which can promote thrombi-dependent zones of no reflow in the myocardium during I/R and exacerbate infarction. IL-6 is associated with acute myocardial infarction (3) and promotes the release of C-reactive protein, an acute-phase protein linked to myocardial infarction and increased production of MCP-1 (142). MCP-1 is involved in neutrophil and macrophage recruitment into the myocardial risk area following I/R, and the release of MCP-1 following I/R injury has been implicated in diminished vagal nerve activity (26). Given the MCP-1 concentrations reported herein and the report that ultrafine carbon particle exposure depresses vagal tone (68), the assessment of vagal tone following C60 exposure may be important in future studies.

We also examined pharmacological responsiveness of isolated LAD in order to link C60 exposure to enhanced coronary artery tone. Vascular tone is an important physiological determinant of tissue perfusion and blood flow by impacting artery diameter and vascular resistance. As vascular tone increases, vessel diameter decreases and thus perfusion flow decreases (5). Coronary perfusion of the myocardial zone at risk for infarction during I/R can occur by collateral flow during ischemia and reflow during reperfusion. Enhanced coronary arterial tone due to particle exposure could impair collateral flow during ischemia and promote zones of no reflow during reperfusion. The LAD from IT C60 exposed male rats did show a trend for sensitized 5-HT mediated vascular smooth muscle contraction in our initial assessment of a vascular contribution to the cardiac I/R injury following IT exposure to C60. Those LAD experiments also indicated that IV C60 exposure may have impacted vascular tone uniquely

from IT exposure to C60 by promoting impaired ACh endothelium-dependent vascular smooth muscle relaxation in the LAD. Unexpectedly, these experiments indicated that in male rats, LAD from the IT vehicle group had diminished ACh responsiveness when compared to the naïve group. In female rats, 5-HT responsiveness and ACh responses were only minimally altered, but a rightward shift in the LAD relaxation response to ACh in the IV C60 group was noticeable. The larger changes in the pharmacological assessments of female LAD came in the SNP concentration response studies, in which the route of exposure seemed to play a role. In these experiments the female IT C60 group had diminished responsiveness to the NO donor SNP. This response was not recapitulated in the female IV C60 group and the response also offers a possible explanation for why the female IT C60 group had larger I/R infarct sizes than the IV C60 group.

It is possible that slight shifts toward enhanced vascular tone during pharmacological assessments of LAD segments may function as an indicator of more robust vascular tone in the greater coronary circulation, especially during a period of cardiac reperfusion following an ischemic bout. We have previously reported that one day after IT exposure to MWCNT in rats, isolated LAD segments generated slightly more stress in response to ET-1 but coronary flow was significantly depressed during post-ischemic reperfusion of isolated Langendorff rat hearts (159). Those enhanced isolated LAD ET-1 responses appeared to be associated with the COX pathway, a physiological response mechanism documented in various vascular beds following pulmonary exposure to nanoparticles (88; 95). These reports prompted us to examine COX-dependent ET-1 stress responses in isolated LAD from rats exposed to IT C60 and vehicle. Maximal stress responses to ET-1 were more pronounced in the IT C60 exposed group compared to the IT

vehicle group. Inhibition with 10 μM Indomethacin, a general COX inhibitor, prevented the increased LAD stress in response to ET-1 seen in the IT C60 group and had no effect in LAD from IT vehicle exposed rats. These data support our hypothesis that enhanced coronary tone may have contributed to exacerbation of post-I/R myocardial infarction we found in the IT C60 exposed rats as compared to the IT vehicle exposed rats. As with the PAI-1 and ACh data we did note that ET-1 Hillslope values were diminished in the vehicle group compared to the naïve group.

The findings in this study provide support that the cardiovascular system as a whole is susceptible to nanoparticle exposure, especially at the pulmonary interface. While the entire set of mechanisms that contribute to exacerbation of I/R infarction are unclear, the vascular system appears to contribute to the deleterious cardiovascular consequences of nanoparticle exposure. The arterial system must maintain appropriate sensitivity to stimuli present in the immediate extracellular environment in order to adequately respond to the perfusion needs of the tissue and organ. If the ability of the arterial system loses its ability to respond to stimuli appropriately, the homeostatic window for organ perfusion may narrow and may leave the tissue/organ susceptible to injury should an insult arise. It appears from our data reported here, and in previous work (159), that 24 hours following nanoparticle exposure, pharmacological responsiveness to chemical ligands may be disrupted in coronary arteries. Our findings of coronary dysfunction following nanoparticle exposure are also consistent with other investigations into coronary endpoints following nanoparticle exposure (95; 111; 153). Such changes in coronary artery physiology can have serious detrimental health effects, especially during an ischemic emergency.

5.5. Chapter 5 conclusion

Chapter 5 demonstrates that the heart is susceptible to I/R injury 24 hours following IT or IV exposure to C60 despite minimal pulmonary inflammation. Novel to our initial predictions, administration of IV C60 also promoted infarct expansion following cardiac I/R 24 hrs post-exposure, suggesting that translocation of C60 to the vascular compartment following pulmonary exposure is not solely responsible for infarct expansion during I/R. We also offer evidence that the mechanisms that drive that injury may be unique from IT exposure. These mechanisms include differential impacts on the coronary vasculature that promote enhanced coronary tone. These ranged from enhanced ET-1 stress generation to depressed ACh responsiveness. Additionally there may be some gender sensitivity to C60 administration routes. IV exposure to C60 may uniquely modulate cytokine release during cardiac I/R. We further caution that the choice of vehicles and dispersants used may have uniquely alter arterial responsiveness and have further unexpected cardiovascularconsequences. Since C60 applications are growing in industry and medicine, awareness of potential cardiovascular consequences of exposure may improve safety regulations, broaden the medical uses of C60 through directed toxicity, and improve physicochemical modifications of C60.

CHAPTER 6

INTEGRATED DISCUSSION AND CONCLUSION

6.1. Integrated discussion

6.1.1. Summary of findings

Experiments from Specific Aim 1 demonstrated that pulmonary exposure to MWCNT 24 hours prior to cardiovascular assessment resulted in exposure mass-dependent increases in PVC at baseline (Figure 3.1). The 100 μg MWCNT group also displayed increased in TXB2 concentration in coronary effluents at baseline but the difference was not statistically significant (Figure 3.1). After 20 minutes of ischemia, hearts isolated from rats exposed to 100 μg of MWCNT demonstrated significant depressions in early coronary reperfusion flow (Figure 3.2), concomitant with significantly increased ET-1 concentration in coronary effluents and TXB2 concentrations that were not significantly elevated (Figure 3.2). Hearts isolated from rats exposed to MWCNT showed had shortened time into reperfusion before the first episode of VT/VF occurred but the differences were not statistically different (Figure 3.4). Following the reperfusion period hearts from the 100 μg MWCNT group had significantly larger infarct sizes than the infarctions that resulted in hearts from rats instilled with vehicle, and rats instilled with 1 or 10 μg of MWCNT had significant losses in LVDP by the end of reperfusion when compared to the vehicle group (Figure 3.4).

Experiments from Specific Aim 2 demonstrated that 24 hours after pulmonary exposure to 100 μg of MWCNT, isolated LAD segments yielded enhanced stress generation in response to increasing concentrations of ET-1 by wire myography compared to LAD isolated from the

vehicle group (Figure 4.1). The enhanced stress response to ET-1 in the MWCNT group was also evident using non-linear regression analysis. However, examination of LAD responses to the TXA2 mimetic U46619 did not yield increases in coronary artery stress following MWCNT exposure but non-linear regression analysis of the vehicle and MWCNT group curves did indicate significant differences between the two groups (Figure 4.1). Our investigation into the enhanced ET-1-mediated coronary artery stress response of the MWCNT group indicated the response was dependent on TXS, TP (Figure 4.5) and COX-2 signaling, with indication of a COX-1 element (Figure 4.4) according to non-linear regression analysis. Evidence that the enhancement of ET-1-mediated coronary artery stress was due to endothelial/ETBR-dependent mechanisms was minimal and further investigations are necessary to clarify the role of these elements in augmentation of LAD stress generation following MWCNT exposure.

Experiments from Specific Aim 3 demonstrated that the hearts were also susceptible to I/R injury expansion, 24 hours following IT exposure to C60 in male and female rats (Figure 5.1), with minimal pulmonary inflammation (Tables 5.2 and 5.3). One day following IV exposure to C60 in male and female rats, myocardial infarction was also worsened in response to I/R (Figure 5.1). Post-cardiac I/R serum cytokines IL-6 and MCP-1 were both elevated in the male IV C60 group when compared to the male IV vehicle, male IT C60, and female IV C60 groups (Figure 5.2). Experiments from Specific Aim 3 also yielded data suggesting that IT exposure to C60 in males results in enhanced ET-1-mediated coronary artery stress response not seen in following IV exposure to C60 in males or C60 exposure by both routes in females (Figure 5.5). Further experiments demonstrated that the enhanced LAD stress response to ET-1 in IT C60 instilled males was sensitive to Indomethacin, a response that was not recapitulated in LAD isolated from

IT vehicle instilled males (Figure 5.6). We did provide evidence unique to LAD isolated from IV C60 exposed male rats, which demonstrated desensitized ACh-mediated relaxation compared to LAD isolated from IV vehicle exposed males (Figure 5.3). LAD isolated from IT C60-instilled female rats demonstrated diminished coronary artery VSMC relaxation in response to SNP when compared to isolated LAD from IV vehicle-instilled females (Figure 5.4).

6.1.2. Considerations

6.1.2.1. Particle characteristics

This dissertation focuses on 2 types of carbon-based ENP: MWCNT and C60. These ENP have similar chemical composition but very different aspect ratios. Because the carbon structures of MWCNT and C60 are hydrophobic, they required a dispersion media in order to increase their solubility and stability in aqueous solution. In experiments designed to address Specific Aims 1 and 2 we utilized an intratracheal instillation of MWCNT, the results for which can be found in Chapters 3 and 4. We selected a medical grade pulmonary surfactant (Infasurf™) diluted to 10% in saline for the MWCNT suspensions. The experiments described for Specific Aim 3 utilized intratracheal and intravenous delivery of C60, the results for which can be found in Chapter 5. The intravenous route of exposure in this study made the use of a pulmonary surfactant less desirable (169). Instead, we selected PVP, a water-soluble polymer often used to increase the water solubility of C60 (77), diluted to 1.4% in saline. The difference in dispersion media and suspension stabilities are important factors to consider in the interpretation of results across the MWCNT and C60 studies. We analyzed suspension stability by assessing zeta potential. The MWCNT had a zeta potential of -44.6 mV (Tables 3.1 and 6.1) in the suspensions used in experiments reported in Chapters 3 and 4, indicating that MWCNT were much more stable in

suspension than the C60 used in experiments reported in Chapter 5, which had a zeta potential of 1.7 mV in suspension (Tables 5.1 and 6.1).

Despite the use of dispersion media, MWCNT and C60 can still agglomerate in solution, thus physical characterization of the particles in solution is necessary in order to understand the working characteristics of suspensions that rats would be exposed to. We analyzed the MWCNT and C60 suspensions by dynamic light scattering in order to obtain hydrodynamic sizes. Our MWCNT suspensions used in experiments from Specific Aims 1 and 2, as reported in Chapters 3 and 4, demonstrated bimodal size distributions with the major peak occurring at 200 nm and a smaller peak occurring 1000 nm (Tables 3.1 and 6.1). Assessing MWCNT hydrodynamic size by dynamic light scattering can be problematic due to the aspect ratio of MWCNT. For example, the bimodal distribution of peak values for MWCNT in suspension could have either indicated (i) the presence of two major size fractions of MWCNT agglomerates at 200 and 1000 nm; or (ii) MWCNT agglomerate diameter at 200 nm and MWCNT agglomerate length at 1000 nm. Conversely, assessment of C60 hydrodynamic size by dynamic light scattering during Specific Aim 3 as reported in Chapter 5, was less problematic, yielding one peak during each measurement with a mean of 371 nm (Tables 5.1 and 6.1). The extent of MWCNT and C60 agglomeration is also able to impact particle numbers in suspension. We analyzed particle numbers of the MWCNT and C60 suspensions by flow cytometry. In Chapter 3 we reported that 100 μg MWCNT instillation suspension contained 37,147 ± 625 particles per 10 μL of suspension (Table 3.1). In Chapter 5 we reported that C60 suspensions contained 25,791 ± 1351 particles per 10 μL of suspension (Table 3.1).

Table 6.1 Particle suspension comparisons

	Comparison of MWCNT and C60 suspensions physical characterization (mean ± SEM)	
	MWCNT	**C60**
Zeta potential	-44.6 mV	1.7 mV
Hydrodynamic size, nm	200 ± 50, 1000 ± 150	371 ± 0.6
Particle mass (per rat)	100 μg	28 μg
Particle number (per rat)	742,940 ± 12,500	515,820 ± 27,020
Calculated surface area (per rat)	467 mm^2	224 mm^2

Surface area calculation for MWCNT based on tube surface area ($2\pi rh$; r was taken as 100 and h was taken as 1000 nm) and C60 based on sphere surface area ($4\pi r^2$; r was taken as 186 nm)

6.1.2.2. Particle dosimetry

A recent publication by Erdely *et al* .identified a mean airborne mass concentration of 10.6 $\mu g/m^3$ MWCNT across 8 different facilities that handle carbon nanotubes in the United States, which was calculated to correspond with a human alveolar deposition of 4.07 μg/day (49). This suggests that airborne concentrations of MWCNT are being relatively well controlled in the facilities investigated. Scenarios and locations in which safety measures are not in place to minimize airborne particle dispersal are likely of low probability, but in a study designed to mimic such conditions while weighing and moving dry materials, MWCNTwere found to range from 4,514 – 123,403 particles/L of air (79). Considering that average tidal volume in humans is 500 mL of air and average respiration rate is 12 breaths a minute, humans breathe approximately 360 L air/hour on average (11). This could potentially result in a deposition of 1,625,040 – 44,425,080 MWCNT particles into the lungs in 1 hour. In experiments from Specific Aim 1, which are reported in Chapter 3 of this dissertation, we selected the use of 100 μg, 10 μg and 1 μg of MWCNT to compare against vehicle exposure. This allowed us to develop an exposure mass-response relationship for MWCNT and isolated cardiac I/R injury. In experiments from

Specific Aim 2, which are reported in Chapter 4, we utilized 100 μg MWCNT to compare against vehicle exposure because coronary flow was significantly depressed during early reperfusion, concomitant with increased ET-1 concentration in coronary effluents during early reperfusion in the 100 μg MWCNT group compared to vehicle during experiments from Specific Aim 1 (Figure 3.2). Based on calculations from the flow cytometry data, the 100 μg MWCNT group exposure mass corresponded with approximately 742,940 ± 12,500 particles per rat (Table 6.1). Considering the difference in a male rat at approximately 300 g and an ideal adult male human at 70 kg (4), humans are approximately 233.33 times larger than a rat. If 742,940 particles of MWCNT is multiplied by 233.33, the particle number would be >173 Million. This would require between 3-107 hours of constant occupational exposure in work conditions with no safety measures to reduce the number of airborne MWCNT. This means that the IT MWCNT instillation model used in this dissertation describes an unlikely real world scenario in terms of modern day occupational exposure.

In experiments from Specific Aim 3, which are reported in Chapter 5, because of the solubility of C60, we could not achieve the same mass concentration of the 100 μg MWCNT instillation suspension (0.5 μg/μL). Instead we examined the highest achievable concentration (0.14 μg/μL) of PVP formulated C60, which translated to 28 μg of C60 exposure to compare against the vehicle group. Based on calculations from flow cytometry data, the 28 μg C60 exposure mass translated to approximately 515,820 ± 27,020 particles per rat (Table 6.1). While it is not expected that airborne concentrations of C60 would be much higher than those found in modern facilities handling MWCNT with safety measures in place (49), a study designed to test airborne C60 concentrations in a occupational environment without safety measures reported to C60

particle numbers to range between 23,856 – 53,119 particles/L of airresearch laboratories (79). Based on the same considerations made for MWCNT, C60 deposition in human lungs could potentially range from 8,588,160 – 31,871,400 particles of C60 in 1 hour. Based on the same human to rat size difference factor, if 515,820 particles of C60 is multiplied by 233.33, the particle number would be >120 Million, which would take between 4-14 hours of constant occupational exposurein work conditions with no safety measures to reduce the number of airborne C60. This means that the IT C60 instillation model used in this dissertation describes an unlikely real world scenario in terms of modern day occupational exposure.

In this dissertation we wanted to make broad comparisons across the MWCNT and C60 studies. Therefore it should be noted that despite the difference in exposure mass between the MWCNT and C60 studies, the differences in the sizes and aspect ratios of MWCNT and C60 in their respective suspensions allows us to consider the cardiovascular endpoints as they relate to differences in calculated particle surface area and particle number dosimetries (see Table 6.1). Rats in the MWCNT studies were exposed to nearly 4 times the particle mass than rats in the C60 study (100 µg vs. 28 µg). However, when the exposure is considered by particle numbers, we delivered only 30% more MWCNT particles than C60 particles to each rat. Furthermore, based on approximated calculations, rats exposed to MWCNT were only exposed to about half of the particle surface area than rats exposed to C60. The only truly common endpoint examined between IT MWCNT and IT C60 studies was the cumulative concentration responses to ET-1 in isolated LAD. As presented in Figure 6.1, when the increased LAD stress responses from both ENP groups (Figure 6.1A) are considered as a function of different dosimetries, the greatest difference between IT MWCNT and IT C60 responses occurred as a function of mass (Figure

6.1B). The least difference between IT MWCNT and IT C60 response occurred as a function of particle number (Figure 6.1C). When the difference between IT MWCNT and IT C60 responses were taken as a function of calculated surface area (Figure 6.1D), the difference was less than that of exposure mass and greater than that of particle number. One possible explanation for the difference in LAD responses when taken as a function of calculated surface area is a potential difference in MWCNT and C60 biological surface area interaction. Considering the differences in MWCNT and C60 agglomerate size and aspect ratios, it may be possible that the amount of particle surface area that interacts with biological tissue and thus initiating a response mechanism may be different between the two ENP. This evidence suggests that C60 may potentially induce greater cardiovascular toxicity than MWCNT on a per mass basis, but that the responses to C60 and MWCNT appear to be normalized as a function of particle number and/or particle surface area.

Figure 6.1 Coronary artery endothelin-1 stress responses as a function of dosimetry

(A) ET-1 stress responses from male rats exposed either to IT MWCNT or IT C60 normalized to each respective vehicle group. (B) ET-1 stress responses from male rats exposed either to IT MWCNT or IT C60 normalized to each respective vehicle group, and presented as a function of ENP mass. (C) ET-1 stress responses from male rats exposed either to IT MWCNT or IT C60 normalized to each respective vehicle group, and presented as a function of ENP particle number. (D) ET-1 stress responses from male rats exposed either to IT MWCNT or IT C60 normalized to each respective vehicle group, and presented as a function of calculated surface area.

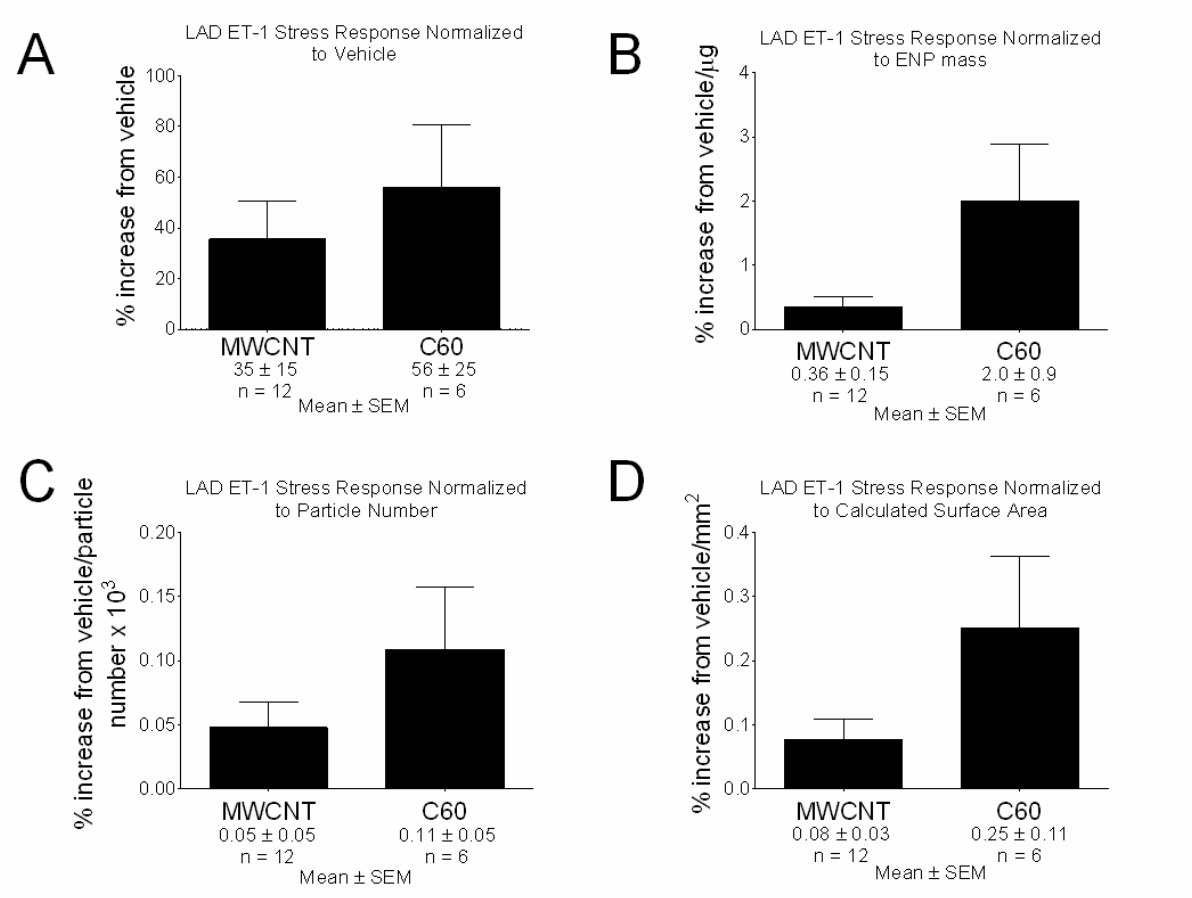

6.1.3. Interpretation of results

The literature review indicated that populations exposed to relatively high levels ofparticulate matter have increased risks for cardiovascular disease. However, while the cardiovascular detriments associated with pulmonary exposure to NP are expected and evident, the physiological mechanisms by which the cardiovascular derangements are brought about are enigmatic. We proposed that pulmonary exposure to ENP could promote intrinsic changes in the heart and coronary vasculature that could drive expansion of myocardial infarction after I/R. In Chapter 3 we provided evidence that pulmonary exposure to MWCNT generated intrinsic changes in the heart that enhanced cardiac arrhythmogenesis when neurohumoral influences were removed. With the exception of resident inflammatory cells, this left the possibility that local autonomic/paracrine signaling, altered coronary perfusion, and/or cellular dysfunction in nodal/conducting tissue may have been contributing factors. The only evidence we were able to uncover at baseline that provided a possible explanation for the aberrant ECG and increased PVC generation in the MWCNT groups was the trend ($P = 0.06$) for increased TXB2 concentration in the coronary effluents from the 100 μg MWCNT group at baseline. In any case, this finding is consistent with cardiac arrhythmogenic responses documented following exposure to air pollution particulate matter (69; 80; 83). More substantial evidence that IT MWCNT instillation had caused alterations in intrinsic factors of the heart was found during early reperfusion. These manifested through increased ET-1 concentrations within the coronary effluents and depression of coronary flow. Increased ET-1 release has also been documented following exposure to air pollution particulate matter and myocardial infarction (80). By the end of reperfusion protocols reported in Chapter 3, LVDP was significantly reduced in hearts isolated from 1 and 10 μg MWCNT-instilled rats and infarct size was significantly larger in hearts isolated from rats

instilled with 100 μg MWCNT. These findings support a generalized hypothesis that pulmonary exposure to ENP can cause cardiovascular detriments within the heart itself, which could possibly be broadened to include augmentation of local inflammatory cells responses residing within heart tissue. Perhaps more importantly we learned that that there was an underlying correlation between the number of PVC that occurred at baseline and the size of myocardial infarction following I/R (Figure 6.2). Therefore, examining individuals for sustained PVC who have recently been exposed to inhalation of high levels of MWCNT or other ENP in occupational settings, and potentially even other NP in the environment, may potentially indicate an increase in the susceptibility for cardiac I/R injury.

Figure 6.2 **In Chapter 3 premature ventricular contractions from baseline correlated with myocardial infarct size following cardiac ischemia/reperfusion**

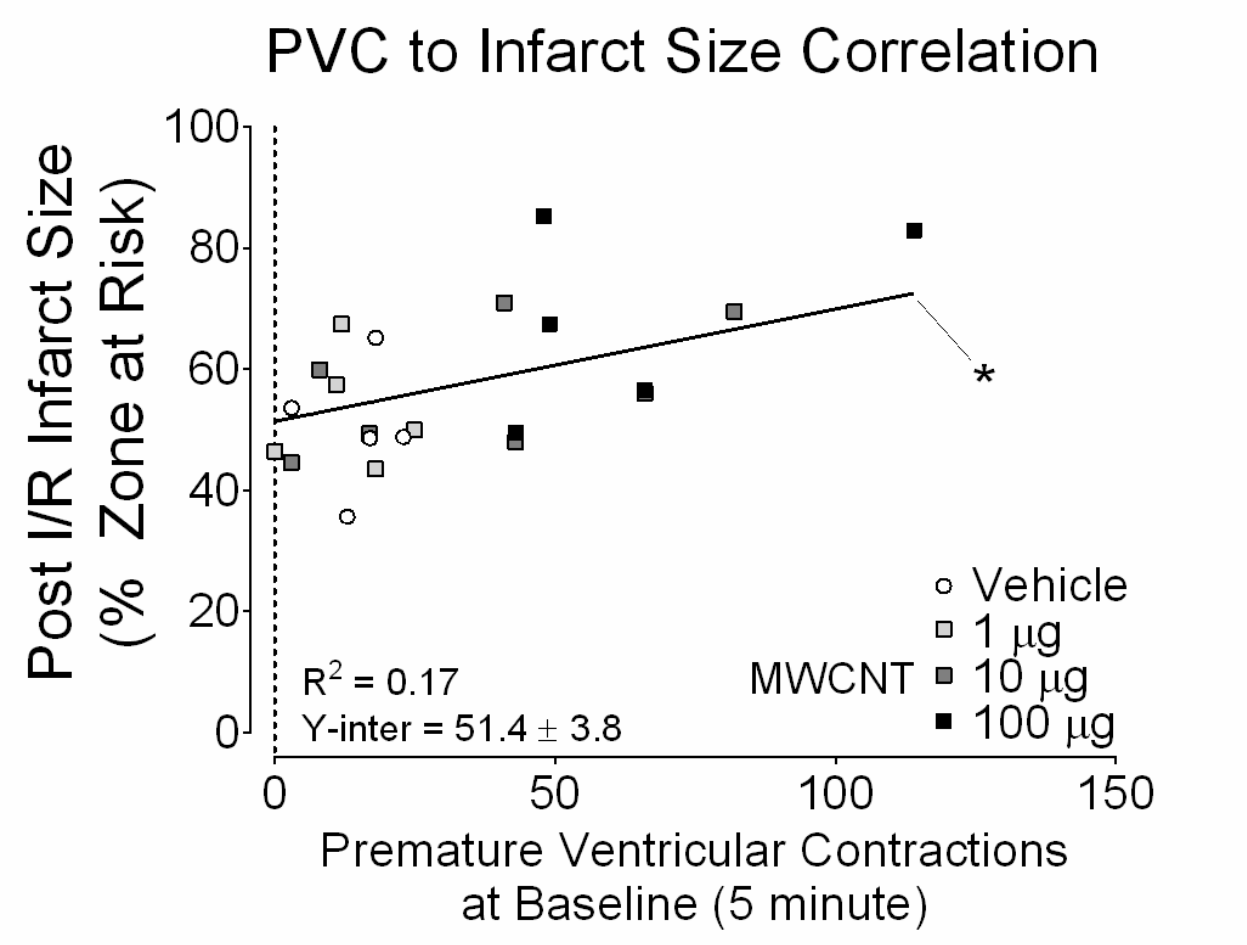

In Chapter 4 we uncovered evidence indicating that isolated LAD from male rats instilled with MWCNT responded to ET-1 with enhanced stress. This supported Chapter 3 findings that hearts isolated from MWCNT exposed rats had increased effluent ET-1 concentrations and depressed coronary flow during early reperfusion. Subsequent studies in Chapter 4 indicated that COX-2 and TP were involved in the enhanced ET-1-mediated coronary artery stress production in the MWCNT group. Figure 6.3 shows a flow chart proposing how MWCNT exposure results in enhanced coronary stress in response to ET-1. These findings, while unique in regards to enhanced ET-1 stress responses in LAD, are in agreement with another report that pulmonary exposure to MWCNT can adversely impact coronary arteries (153).

Figure 6.3 Proposed mechanism of increased coronary artery stress in response to ET-1 following pulmonary exposure to multi-walled carbon nanotubes(159)

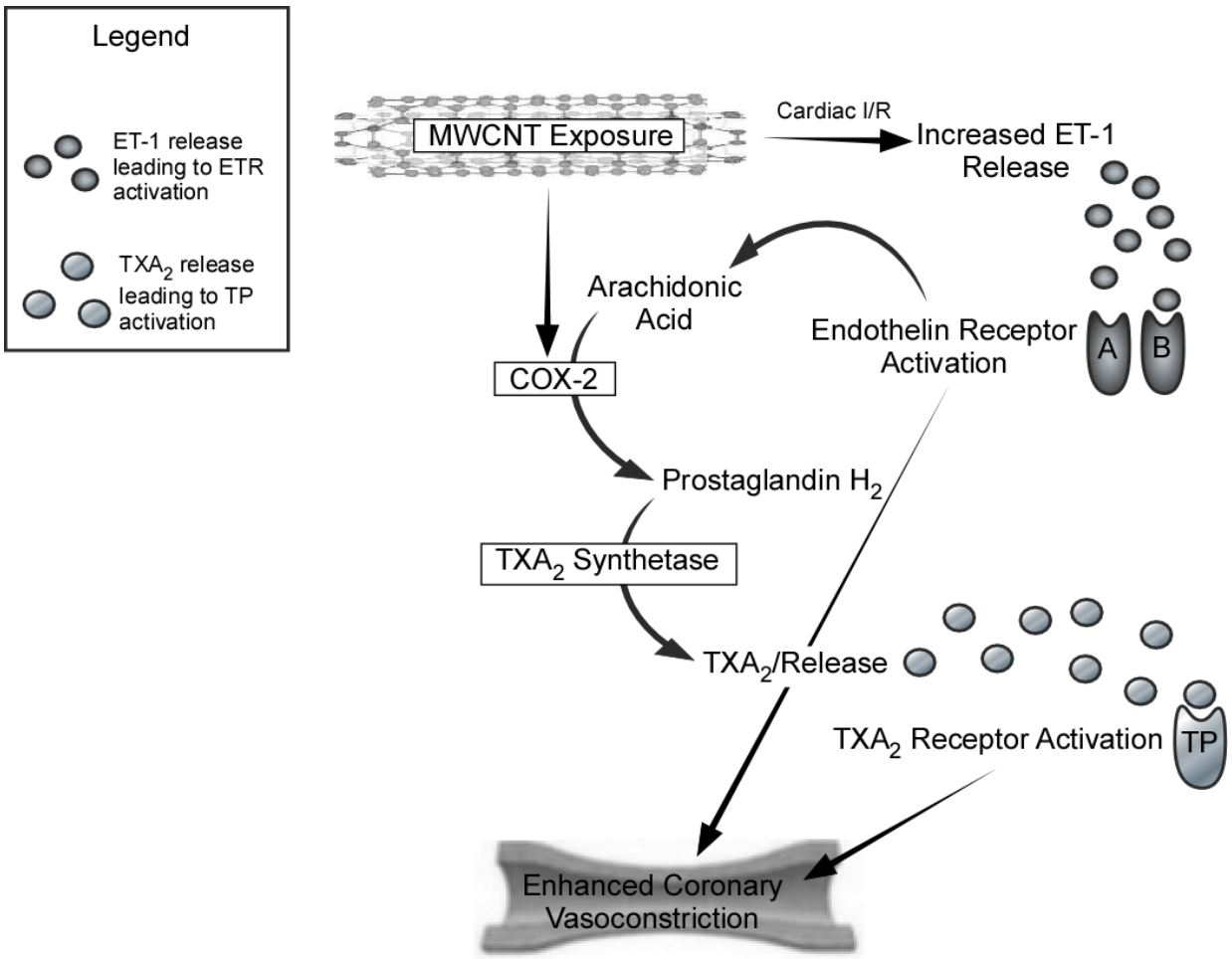

Modified from:
Thompson LC, Frasier CR, Sloan RC, Mann EE, Harrison BS, Brown JM, Brown DA and Wingard CJ. Pulmonary instillation of multi-walled carbon nanotubes promotes coronary vasoconstriction and exacerbates injury in isolated hearts. *Nanotoxicology* (November 23, 2012); doi:10.3109/17435390.2012.744858.

Considering the rate that new ENP are being developed, establishing a physiological mechanism that can be used to classify ENP as potentially cardiotoxic would provide an important tool in toxicological assessments of new ENP that come to market. To this end we examined C60 exposure using the *in situ* cardiac I/R endpoint previously established in our laboratory and the isolated coronary artery assessment of ET-1-mediated stress production via wire myography established with in Chapter 4. We also examined IT and IV exposure routes because (i) C60 has potential medical uses like contrast imaging agents and drug delivery devices that could require C60 be delivered IV and (ii) the size and shape of C60 should give it a relatively high probability to translocate through the lung and into the vascular compartment following pulmonary exposure. Comparing IT and IV responses should provide a means to potentially assess if detrimental cardiovascular responses to IT C60 are due to an interaction at the pulmonary interface or possibly due to translocation into circulation. The initial finding was that cardiac I/R infarction expanded in male rats exposed to either IT or IV C60. This finding provides some plausibility to the claim that IT C60 translocation from the lung to the vascular compartment was responsible for cardiac I/R infarct expansion, but further research would be needed to substantiate that claim. Alternatively, we uncovered stronger evidence to the contrary, in which serum cytokine profiles following cardiac I/R and isolated LAD experiments both suggested that the mechanisms responsible for cardiac I/R injury exacerbation are likely unique between IT and IV C60 exposure.

The common link between IT MWCNT and IT C60 exposed male rats was that the exposure resulted increased LAD stress in response to ET-1 when compared to their respective vehicle groups. In both ENP groups, the LAD responses to ET-1 were returned to the stress level seen in vehicle control groups, with little change in ET-1 stress responses found in LAD from the vehicle groups inhibited with Indomethacin. This suggests that COX is likely the contributing source of enhanced ET-1-mediated stress in LAD isolated from IT ENP instilled rats. These findings, while exciting, must be interpreted with caution as ET-1 is a pleiotropic peptide and is influential in the cardiovascular system in many ways (see Figure 6.4) (58). Altered ET-1 responses in coronary arteries can be detrimental, as data from this dissertation suggests. However, if altered physiological responses to ET-1 following ENP exposure are not confined to coronary arteries, then ET-1 signaling may be of greater importance to examine following pulmonary exposure to ENP.

It should also be noted that experiments for this project utilized IT exposures in rats. Given that rats are obligatory nose breathers and that IT instillation bypasses nasal tissue, evidence that the LAD/ET-1/COX responses are likely dependent on ENP exposure at the pulmonary interface. Also, while this dissertation addressed an acute exposure associated with relatively large mass exposures to ENP, real world exposures in humans may be of lower mass, but small changes in physiological responses to ligands like ET-1 as described in Figure 6.4 could provide an explanation for the high incidence of cardiovascular disease and mortality that have been linked to airborne particulate matter. Therefore based on the evidence provided in this dissertation, ET-1/COX-associated mechanisms should be carefully examined following ENP inhalation

exposures in order to determine if long term exposure to ENP could potentially increase the incidence of cardiovascular disease and mortality in individuals chronically exposed to ENP.

Figure 6.4 Potential cardiovascular consequences of dysregulated endothelin-1 signaling(58)

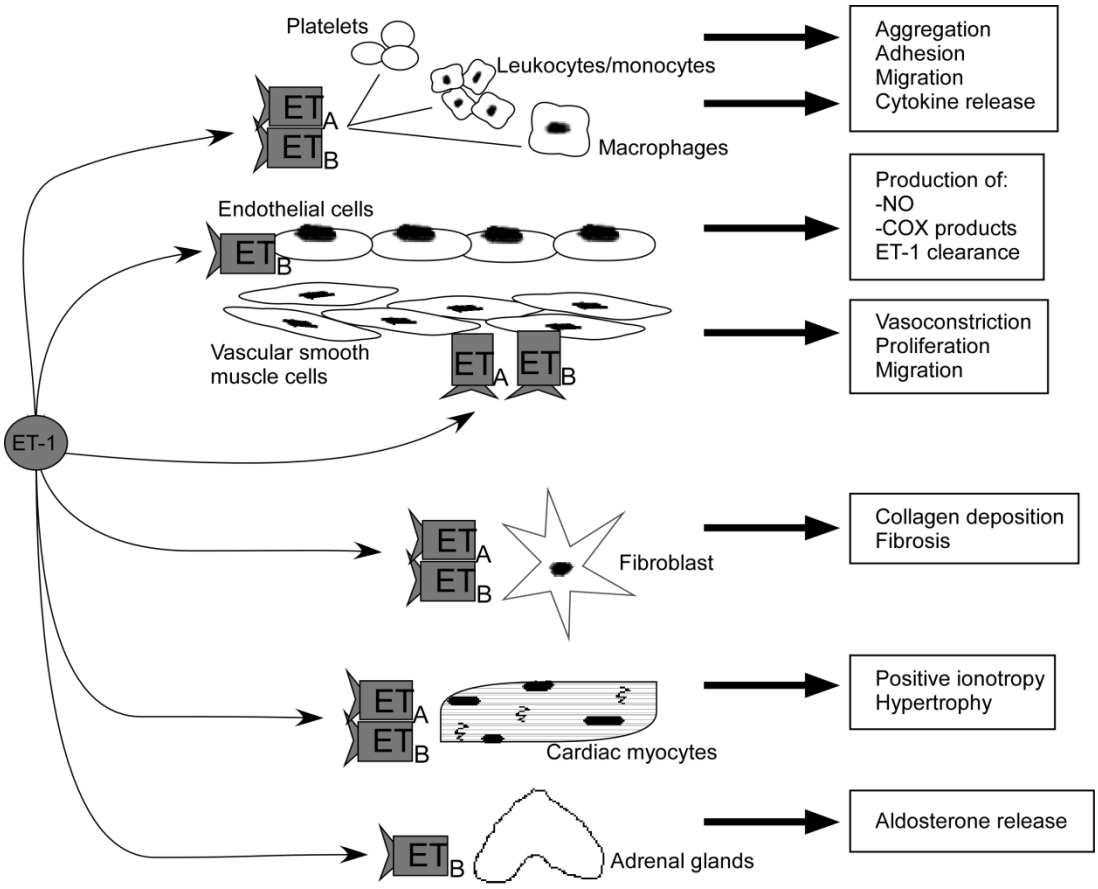

Modified from:
Galie N, Manes A and Branzi A. The endothelin system in pulmonary arterial hypertension. *Cardiovasc Res* 61: 227-237, 2004.

6.2. Dissertation conclusion

This dissertation has outlined important points from the literature that merit concern that the cardiovascular system could be particularly susceptible to ENP-induced toxicity. Experiments were performed herein that indicated the potential for pulmonary exposureto ENP to produce dysfunction in heart rhythm and the coronary artery ET-1/COX axis. We provide evidence that ENP have the potential to generate cardiovascular detriments unique to exposure route, and further that males and females may respond to ENP exposure through different mechanisms. By considering particle dosimetry, it appears that isolated coronary artery responses to ET-1 following MWCNT or C60 exposure can be normalized when they are considered as a function of particle number/particle surface area. In either case, pulmonary exposure to MWCNT or C60 produced augmented coronary artery responses to ET-1. Given the broad reaching consequences of altered ET-1signaling throughout the cardiovascular system, if exposure to ENP is a concern, therapeutic targeting of the ET-1 and/or COX signaling pathways could potentially alleviate cardiovascular detriments associated with ENP exposures.

REFERENCE LIST

1. **Abarbanell AM, Herrmann JL, Weil BR, Wang Y, Tan J, Moberly SP, Fiege JW and Meldrum DR**. Animal models of myocardial and vascular injury. *J Surg Res* 162: 239-249, 2010.

2. **Aird WC**. Phenotypic heterogeneity of the endothelium: I. Structure, function, and mechanisms. *Circ Res* 100: 158-173, 2007.

3. **Anderson DR, Poterucha JT, Mikuls TR, Duryee MJ, Garvin RP, Klassen LW, Shurmur SW and Thiele GM**. IL-6 and its receptors in coronary artery disease and acute myocardial infarction. *Cytokine* 62: 395-400, 2013.

4. **Aronson PS, Boron WF and Boulpaep EL**. Transport of Solutes and Water. In: *Medical Physiology: A Cellular and Molecular Approach*, edited by Boron WF and Boulpaep EL. Philidelphia, PA: Saunders Elsevier, 2009.

5. **Badeer HS**. Hemodynamics for medical students. *Adv Physiol Educ* 25: 44-52, 2001.

6. **Baker GL, Gupta A, Clark ML, Valenzuela BR, Staska LM, Harbo SJ, Pierce JT and Dill JA**. Inhalation toxicity and lung toxicokinetics of C60 fullerene nanoparticles and microparticles. *Toxicol Sci* 101: 122-131, 2008.

7. **Bakry R, Vallant RM, Najam-ul-Haq M, Rainer M, Szabo Z, Huck CW and Bonn GK**. Medicinal applications of fullerenes. *Int J Nanomedicine* 2: 639-649, 2007.

8. **Belevych AE, Terentyev D, Viatchenko-Karpinski S, Terentyeva R, Sridhar A, Nishijima Y, Wilson LD, Cardounel AJ, Laurita KR, Carnes CA, Billman GE and Gyorke S**. Redox modification of ryanodine receptors underlies calcium alternans in a canine model of sudden cardiac death. *Cardiovasc Res* 84: 387-395, 2009.

9. **Bell RM, Mocanu MM and Yellon DM**. Retrograde heart perfusion: the Langendorff technique of isolated heart perfusion. *J Mol Cell Cardiol* 50: 940-950, 2011.

10. **Bonner JC**. Nanoparticles as a potential cause of pleural and interstitial lung disease. *Proc Am Thorac Soc* 7: 138-141, 2010.

11. **Boron WF**. Organization of the Respiratory System. In: *Medical Physiology: A Cellular and Molecular Approach*, edited by Boron WF and Boulpaep EL. Philidelphia, PA: Saunders Elsevier, 2009.

12. **Boulpaep EL**. Arteries and Veins. In: *Medical Physiology: A Cellular and Molecular Approach*, edited by Boron WF and Boulpaep EL. Philidelphia, PA: Saunders Elsevier, 2009.

13. **Bourdon JA, Halappanavar S, Saber AT, Jacobsen NR, Williams A, Wallin H, Vogel U and Yauk CL**. Hepatic and pulmonary toxicogenomic profiles in mice intratracheally instilled with carbon black nanoparticles reveal pulmonary inflammation, acute phase response and alterations in lipid homeostasis. *Toxicol Sci* 2012.

14. **Brasier AR**. The nuclear factor-kappaB-interleukin-6 signalling pathway mediating vascular inflammation. *Cardiovasc Res* 86: 211-218, 2010.

15. **Brook RD**. Cardiovascular effects of air pollution. *Clin Sci (Lond)* 115: 175-187, 2008.

16. **Brook RD, Rajagopalan S, Pope CA, III, Brook JR, Bhatnagar A, ez-Roux AV, Holguin F, Hong Y, Luepker RV, Mittleman MA, Peters A, Siscovick D, Smith SC, Jr., Whitsel L and Kaufman JD**. Particulate matter air pollution and cardiovascular disease: An update to the scientific statement from the American Heart Association. *Circulation* 121: 2331-2378, 2010.

17. **Brown DA, Jew KN, Sparagna GC, Musch TI and Moore RL**. Exercise training preserves coronary flow and reduces infarct size after ischemia-reperfusion in rat heart. *J Appl Physiol* 95: 2510-2518, 2003.

18. **Brown DA and O'Rourke B**. Cardiac mitochondria and arrhythmias. *Cardiovasc Res* 88: 241-249, 2010.

19. **Brunner F, du Toit EF and Opie LH**. Endothelin release during ischaemia and reperfusion of isolated perfused rat hearts. *J Mol Cell Cardiol* 24: 1291-1305, 1992.

20. **Budinger GR, McKell JL, Urich D, Foiles N, Weiss I, Chiarella SE, Gonzalez A, Soberanes S, Ghio AJ, Nigdelioglu R, Mutlu EA, Radigan KA, Green D, Kwaan HC and Mutlu GM**. Particulate matter-induced lung inflammation increases systemic levels of PAI-1 and activates coagulation through distinct mechanisms. *PLoS One* 6: e18525, 2011.

21. **Buja LM**. Myocardial ischemia and reperfusion injury. *Cardiovasc Pathol* 14: 170-175, 2005.

22. **Bunz H, Plankenhorn S and Klein R**. Effect of buckminsterfullerenes on cells of the innate and adaptive immune system: an in vitro study with human peripheral blood mononuclear cells. *Int J Nanomedicine* 7: 4571-4580, 2012.

23. **Buus NH, Vanbavel E and Mulvany MJ**. Differences in sensitivity of rat mesenteric small arteries to agonists when studied as ring preparations or as cannulated preparations. *Br J Pharmacol* 112: 579-587, 1994.

24. **Cadenas S, Aragones J and Landazuri MO**. Mitochondrial reprogramming through cardiac oxygen sensors in ischaemic heart disease. *Cardiovasc Res* 88: 219-228, 2010.

25. **Callera G, Tostes R, Savoia C, Muscara MN and Touyz RM**. Vasoactive peptides in cardiovascular (patho)physiology. *Expert Rev Cardiovasc Ther* 5: 531-552, 2007.

26. **Calvillo L, Vanoli E, Andreoli E, Besana A, Omodeo E, Gnecchi M, Zerbi P, Vago G, Busca G and Schwartz PJ**. Vagal stimulation, through its nicotinic action, limits infarct size and the inflammatory response to myocardial ischemia and reperfusion. *J Cardiovasc Pharmacol* 58: 500-507, 2011.

27. **Campen MJ, Lund A and Rosenfeld M**. Mechanisms linking traffic-related air pollution and atherosclerosis. *Curr Opin Pulm Med* 18: 155-160, 2012.

28. **Cascio WE, Cozzi E, Hazarika S, Devlin RB, Henriksen RA, Lust RM, Van Scott MR and Wingard CJ**. Cardiac and vascular changes in mice after exposure to ultrafine particulate matter. *Inhal Toxicol* 19 Suppl 1: 67-73, 2007.

29. **Chen Z, Meng H, Xing G, Yuan H, Zhao F, Liu R, Chang X, Gao X, Wang T, Jia G, Ye C, Chai Z and Zhao Y**. Age-related differences in pulmonary and cardiovascular responses to SiO2 nanoparticle inhalation: nanotoxicity has susceptible population. *Environ Sci Technol* 42: 8985-8992, 2008.

30. **Cherng TW, Campen MJ, Knuckles TL, Gonzalez BL and Kanagy NL**. Impairment of coronary endothelial cell ET(B) receptor function after short-term inhalation exposure to whole diesel emissions. *Am J Physiol Regul Integr Comp Physiol* 297: R640-R647, 2009.

31. **Cherng TW, Paffett ML, Jackson-Weaver O, Campen MJ, Walker BR and Kanagy NL**. Mechanisms of diesel-induced endothelial nitric oxide synthase dysfunction in coronary arterioles. *Environ Health Perspect* 119: 98-103, 2011.

32. **Cho WS, Duffin R, Poland CA, Howie SE, MacNee W, Bradley M, Megson IL and Donaldson K**. Metal oxide nanoparticles induce unique inflammatory footprints in the lung: important implications for nanoparticle testing. *Environ Health Perspect* 118: 1699-1706, 2010.

33. **Choi HS, Ashitate Y, Lee JH, Kim SH, Matsui A, Insin N, Bawendi MG, Semmler-Behnke M, Frangioni JV and Tsuda A**. Rapid translocation of nanoparticles from the lung airspaces to the body. *Nat Biotechnol* 28: 1300-1303, 2010.

34. **Coker SJ, Parratt JR, Ledingham IM and Zeitlin IJ**. Thromboxane and prostacyclin release from ischaemic myocardium in relation to arrhythmias. *Nature* 291: 323-324, 1981.

35. **Cox RH**. Differences in mechanics of arterial smooth muscle from hindlimb arteries. *Am J Physiol* 235: H649-H656, 1978.

36. **Cozzi E, Hazarika S, Stallings HW, III, Cascio WE, Devlin RB, Lust RM, Wingard CJ and Van Scott MR**. Ultrafine particulate matter exposure augments ischemia-reperfusion injury in mice. *Am J Physiol Heart Circ Physiol* 291: H894-H903, 2006.

37. **Cuevas AK, Liberda EN, Gillespie PA, Allina J and Chen LC**. Inhaled nickel nanoparticles alter vascular reactivity in C57BL/6 mice. *Inhal Toxicol* 22 Suppl 2: 100-106, 2010.

38. **Davis MJ and Gore RW**. Length-tension relationship of vascular smooth muscle in single arterioles. *Am J Physiol* 256: H630-H640, 1989.

39. **Delfino RJ, Sioutas C and Malik S**. Potential role of ultrafine particles in associations between airborne particle mass and cardiovascular health. *Environ Health Perspect* 113: 934-946, 2005.

40. **Desjardins F, Aubin MC, Carrier M and Perrault LP**. Decrease of endothelin receptor subtype ETB and release of COX-derived products contribute to endothelial dysfunction of porcine epicardial coronary arteries in left ventricular hypertrophy. *J Cardiovasc Pharmacol* 45: 499-508, 2005.

41. **Dogan S, Turnbaugh D, Zhang M, Cofie DQ, Fugate RD and Kem DC**. Thromboxane A2 receptor mediation of calcium and calcium transients in rat cardiomyocytes. *Life Sci* 60: 943-952, 1997.

42. **Donaldson K, Brown D, Clouter A, Duffin R, MacNee W, Renwick L, Tran L and Stone V**. The pulmonary toxicology of ultrafine particles. *J Aerosol Med* 15: 213-220, 2002.

43. **Driscoll KE, Costa DL, Hatch G, Henderson R, Oberdorster G, Salem H and Schlesinger RB**. Intratracheal instillation as an exposure technique for the evaluation of respiratory tract toxicity: uses and limitations. *Toxicol Sci* 55: 24-35, 2000.

44. **Du Z, Zhao D, Jing L, Cui G, Jin M, Li Y, Liu X, Liu Y, Du H, Guo C, Zhou X and Sun Z**. Cardiovascular Toxicity of Different Sizes Amorphous Silica Nanoparticles in Rats After Intratracheal Instillation. *Cardiovasc Toxicol* 2013.

45. **Duling BR, Gore RW, Dacey RG, Jr. and Damon DN**. Methods for isolation, cannulation, and in vitro study of single microvessels. *Am J Physiol* 241: H108-H116, 1981.

46. **Duncker DJ and Bache RJ**. Regulation of coronary blood flow during exercise. *Physiol Rev* 88: 1009-1086, 2008.

47. **Duru F, Barton M, Luscher TF and Candinas R**. Endothelin and cardiac arrhythmias: do endothelin antagonists have a therapeutic potential as antiarrhythmic drugs? *Cardiovasc Res* 49: 272-280, 2001.

48. **Emmerechts J, Alfaro-Moreno E, Vanaudenaerde BM, Nemery B and Hoylaerts MF**. Short-term exposure to particulate matter induces arterial but not venous thrombosis in healthy mice. *J Thromb Haemost* 8: 2651-2661, 2010.

49. **Erdely A, Dahm M, Chen BT, Zeidler-Erdely PC, Fernback JE, Birch ME, Evans DE, Kashon ML, Deddens JA, Hulderman T, Bilgesu SA, Battelli L, Schwegler-Berry D, Leonard HD, McKinney W, Frazer DG, Antonini JM, Porter DW, Castranova V and Schubauer-Berigan MK**. Carbon nanotube dosimetry: from workplace exposure assessment to inhalation toxicology. *Part Fibre Toxicol* 10: 53, 2013.

50. **Fan J, Fang G, Zeng F, Wang X and Wu S**. Water-dispersible fullerene aggregates as a targeted anticancer prodrug with both chemo- and photodynamic therapeutic actions. *Small* 9: 613-621, 2013.

51. **Faunce TA, White J and Matthaei KI**. Integrated research into the nanoparticle-protein corona: a new focus for safe, sustainable and equitable development of nanomedicines. *Nanomedicine (Lond)* 3: 859-866, 2008.

52. **Feletou M, Huang Y and Vanhoutte PM**. Endothelium-mediated control of vascular tone: COX-1 and COX-2 products. *Br J Pharmacol* 164: 894-912, 2011.

53. **Feletou M, Vanhoutte PM and Verbeuren TJ**. The thromboxane/endoperoxide receptor (TP): the common villain. *J Cardiovasc Pharmacol* 55: 317-332, 2010.

54. **Ferroni P, Riondino S, Vazzana N, Santoro N, Guadagni F and Davi G**. Biomarkers of platelet activation in acute coronary syndromes. *Thromb Haemost* 108: 1109-1123, 2012.

55. **Flannery PJ and Spurney RF**. Desensitization of the mouse thromboxane A2 receptor (TP) by G protein-coupled receptor kinases (Grks). *Prostaglandins Other Lipid Mediat* 70: 79-90, 2002.

56. **Frangogiannis NG, Smith CW and Entman ML**. The inflammatory response in myocardial infarction. *Cardiovasc Res* 53: 31-47, 2002.

57. **Frasier CR, Sloan RC, Bostian PA, Gonzon MD, Kurowicki J, Lopresto SJ, Anderson EJ and Brown DA**. Short-term exercise preserves myocardial glutathione and decreases arrhythmias after thiol oxidation and ischemia in isolated rat hearts. *J Appl Physiol* 111: 1751-1759, 2011.

58. **Galie N, Manes A and Branzi A**. The endothelin system in pulmonary arterial hypertension. *Cardiovasc Res* 61: 227-237, 2004.

59. **Gasser M, Wick P, Clift MJ, Blank F, Diener L, Yan B, Gehr P, Krug HF and Rothen-Rutishauser B**. Pulmonary surfactant coating of multi-walled carbon nanotubes (MWCNTs) influences their oxidative and pro-inflammatory potential in vitro. *Part Fibre Toxicol* 9: 17, 2012.

60. **Geraets L, Oomen AG, Schroeter JD, Coleman VA and Cassee FR**. Tissue Distribution of Inhaled Micro- and Nano-sized Cerium Oxide Particles in Rats: Results from a 28-day Exposure Study. *Toxicol Sci* 2012.

61. **Geys J, Nemmar A, Verbeken E, Smolders E, Ratoi M, Hoylaerts MF, Nemery B and Hoet PH**. Acute toxicity and prothrombotic effects of quantum dots: impact of surface charge. *Environ Health Perspect* 116: 1607-1613, 2008.

62. **Go AS, Mozaffarian D, Roger VL, Benjamin EJ, Berry JD, Borden WB, Bravata DM, Dai S, Ford ES, Fox CS, Franco S, Fullerton HJ, Gillespie C, Hailpern SM, Heit JA, Howard VJ, Huffman MD, Kissela BM, Kittner SJ, Lackland DT, Lichtman JH, Lisabeth LD, Magid D, Marcus GM, Marelli A, Matchar DB, McGuire DK, Mohler ER, Moy CS, Mussolino ME, Nichol G, Paynter NP, Schreiner PJ, Sorlie PD, Stein J, Turan TN, Virani SS, Wong ND, Woo D and Turner MB**. Executive summary: heart disease and stroke statistics--2013 update: a report from the American Heart Association. *Circulation* 127: 143-152, 2013.

63. **Godleski JJ, Verrier RL, Koutrakis P, Catalano P, Coull B, Reinisch U, Lovett EG, Lawrence J, Murthy GG, Wolfson JM, Clarke RW, Nearing BD and Killingsworth C**. Mechanisms of morbidity and mortality from exposure to ambient air particles. *Res Rep Health Eff Inst* 5-88, 2000.

64. **Gold DR and Mittleman MA**. New insights into pollution and the cardiovascular system: 2010 to 2012. *Circulation* 127: 1903-1913, 2013.

65. **Guidetti GF, Consonni A, Cipolla L, Mustarelli P, Balduini C and Torti M**. Nanoparticles induce platelet activation in vitro through stimulation of canonical signalling pathways. *Nanomedicine* 8: 1329-1336, 2012.

66. **Gustafsson A, Lindstedt E, Elfsmark LS and Bucht A**. Lung exposure of titanium dioxide nanoparticles induces innate immune activation and long-lasting lymphocyte response in the Dark Agouti rat. *J Immunotoxicol* 8: 111-121, 2011.

67. **Halpern W and Mulvany MJ**. Tension responses to small length changes of vascular smooth muscle cells [proceedings]. *J Physiol* 265: 21P-23P, 1977.

68. **Harder V, Gilmour P, Lentner B, Karg E, Takenaka S, Ziesenis A, Stampfl A, Kodavanti U, Heyder J and Schulz H**. Cardiovascular responses in unrestrained WKY rats to inhaled ultrafine carbon particles. *Inhal Toxicol* 17: 29-42, 2005.

69. **He F, Shaffer ML, Rodriguez-Colon S, Yanosky JD, Bixler E, Cascio WE and Liao D**. Acute effects of fine particulate air pollution on cardiac arrhythmia: the APACR study. *Environ Health Perspect* 119: 927-932, 2011.

70. **Hearse DJ and Sutherland FJ**. Experimental models for the study of cardiovascular function and disease. *Pharmacol Res* 41: 597-603, 2000.

71. **Hoffmann B, Moebus S, Dragano N, Stang A, Mohlenkamp S, Schmermund A, Memmesheimer M, Brocker-Preuss M, Mann K, Erbel R and Jockel KH**. Chronic residential exposure to particulate matter air pollution and systemic inflammatory markers. *Environ Health Perspect* 117: 1302-1308, 2009.

72. **Horie M, Fukui H, Nishio K, Endoh S, Kato H, Fujita K, Miyauchi A, Nakamura A, Shichiri M, Ishida N, Kinugasa S, Morimoto Y, Niki E, Yoshida Y and Iwahashi H**. Evaluation of acute oxidative stress induced by NiO nanoparticles in vivo and in vitro. *J Occup Health* 53: 64-74, 2011.

73. **Horowitz A, Menice CB, Laporte R and Morgan KG**. Mechanisms of smooth muscle contraction. *Physiol Rev* 76: 967-1003, 1996.

74. **Hubbs AF, Mercer RR, Benkovic SA, Harkema J, Sriram K, Schwegler-Berry D, Goravanahally MP, Nurkiewicz TR, Castranova V and Sargent LM**. Nanotoxicology--a pathologist's perspective. *Toxicol Pathol* 39: 301-324, 2011.

75. **Hussain S, Boland S, Baeza-Squiban A, Hamel R, Thomassen LC, Martens JA, Billon-Galland MA, Fleury-Feith J, Moisan F, Pairon JC and Marano F**. Oxidative stress and proinflammatory effects of carbon black and titanium dioxide nanoparticles: role of particle surface area and internalized amount. *Toxicology* 260: 142-149, 2009.

76. **Iversen NK, Frische S, Thomsen K, Laustsen C, Pedersen M, Hansen PB, Bie P, Fresnais J, Berret JF, Baatrup E and Wang T**. Superparamagnetic iron oxide polyacrylic acid coated gamma-Fe2O3 nanoparticles do not affect kidney function but cause acute effect on the cardiovascular function in healthy mice. *Toxicol Appl Pharmacol* 266: 276-288, 2013.

77. **Jensen AW, Wilson SR and Schuster DI**. Biological applications of fullerenes. *Bioorg Med Chem* 4: 767-779, 1996.

78. **Jia G, Wang H, Yan L, Wang X, Pei R, Yan T, Zhao Y and Guo X**. Cytotoxicity of carbon nanomaterials: single-wall nanotube, multi-wall nanotube, and fullerene. *Environ Sci Technol* 39: 1378-1383, 2005.

79. **Johnson DR, Methner MM, Kennedy AJ and Steevens JA**. Potential for occupational exposure to engineered carbon-based nanomaterials in environmental laboratory studies. *Environ Health Perspect* 118: 49-54, 2010.

80. **Kang YJ, Li Y, Zhou Z, Roberts AM, Cai L, Myers SR, Wang L and Schuchke DA**. Elevation of serum endothelins and cardiotoxicity induced by particulate matter (PM2.5) in rats with acute myocardial infarction. *Cardiovasc Toxicol* 2: 253-261, 2002.

81. **Karaa A, Kamoun WS, Xu H, Zhang J and Clemens MG**. Differential effects of oxidative stress on hepatic endothelial and Kupffer cell eicosanoid release in response to endothelin-1. *Microcirculation* 13: 457-466, 2006.

82. **Katwa P, Wang X, Urankar RN, Podila R, Hilderbrand SC, Fick RB, Rao AM, Ke PC, Wingard CJ and Brown JM**. A carbon nanotube toxicity paradigm driven by mast cells and the IL-(3)(3)/ST(2) axis. *Small* 8: 2904-2912, 2012.

83. **Kim JB, Kim C, Choi E, Park S, Park H, Pak HN, Lee MH, Shin DC, Hwang KC and Joung B**. Particulate air pollution induces arrhythmia via oxidative stress and calcium calmodulin kinase II activation. *Toxicol Appl Pharmacol* 259: 66-73, 2012.

84. **Kirkby NS, Hadoke PW, Bagnall AJ and Webb DJ**. The endothelin system as a therapeutic target in cardiovascular disease: great expectations or bleak house? *Br J Pharmacol* 153: 1105-1119, 2008.

85. **Kis A, Jensen K, Aloni S, Mickelson W and Zettl A**. Interlayer forces and ultralow sliding friction in multiwalled carbon nanotubes. *Phys Rev Lett* 97: 025501, 2006.

86. **Kis A and Zettl A**. Nanomechanics of carbon nanotubes. *Philos Transact A Math Phys Eng Sci* 366: 1591-1611, 2008.

87. **Klocke R, Tian W, Kuhlmann MT and Nikol S**. Surgical animal models of heart failure related to coronary heart disease. *Cardiovasc Res* 74: 29-38, 2007.

88. **Knuckles TL, Yi J, Frazer DG, Leonard HD, Chen BT, Castranova V and Nurkiewicz TR**. Nanoparticle inhalation alters systemic arteriolar vasoreactivity through sympathetic and cyclooxygenase-mediated pathways. *Nanotoxicology* 6: 724-735, 2012.

89. **Kohan DE, Rossi NF, Inscho EW and Pollock DM**. Regulation of blood pressure and salt homeostasis by endothelin. *Physiol Rev* 91: 1-77, 2011.

90. **Kubota R, Tahara M, Shimizu K, Sugimoto N, Hirose A and Nishimura T**. Time-dependent variation in the biodistribution of C(6)(0) in rats determined by liquid chromatography-tandem mass spectrometry. *Toxicol Lett* 206: 172-177, 2011.

91. **LaDou J**. The asbestos cancer epidemic. *Environ Health Perspect* 112: 285-290, 2004.

92. **LaDou J, Castleman B, Frank A, Gochfeld M, Greenberg M, Huff J, Joshi TK, Landrigan PJ, Lemen R, Myers J, Soffritti M, Soskolne CL, Takahashi K, Teitelbaum D, Terracini B and Watterson A**. The case for a global ban on asbestos. *Environ Health Perspect* 118: 897-901, 2010.

93. **Lanfranchi PA and Somers VK**. Arterial baroreflex function and cardiovascular variability: interactions and implications. *Am J Physiol Regul Integr Comp Physiol* 283: R815-R826, 2002.

94. **Langrish JP, Bosson J, Unosson J, Muala A, Newby DE, Mills NL, Blomberg A and Sandstrom T**. Cardiovascular effects of particulate air pollution exposure: time course and underlying mechanisms. *J Intern Med* 272: 224-239, 2012.

95. **LeBlanc AJ, Moseley AM, Chen BT, Frazer D, Castranova V and Nurkiewicz TR**. Nanoparticle inhalation impairs coronary microvascular reactivity via a local reactive oxygen species-dependent mechanism. *Cardiovasc Toxicol* 10: 27-36, 2010.

96. **Lee JK, Sayers BC, Chun KS, Lao HC, Shipley-Phillips JK, Bonner JC and Langenbach R**. Multi-walled carbon nanotubes induce COX-2 and iNOS expression via MAP kinase-dependent and -independent mechanisms in mouse RAW264.7 macrophages. *Part Fibre Toxicol* 9: 14, 2012.

97. **Lefer AM, Smith EF, III, Araki H, Smith JB, Aharony D, Claremon DA, Magolda RL and Nicolaou KC**. Dissociation of vasoconstrictor and platelet aggregatory activities of thromboxane by carbocyclic thromboxane A2, a stable analog of thromboxane A2. *Proc Natl Acad Sci U S A* 77: 1706-1710, 1980.

98. **Legramante JM, Valentini F, Magrini A, Palleschi G, Sacco S, Iavicoli I, Pallante M, Moscone D, Galante A, Bergamaschi E, Bergamaschi A and Pietroiusti A**. Cardiac autonomic regulation after lung exposure to carbon nanotubes. *Hum Exp Toxicol* 28: 369-375, 2009.

99. **Li J, Zhang H and Zhang C**. Role of inflammation in the regulation of coronary blood flow in ischemia and reperfusion: mechanisms and therapeutic implications. *J Mol Cell Cardiol* 52: 865-872, 2012.

100. **Li JJ, Muralikrishnan S, Ng CT, Yung LY and Bay BH**. Nanoparticle-induced pulmonary toxicity. *Exp Biol Med (Maywood)* 235: 1025-1033, 2010.

101. **Liu CQ, Leung FP, Wong SL, Wong WT, Lau CW, Lu L, Yao X, Yao T and Huang Y**. Thromboxane prostanoid receptor activation impairs endothelial nitric oxide-dependent vasorelaxations: the role of Rho kinase. *Biochem Pharmacol* 78: 374-381, 2009.

102. **Luca C**. Electrophysiological properties of right heart and atrioventricular conducting system in patients with alcoholic cardiomyopathy. *Br Heart J* 42: 274-281, 1979.

103. **Ludbrook J**. Repeated measurements and multiple comparisons in cardiovascular research. *Cardiovasc Res* 28: 303-311, 1994.

104. **Ma JY, Zhao H, Mercer RR, Barger M, Rao M, Meighan T, Schwegler-Berry D, Castranova V and Ma JK**. Cerium oxide nanoparticle-induced pulmonary inflammation and alveolar macrophage functional change in rats. *Nanotoxicology* 5: 312-325, 2011.

105. **Mann EE, Thompson LC, Shannahan JH and Wingard CJ**. Changes in cardiopulmonary function induced by nanoparticles. *Wiley Interdiscip Rev Nanomed Nanobiotechnol* 4: 691-702, 2012.

106. **Maxwell SR and Lip GY**. Reperfusion injury: a review of the pathophysiology, clinical manifestations and therapeutic options. *Int J Cardiol* 58: 95-117, 1997.

107. **Mercer RR, Hubbs AF, Scabilloni JF, Wang L, Battelli LA, Friend S, Castranova V and Porter DW**. Pulmonary fibrotic response to aspiration of multi-walled carbon nanotubes. *Part Fibre Toxicol* 8: 21, 2011.

108. **Miller AM and Zhang JX**. Altered endothelin-1 signaling in production of thromboxane A2 in kupffer cells from bile duct ligated rats. *Cell Mol Immunol* 6: 441-452, 2009.

109. **Mills NL, Donaldson K, Hadoke PW, Boon NA, MacNee W, Cassee FR, Sandstrom T, Blomberg A and Newby DE**. Adverse cardiovascular effects of air pollution. *Nat Clin Pract Cardiovasc Med* 6: 36-44, 2009.

110. **Min J, Shah PN, Chae CG and Lee JS**. Arrangement of C60 via the self-assembly of post-functionalizable polyisocyanate block copolymer. *Macromol Rapid Commun* 33: 2029-2034, 2012.

111. **Minarchick VC, Stapleton PA, Porter DW, Wolfarth MG, Ciftyurek E, Barger M, Sabolsky EM and Nurkiewicz TR**. Pulmonary Cerium Dioxide Nanoparticle Exposure Differentially Impairs Coronary and Mesenteric Arteriolar Reactivity. *Cardiovasc Toxicol* 2013.

112. **Miyagawa H, Misra M and Mohanty AK**. Mechanical properties of carbon nanotubes and their polymer nanocomposites. *J Nanosci Nanotechnol* 5: 1593-1615, 2005.

113. **Monopoli MP, Aberg C, Salvati A and Dawson KA**. Biomolecular coronas provide the biological identity of nanosized materials. *Nat Nanotechnol* 7: 779-786, 2012.

114. **Morimoto Y, Hirohashi M, Ogami A, Oyabu T, Myojo T, Nishi K, Kadoya C, Todoroki M, Yamamoto M, Murakami M, Shimada M, Wang WN, Yamamoto K, Fujita K, Endoh S, Uchida K, Shinohara N, Nakanishi J and Tanaka I**. Inflammogenic effect of well-characterized fullerenes in inhalation and intratracheal instillation studies. *Part Fibre Toxicol* 7: 4, 2010.

115. **Morinaka Y, Nobori M, Murata M, Wakamiya A, Sagawa T, Yoshikawa S and Murata Y**. Synthesis and photovoltaic properties of acceptor materials based on the dimerization of fullerene C60 for use in efficient polymer solar cells. *Chem Commun (Camb)* 49: 3670-3672, 2013.

116. **Mulvany MJ and Aalkjaer C**. Structure and function of small arteries. *Physiol Rev* 70: 921-961, 1990.

117. **Mulvany MJ and Halpern W**. Mechanical properties of vascular smooth muscle cells in situ. *Nature* 260: 617-619, 1976.

118. **Murphy E and Steenbergen C**. Gender-based differences in mechanisms of protection in myocardial ischemia-reperfusion injury. *Cardiovasc Res* 75: 478-486, 2007.

119. **Nemmar A, Delaunois A, Nemery B, Dessy-Doize C, Beckers JF, Sulon J and Gustin P**. Inflammatory effect of intratracheal instillation of ultrafine particles in the rabbit: role of C-fiber and mast cells. *Toxicol Appl Pharmacol* 160: 250-261, 1999.

120. **Nessim GD**. Properties, synthesis, and growth mechanisms of carbon nanotubes with special focus on thermal chemical vapor deposition. *Nanoscale* 2: 1306-1323, 2010.

121. **Nguyen A, Thorin-Trescases N and Thorin E**. Working under pressure: coronary arteries and the endothelin system. *Am J Physiol Regul Integr Comp Physiol* 298: R1188-R1194, 2010.

122. **Niwa Y, Hiura Y, Sawamura H and Iwai N**. Inhalation exposure to carbon black induces inflammatory response in rats. *Circ J* 72: 144-149, 2008.

123. **Nurkiewicz TR, Porter DW, Hubbs AF, Stone S, Chen BT, Frazer DG, Boegehold MA and Castranova V**. Pulmonary nanoparticle exposure disrupts systemic microvascular nitric oxide signaling. *Toxicol Sci* 110: 191-203, 2009.

124. **Oberdorster G, Oberdorster E and Oberdorster J**. Nanotoxicology: an emerging discipline evolving from studies of ultrafine particles. *Environ Health Perspect* 113: 823-839, 2005.

125. **Oberdorster G, Sharp Z, Atudorei V, Elder A, Gelein R, Lunts A, Kreyling W and Cox C**. Extrapulmonary translocation of ultrafine carbon particles following whole-body inhalation exposure of rats. *J Toxicol Environ Health A* 65: 1531-1543, 2002.

126. **Ogami A, Yamamoto K, Morimoto Y, Fujita K, Hirohashi M, Oyabu T, Myojo T, Nishi K, Kadoya C, Todoroki M, Yamamoto M, Murakami M, Shimada M, Wang WN, Shinohara N, Endoh S, Uchida K, Nakanishi J and Tanaka I**. Pathological features of rat lung following inhalation and intratracheal instillation of C(60) fullerene. *Inhal Toxicol* 23: 407-416, 2011.

127. **Ozdemir R, Parlakpinar H, Polat A, Colak C, Ermis N and Acet A**. Selective endothelin a (ETA) receptor antagonist (BQ-123) reduces both myocardial infarct size and oxidant injury. *Toxicology* 219: 142-149, 2006.

128. **Pacurari M, Castranova V and Vallyathan V**. Single- and multi-wall carbon nanotubes versus asbestos: are the carbon nanotubes a new health risk to humans? *J Toxicol Environ Health A* 73: 378-395, 2010.

129. **Pacurari M, Qian Y, Fu W, Schwegler-Berry D, Ding M, Castranova V and Guo NL**. Cell permeability, migration, and reactive oxygen species induced by multiwalled carbon nanotubes in human microvascular endothelial cells. *J Toxicol Environ Health A* 75: 112-128, 2012.

130. **Park EJ, Kim H, Kim Y, Yi J, Choi K and Park K**. Inflammatory responses may be induced by a single intratracheal instillation of iron nanoparticles in mice. *Toxicology* 275: 65-71, 2010.

131. **Pernow J and Wang QD**. Endothelin in myocardial ischaemia and reperfusion. *Cardiovasc Res* 33: 518-526, 1997.

132. **Plante M, Honore JC, Neugebauer W and Orleans-Juste P**. Endothelin-1 (1-31) induces a thiorphan-sensitive release of eicosanoids via ET(B) receptors in the guinea pig perfused lung. *Clin Sci (Lond)* 103 Suppl 48: 128S-131S, 2002.

133. **Porter DW, Hubbs AF, Mercer RR, Wu N, Wolfarth MG, Sriram K, Leonard S, Battelli L, Schwegler-Berry D, Friend S, Andrew M, Chen BT, Tsuruoka S, Endo M and Castranova V**. Mouse pulmonary dose- and time course-responses induced by exposure to multi-walled carbon nanotubes. *Toxicology* 269: 136-147, 2010.

134. **Prisby RD, Muller-Delp J, Delp MD and Nurkiewicz TR**. Age, gender, and hormonal status modulate the vascular toxicity of the diesel exhaust extract phenanthraquinone. *J Toxicol Environ Health A* 71: 464-470, 2008.

135. **Pryshchep O, Ma-Krupa W, Younge BR, Goronzy JJ and Weyand CM**. Vessel-specific Toll-like receptor profiles in human medium and large arteries. *Circulation* 118: 1276-1284, 2008.

136. **Qi W, Wei JX, Dorairaj I, Mahajan RP and Wilson VG**. Evidence that a prostanoid produced by cyclo-oxygenase-2 enhances contractile responses of the porcine isolated coronary artery following exposure to lipopolysaccharide. *Br J Anaesth* 98: 323-330, 2007.

137. **Reddy AR, Rao MV, Krishna DR, Himabindu V and Reddy YN**. Evaluation of oxidative stress and anti-oxidant status in rat serum following exposure of carbon nanotubes. *Regul Toxicol Pharmacol* 59: 251-257, 2011.

138. **Ricciotti E and FitzGerald GA**. Prostaglandins and inflammation. *Arterioscler Thromb Vasc Biol* 31: 986-1000, 2011.

139. **Ryman-Rasmussen JP, Cesta MF, Brody AR, Shipley-Phillips JK, Everitt JI, Tewksbury EW, Moss OR, Wong BA, Dodd DE, Andersen ME and Bonner JC**. Inhaled carbon nanotubes reach the subpleural tissue in mice. *Nat Nanotechnol* 4: 747-751, 2009.

140. **Sayers BC, Taylor AJ, Glista-Baker EE, Shipley-Phillips JK, Dackor RT, Edin ML, Lih FB, Tomer KB, Zeldin DC, Langenbach R and Bonner JC**. Role of cyclooxygenase-2 in exacerbation of allergen-induced airway remodeling by multiwalled carbon nanotubes. *Am J Respir Cell Mol Biol* 49: 525-535, 2013.

141. **Schubert R and Mulvany MJ**. The myogenic response: established facts and attractive hypotheses. *Clin Sci (Lond)* 96: 313-326, 1999.

142. **Schuett H, Luchtefeld M, Grothusen C, Grote K and Schieffer B**. How much is too much? Interleukin-6 and its signalling in atherosclerosis. *Thromb Haemost* 102: 215-222, 2009.

143. **Semmler-Behnke M, Kreyling WG, Lipka J, Fertsch S, Wenk A, Takenaka S, Schmid G and Brandau W**. Biodistribution of 1.4- and 18-nm gold particles in rats. *Small* 4: 2108-2111, 2008.

144. **Shannahan JH, Kodavanti UP and Brown JM**. Manufactured and airborne nanoparticle cardiopulmonary interactions: a review of mechanisms and the possible contribution of mast cells. *Inhal Toxicol* 24: 320-339, 2012.

145. **Shinohara N, Gamo M and Nakanishi J**. Fullerene c60: inhalation hazard assessment and derivation of a period-limited acceptable exposure level. *Toxicol Sci* 123: 576-589, 2011.

146. **Shinohara N, Nakazato T, Tamura M, Endoh S, Fukui H, Morimoto Y, Myojo T, Shimada M, Yamamoto K, Tao H, Yoshida Y and Nakanishi J**. Clearance kinetics of fullerene C(6)(0) nanoparticles from rat lungs after intratracheal C(6)(0) instillation and inhalation C(6)(0) exposure. *Toxicol Sci* 118: 564-573, 2010.

147. **Skrzypiec-Spring M, Grotthus B, Szelag A and Schulz R**. Isolated heart perfusion according to Langendorff---still viable in the new millennium. *J Pharmacol Toxicol Methods* 55: 113-126, 2007.

148. **Sloan RC, Rosenbaum M, O'Rourke D, Oppelt K, Frasier CR, Waston CA, Allan AG and Brown DA**. High doses of ketamine-xylazine anesthesia reduce cardiac ischemia-reperfusion injury in guinea pigs. *J Am Assoc Lab Anim Sci* 50: 349-354, 2011.

149. **Smita S, Gupta SK, Bartonova A, Dusinska M, Gutleb AC and Rahman Q**. Nanoparticles in the environment: assessment using the causal diagram approach. *Environ Health* 11 Suppl 1: S13, 2012.

150. **Somlyo AP and Somlyo AV**. Ca2+ sensitivity of smooth muscle and nonmuscle myosin II: modulated by G proteins, kinases, and myosin phosphatase. *Physiol Rev* 83: 1325-1358, 2003.

151. **Soto D and Salcedo R**. Coordination modes and different hapticities for fullerene organometallic complexes. *Molecules* 17: 7151-7168, 2012.

152. **Stampfl A, Maier M, Radykewicz R, Reitmeir P, Gottlicher M and Niessner R**. Langendorff heart: a model system to study cardiovascular effects of engineered nanoparticles. *ACS Nano* 5: 5345-5353, 2011.

153. **Stapleton PA, Minarchick VC, Cumpston AM, McKinney W, Chen BT, Sager TM, Frazer DG, Mercer RR, Scabilloni J, Andrew ME, Castranova V and Nurkiewicz TR**. Impairment of coronary arteriolar endothelium-dependent dilation after multi-walled carbon nanotube inhalation: a time-course study. *Int J Mol Sci* 13: 13781-13803, 2012.

154. **Stapleton PA, Minarchick VC, McCawley M, Knuckles TL and Nurkiewicz TR**. Xenobiotic particle exposure and microvascular endpoints: a call to arms. *Microcirculation* 19: 126-142, 2012.

155. **Steenland K, Fletcher T and Savitz DA**. Epidemiologic evidence on the health effects of perfluorooctanoic acid (PFOA). *Environ Health Perspect* 118: 1100-1108, 2010.

156. **Sumner SC, Fennell TR, Snyder RW, Taylor GF and Lewin AH**. Distribution of carbon-14 labeled C60 ([14C]C60) in the pregnant and in the lactating dam and the effect of C60 exposure on the biochemical profile of urine. *J Appl Toxicol* 30: 354-360, 2010.

157. **Sung JH, Ji JH, Park JD, Song MY, Song KS, Ryu HR, Yoon JU, Jeon KS, Jeong J, Han BS, Chung YH, Chang HK, Lee JH, Kim DW, Kelman BJ and Yu IJ**. Subchronic inhalation toxicity of gold nanoparticles. *Part Fibre Toxicol* 8: 16, 2011.

158. **Tawfik HE, Cena J, Schulz R and Kaufman S**. Role of oxidative stress in multiparity-induced endothelial dysfunction. *Am J Physiol Heart Circ Physiol* 295: H1736-H1742, 2008.

159. **Thompson LC, Frasier CR, Sloan RC, Mann EE, Harrison BS, Brown JM, Brown DA and Wingard CJ**. Pulmonary instillation of multi-walled carbon nanotubes promotes coronary vasoconstriction and exacerbates injury in isolated hearts. *Nanotoxicology* (November 23, 2012); doi:10.3109/17435390.2012.744858.

160. **Thompson, L. C., Urankar, R. N., holland, N. A., Vidanapathirana, A. K., Plankenhorn, S., Han, L., Sumner, S. J., Lewin, A. H., Fennell, T. R., Lust, R. M., Brown, J. M., and Wingard, C. J**. C60 exposure augments cardiac ischemia/reperfusion injury and coronary tone in Sprague-Dawley rats. Toxicol.Sci. (Resubmitted 11/8/2013)

161. **Thorin E and Clozel M**. The cardiovascular physiology and pharmacology of endothelin-1. *Adv Pharmacol* 60: 1-26, 2010.

162. **Tong H, McGee JK, Saxena RK, Kodavanti UP, Devlin RB and Gilmour MI**. Influence of acid functionalization on the cardiopulmonary toxicity of carbon nanotubes and carbon black particles in mice. *Toxicol Appl Pharmacol* 239: 224-232, 2009.

163. **Turco RF, Bischoff M, Tong ZH and Nies L**. Environmental implications of nanomaterials: are we studying the right thing? *Curr Opin Biotechnol* 22: 527-532, 2011.

164. **Uchida E, Bohr DF and Hoobler SW**. A method for studying isolated resistance vessels from rabbit mesentery and brain and their responses to drugs. *Circ Res* 21: 525-536, 1967.

165. **Urankar RN, Lust RM, Mann E, Katwa P, Wang X, Podila R, Hilderbrand SC, Harrison BS, Chen P, Ke PC, Rao AM, Brown JM and Wingard CJ**. Expansion of cardiac ischemia/reperfusion injury after instillation of three forms of multi-walled carbon nanotubes. *Part Fibre Toxicol* 9: 38, 2012.

166. **Utell MJ, Frampton MW, Zareba W, Devlin RB and Cascio WE**. Cardiovascular effects associated with air pollution: potential mechanisms and methods of testing. *Inhal Toxicol* 14: 1231-1247, 2002.

167. **Van ES, Leipsic J, Paul Man SF and Sin DD**. The relationship between lung inflammation and cardiovascular disease. *Am J Respir Crit Care Med* 186: 11-16, 2012.

168. **Vesterdal LK, Folkmann JK, Jacobsen NR, Sheykhzade M, Wallin H, Loft S and Moller P**. Pulmonary exposure to carbon black nanoparticles and vascular effects. *Part Fibre Toxicol* 7: 33, 2010.

169. **Vidanapathirana AK, Lai X, Hilderbrand SC, Pitzer JE, Podila R, Sumner SJ, Fennell TR, Wingard CJ, Witzmann FA and Brown JM**. Multi-walled carbon nanotube directed gene and protein expression in cultured human aortic endothelial cells is influenced by suspension medium. *Toxicology* 302: 114-122, 2012.

170. **Wade ML and Fitzpatrick FA**. Nitric oxide modulates the activity of the hemoproteins prostaglandin I2 synthase and thromboxane A2 synthase. *Arch Biochem Biophys* 347: 174-180, 1997.

171. **Wang L, Wang L, Ding W and Zhang F**. Acute toxicity of ferric oxide and zinc oxide nanoparticles in rats. *J Nanosci Nanotechnol* 10: 8617-8624, 2010.

172. **Wang M, Baker L, Tsai BM, Meldrum KK and Meldrum DR**. Sex differences in the myocardial inflammatory response to ischemia-reperfusion injury. *Am J Physiol Endocrinol Metab* 288: E321-E326, 2005.

173. **Wang X, Katwa P, Podila R, Chen P, Ke PC, Rao AM, Walters DM, Wingard CJ and Brown JM**. Multi-walled carbon nanotube instillation impairs pulmonary function in C57BL/6 mice. *Part Fibre Toxicol* 8: 24, 2011.

174. **Wang X, Xia T, Addo NS, Ji Z, Lin S, Meng H, Chung CH, George S, Zhang H, Wang M, Li N, Yang Y, Castranova V, Mitra S, Bonner JC and Nel AE**. Dispersal state of multiwalled carbon nanotubes elicits profibrogenic cellular responses that correlate with fibrogenesis biomarkers and fibrosis in the murine lung. *ACS Nano* 5: 9772-9787, 2011.

175. **Watras JM**. Smooth Muscle Physiology. In: *Physiology*, edited by Berne RM, Levy MN, Koeppen BM and Stanton BA. St. Louis, MO: Mosby, 2004.

176. **Wingard CJ, Walters DM, Cathey BL, Hilderbrand SC, Katwa P, Lin S, Ke PC, Podila R, Rao A, Lust RM and Brown JM**. Mast cells contribute to altered vascular reactivity and ischemia-reperfusion injury following cerium oxide nanoparticle instillation. *Nanotoxicology* 5: 531-545, 2011.

177. **Wong BA**. Inhalation exposure systems: design, methods and operation. *Toxicol Pathol* 35: 3-14, 2007.

178. **Xu H, Korneszczuk K, Karaa A, Lin T, Clemens MG and Zhang JX**. Thromboxane A2 from Kupffer cells contributes to the hyperresponsiveness of hepatic portal circulation to endothelin-1 in endotoxemic rats. *Am J Physiol Gastrointest Liver Physiol* 288: G277-G283, 2005.

179. **Yazdi AS, Guarda G, Riteau N, Drexler SK, Tardivel A, Couillin I and Tschopp J**. Nanoparticles activate the NLR pyrin domain containing 3 (Nlrp3) inflammasome and

cause pulmonary inflammation through release of IL-1alpha and IL-1beta. *Proc Natl Acad Sci U S A* 107: 19449-19454, 2010.

180. **Ytrehus K**. The ischemic heart--experimental models. *Pharmacol Res* 42: 193-203, 2000.

181. **Zakynthinos E and Pappa N**. Inflammatory biomarkers in coronary artery disease. *J Cardiol* 53: 317-333, 2009.

182. **Zhang RZ, Gashev AA, Zawieja DC and Davis MJ**. Length-tension relationships of small arteries, veins, and lymphatics from the rat mesenteric microcirculation. *Am J Physiol Heart Circ Physiol* 292: H1943-H1952, 2007.

183. **Zimmer HG**. The Isolated Perfused Heart and Its Pioneers. *News Physiol Sci* 13: 203-210, 1998.

184. **Zweier JL and Talukder MA**. The role of oxidants and free radicals in reperfusion injury. *Cardiovasc Res* 70: 181-190, 2006.

APPENDIX A: IACUC APPROVAL LETTERS FOR ANIMAL USE PROTOCOLS

East Carolina University

1907-2007 CENTENNIAL

Animal Care and Use Committee
212 Ed Warren Life Sciences Building
East Carolina University
Greenville, NC 27834

252-744-2436 office
252-744-2355 fax

January 21, 2010

Christopher Wingard, Ph.D.
Department Physiology
Brody 6N-98
ECU Brody School of Medicine

Dear Dr. Wingard:

Your Animal Use Protocol entitled, "Cardiovascular Impact of Inhaled Multiwalled Carbon Nanotubes," (AUP #Q240a) was reviewed by this institution's Animal Care and Use Committee on 1/21/10. The following action was taken by the Committee:

"Approved as submitted"

Please contact Dale Aycock at 744-2997 prior to biohazard use

A copy is enclosed for your laboratory files. Please be reminded that all animal procedures must be conducted as described in the approved Animal Use Protocol. Modifications of these procedures cannot be performed without prior approval of the ACUC. The Animal Welfare Act and Public Health Service Guidelines require the ACUC to suspend activities not in accordance with approved procedures and report such activities to the responsible University Official (Vice Chancellor for Health Sciences or Vice Chancellor for Academic Affairs) and appropriate federal Agencies.

Sincerely yours,

Robert G. Carroll, Ph.D.
Chairman, Animal Care and Use Committee

RGC/jd

enclosure

East Carolina University

Animal Care and Use Commitee
212 Ed Warren Life Sciences Building
East Carolina University
Greenville, NC 27834

252-744-2436 office
252-744-2355 fax

February 15, 2012

Chris Wingard, Ph.D.
Department of Physiology
Brody 6N-98
ECU Brody School of Medicine

Dear Dr. Wingard:

The Amendment to your Animal Use Protocol entitled, "Cardiovascular and Cytokine Changes Following RTIs C60 and MWCNT Administration to Non-Pregnant, Pregnant and Lactating Rats", (AUP #Q300) was reviewed by this institution's Animal Care and Use Committee on 2/15/12. The following action was taken by the Committee:

"Approved as amended"

****Please contact Dale Aycock prior to any hazard use**

A copy of the Amendment is enclosed for your laboratory files. Please be reminded that all animal procedures must be conducted as described in the approved Animal Use Protocol. Modifications of these procedures cannot be performed without prior approval of the ACUC. The Animal Welfare Act and Public Health Service Guidelines require the ACUC to suspend activities not in accordance with approved procedures and report such activities to the responsible University Official (Vice Chancellor for Health Sciences or Vice Chancellor for Academic Affairs) and appropriate federal Agencies.

Sincerely yours,

Scott E. Gordon, Ph.D.
Chairman, Animal Care and Use Committee

SEG/jd

enclosure